1969

A theoretical study on the interpretation of resistivity sounding data measured by the Wenner electrode system

Siew Hung Chan

A THEORETICAL STUDY ON THE INTERPRETATION OF RESISTIVITY SOUNDING DATA MEASURED BY THE WENNER ELECTRODE SYSTEM

by

SIEW HUNG CHAN

A DISSERTATION

Presented to the Faculty of the Graduate School of the

UNIVERSITY OF MISSOURI AT ROLLA

In Partial Fulfillment of the Requirements for the Degree

DOCTOR OF PHILOSOPHY

in

GEOPHYSICAL ENGINEERING

Rolla, Missouri

1969

Advisor

ABSTRACT

This thesis deals with a theoretical study on the interpretation of resistivity sounding data measured by the Wenner electrode system. The objectives of this investigation are twofold: (i) to derive from the apparent resistivity data some suitable functions from which the resistivity and thickness of each member of the sequence of layers composing the earth may be determined, and (ii) to devise suitable methods for analyzing the resulting functions.

In this investigation it is shown that the solution of the boundary value problem associated with an n-layered earth model leads to an integral equation for the Wenner electrode system. This integral equation relates the apparent resistivity function to an unknown function, termed the kernel, which is dependent on the layer resistivities and thicknesses. By solving this integral equation one does not obtain the kernel directly, but rather a related function, termed the associated kernel, from which an explicit integral expression for the kernel can be derived. Formulas for numerical integration are developed for the calculation of both the kernel and associated kernel from apparent resistivity data. These formulas are found to give satisfactory results.

A numerical-graphical method is developed for the analysis of the kernel and the associated kernel. A further

technique based on the principle of logarithmic curve matching is developed for the decomposition of the kernel alone. These methods are found to yield reasonably accurate values for the layer resistivities and thicknesses.

ACKNOWLEDGEMENTS

The author wishes to express his gratitude first to his wife, for her patience throughout this research and the graduate studies which preceded it. He is especially grateful to Dr. Hughes M. Zenor, his dissertation advisor, for his encouragement and guidance. He also wishes to express his sincere thanks to Dr. Richard D. Rechtien for critical reading of this thesis; and to Dr. Ernest M. Spokes, Chairman of Department of Mining and Petroleum Engineering, for financial support through research appointment. To the authorities of the University of Malaya he is grateful for the study leave and grant that together made possible his return to the University of Missouri at Rolla for his doctoral study.

TABLE OF CONTENTS

LIST OF FIGURES

LIST OF TABLES

CHAPTER I

INTRODUCTION

One of the most popular techniques in shallow geophysical exploration is the use of d. c. (d. c. = direct current) resistivity depth soundings. In such measurements the resistivity of the earth is studied with an array of four electrode contacts, two of which are used to supply a current to the ground, and two of which are used to detect the electric field established in the ground by the current. A widely used electrode array is the Wenner system, the description of which can be found in Appendix A. By assuming the materials beneath the surface of the ground to be uniform, values of apparent resistivity are calculated from the measurements. The concept of apparent resistivity (see Appendix A for definition) permits the use of very simple mathematical formulas expressing the relationships between voltage, current, electrode spacing and the resistivity of the supposedly uniform earth. If the ground is not uniform, but consists of a series of strata in which the electrical properties within each stratum are uniform, then the variation of resistivity with depth in the ground may be studied by making apparent resistivity determinations with an increasing sequence of separations between the electrodes. Generally speaking the larger the electrode spacing the more the observed data will reflect the resistivity of layers at depth in the earth.

The interpretation of apparent resistivity data of depth soundings generally involves complicated mathematical analysis. Theoretically speaking we are concerned with an unusual boundary value problem in potential theory. In this problem the function to be determined is one which expresses the unknown variation of the resistivity with depth, whereas the potential function itself is considered to be known on the boundary, which in this problem is the surface of the earth.

Apart from the empirical methods, the interpretation of resistivity data may be broadly classified either as indirect or direct. The indirect methods of interpretation involves the comparison of the field sounding curves with theoretical apparent resistivity curves computed for an assumed sequence of resistivities and layer thicknesses. It is obvious that the indirect methods require the use of extensive tables or curves of theoretical solutions or both. At present the indirect methods are most popular among the field geophysicists because these methods are relatively simple in principle and easy to apply in practice. On account of their popularity there exists a large body of literatures concerning the indirect methods of interpreting resistivity data. A comprehensive bibliography is given by Van Nostrand and Cook (1966). Keller and Frischknacht (1966) give a detailed review on the various techniques of curve matching in their book on electrical methods in geophysical prospecting.

In the direct methods of interpretation no assumptions about the layer resistivities and thicknesses are necessary, but some geometric limitations are generally imposed on the earth model used. The general procedure of the direct methods of interpretation involves two main steps: (1) the calculation of a function which is termed the Slichter's kernel from the observed apparent resistivity data, and (2) the determination of the layer resistivities and thicknesses from the resulting Slichter's kernel. From the theoretical point of view the direct approach is equivalent to the search for a solution of the integral equation relating the apparent resistivity to the true resistivity and thickness of each of the individual layers composing the earth.

The direct methods of interpretation have first been studied in a series of papers by Langer (1933), Slichter (1933), and Stevenson (1934) respectively for the case of a continuous vertical variation of resistivity. In these papers it is assumed that the resistivity $\rho(z)$ can be expressed as a power series in z (the depth); the coefficients of this power series are determined by comparison with the coefficients of another power series representing the Slichter's kernel. The Slichter's kernel must be determined from the field data, namely the electric potentials, through integration. The methods of calculation are extremely cumbersome because of the highly complicated algebraic relations relating the coefficients of the two power series. There

is still another serious drawback in these methods. If a discontinuity in resistivity exists, the power series representations of both the resistivity function and the Slichter's kernel break down. In practice it is found that the function which best approximates the true resistivity variation in layered earth is a stepwise function of depth. Accordingly the methods developed by these earlier investigators have hardly found any application to practical problems.

Pekeris (1940) devised a numerical-graphical method for the analysis of the Slichter's kernel. His method works quite well but subjects to the restriction of small depth values. Later Vozoff (1956) proposed another method for analyzing the kernel. Vozoff's method involves the fitting of a kernel integrated from potential field data with a theoretical kernel calculated from an assumed sequence of layer resistivities and thicknesses. In the process of fitting which is carried out automatically on a digital computer the parameters of the kernel, namely the resistivity and thickness, are changed slowly until a good fit is obtained between the field and theoretical kernels. It must be pointed out that in both the papers by Pekeris and Vozoff respectively the actual computation of the kernel from the field data is not discussed.

In all the papers mentioned above none of these writers shows how the kernel may be calculated from the apparent

resistivity data. All these earlier methods require a knowledge of the electric potentials along the measuring line on the ground surface. But this knowledge is not obtained by the field procedures that are commonly used nowadays. This may be another reason why these methods are never adopted by the field geophysicists.

The most recent study on the direct methods of interpretation is presented by Koefoed in a series of two papers (1965 and 1966). In his first paper Koefoed derived an explicit integral expression for the Slichter's kernel in terms of the apparent resistivity function as measured by the Schlumberger electrode system. Then he proceeded to show how the integral expression of the kernel could be evaluated by approximating the apparent resistivity function with either a set of unrational algebraic functions or a set of exponential functions. In his second paper Koefoed dealt with the Wenner electrode system in a similar manner, but he did not obtain any explicit expression for the kernel in terms of the apparent resistivity function. The derivation of such an expression was later achieved by Paul (1968). Although the formulas derived by Koefoed are not very complicated from the computational point of view it is rather disappointing that he did not show how his formulas could actually be applied to practical situations.

Review of the literatures shows that the major obstacle which prevents the practical application of the direct methods

of interpretation has been that no suitable formulas are available to enable one to compute the Slichter's kernel or related functions directly from the apparent resistivity data. It was one of the main objectives of this thesis to develop a technique for deriving from the apparent resistivity data measured by the Wenner electrode system some functions from which the layer resistivities and thicknesses might be determined. Another objective was to devise methods for the analysis of the resulting functions derived from the field data.

In the following the solution of the boundary value problem associated with an n-layered earth model is first discussed in Chapter II. In the same chapter the solution for the integral equation resulting from solving the boundary value problem is also discussed. It will be shown that the process of solving the integral equation leads to two functions which will be designated as the 'kernel' and the 'associated kernel' respectively. As will be explained later the kernel defined in this thesis is not identical with the Slichter's kernel. Numerical techniques for computing the kernel and the associated kernel are derived in Chapter III. Finally the methods for determining the layer resistivities and thicknesses from the kernel functions are presented in Chapter IV.

CHAPTER II

THEORETICAL EARTH MODEL FOR THE INTERPRETATION OF APPARENT RESISTIVITY DATA

Basic Equations for Direct Current

The flow of direct current in a conducting medium is governed by the Ohm's law:

$$\vec{J} = \sigma \vec{E} \tag{2.1}$$

where $\vec{J}$ = current density measured in amp/m^2,

$\vec{E}$ = electric field intensity measured in volts/m,

σ = conductivity of the medium in mho/m.

It is sometimes more convenient to write (2.1) in the form

$$\vec{J} = \vec{E}/\rho \tag{2.2}$$

where $\sigma = 1/\rho$, ρ being the resistivity expressed in ohm-m. In addition to Ohm's law the current density has to satisfy the divergence condition:

$$\nabla . \vec{J} = 0 \tag{2.3}$$

This divergence condition must be satisfied everywhere in a source-free region.

Since stationary electric fields are conservative, that is $\nabla \times \vec{E} = 0$, $\vec{E}$ may be derivable from a scalar potential function V as follows:

$$\vec{E} = -\nabla V \tag{2.4}$$

where V is measured in volts. By substituting (2.4) into (2.1) we get

$$\vec{J} = -\sigma \nabla V = -\frac{1}{\rho} \nabla V \qquad (2.5)$$

It follows from (2.5) and (2.3) that

$$\nabla.(-\sigma \nabla V) = 0$$

and hence

$$\nabla\sigma.\nabla V + \sigma \nabla^2 V = 0 \qquad (2.6)$$

If the conductivity σ remains constant throughout the entire medium, then

$$\nabla^2 V = 0 \qquad (2.7)$$

which is the well known Laplace's equation. So the potential in this case is a harmonic function.

Suppose that the medium is divided into two regions of different conductivities, but within each region the conductivity is a constant. Let ρ_1 and ρ_2 be the resistivities of these two regions respectively. The potential in each region is still a harmonic function, but at the interface between the two regions two conditions must be satisfied: (i) the potential V must be continuous across the boundary, and (ii) the normal component of the current density $\vec{J}$ must also be continuous. The first condition is equivalent to the fact that the amount of work required to deposit a given charge on one side of the boundary should not differ from that required to deposit the same charge on the other side. The second condition is a consequence of the requirement that the current is conserved - all the current entering the boundary plane

from one side must leave it from the other side. From the conditions $\nabla.\vec{J} = 0$ and $\nabla x\vec{E} = 0$ one can formally deduce that these two boundary conditions can be expressed mathematically by the following equations:

$$V_1 = V_2 \tag{2.8}$$

for the continuity of the potential V, and

$$\vec{J}_1 .\hat{n} = \vec{J}_2 . \hat{n} \tag{2.9}$$

for the continuity of the normal component of the current density $\vec{J}$. In (2.9) $\hat{n}$ is the unit vector normal to the interface. With the use of (2.5) we can write (2.9) as

$$\frac{1}{\rho_1} \frac{\partial V_1}{\partial n} = \frac{1}{\rho_2} \frac{\partial V_2}{\partial n} \tag{2.10}$$

Solution of Boundary Value Problem

In the interpretation of resistivity data of depth soundings it is customary assumed that the ground is made up of two or more horizontal layers, each of which has a constant resistivity and finite thickness except the bottom-most layer being theoretically assumed to extend to infinity. Practical experiences show that such a model of the earth can often be used to approximate very closely the subsurface physical and geological conditions. From the theoretical point of view this model has the advantage that the mathematical theory involved in the analysis of the problem is not too complicated to handle.

The boundary value problem which we are going to consider may be stated as follows: The earth is assumed to consist of n horizontal layers (Fig. 2.1). Each of the first n-1 layers is characterized by a resistivity ρ_i and a finite thickness d_i, i = 1, 2,3,.....,n-1, while the bottom-most layer has a resistivity ρ_n and an infinite thickness. The upper-most layer is bounded at its upper boundary by the air which is assumed to have infinite resistance. The problem is to determine the potentials about a point current electrode located at the surface of the layered earth.

To solve the above problem we first note that the potential function will posses cylindrical symmetry because of the geometry of the model. Hence we shall adopt a cylindrical coordinate system with its origin coinciding with the position of the current electrode, and with the z-axis normal to the layering planes. Let V_1, V_2,.....,V_n be the potential functions in the media 1, 2, 3,.....,n respectively. Within each layer the potential function V_i must satisfy the Laplace's equation, that is,

$$\nabla^2 V_i = \frac{\partial^2 V_i}{\partial r^2} + \frac{1}{r}\frac{\partial V_i}{\partial r} + \frac{\partial V_i}{\partial z^2} = 0 \qquad (2.11)$$

for $z_{i-1} < z < z_i$ and $0 < r < \infty$, and also the following boundary conditions:

(i) $V_i(r,z) \to 0$ as $r \to \infty$ and in the bottom-most layer V_n must also vanish when z approaches infinity; and

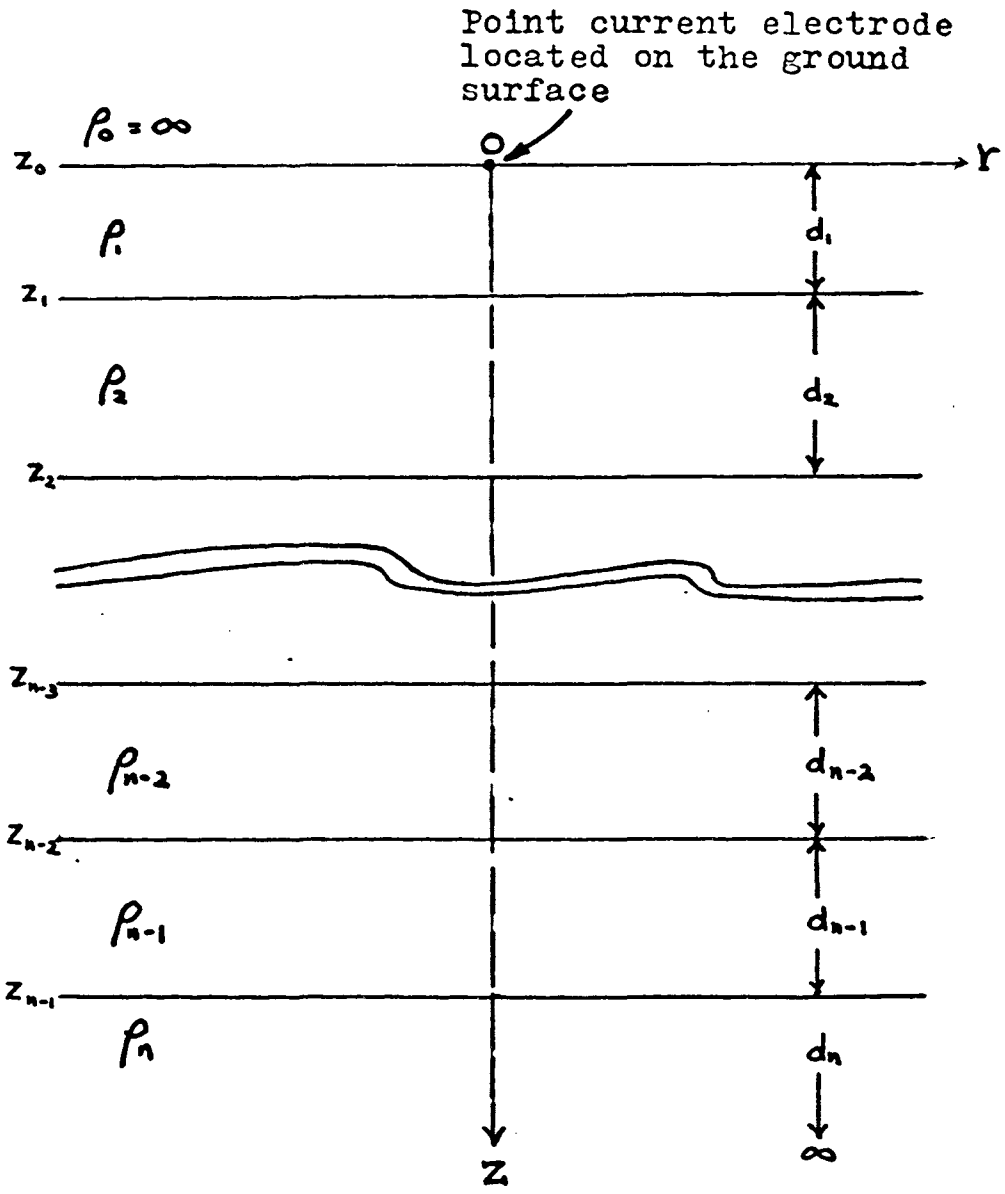

Fig. 2.1. n-layer earth model

(ii) at the interface z_i between layer i and layer i+1

$$V_i = V_{i+1}$$

and

$$\frac{1}{\rho_i} \frac{\partial V_i}{\partial z} \bigg|_{z = z_i} = \frac{1}{\rho_{i+1}} \frac{\partial V_{i+1}}{\partial z} \bigg|_{z = z_i}$$

In addition to the above conditions the potential function V_1 in the first layer has to satisfy two further conditions:

(i) since no current can flow across the boundary the normal component of the current density must vanish at z = 0. This implies that

$$\frac{\partial V_1}{\partial z} \bigg|_{z = 0} = 0 \ ;$$

and (ii) V_1 must approach the correct expression for the potential about a single point source in a uniform medium, that is,

$$V_1(r,z) \rightarrow \frac{I \rho_1}{2\pi R} \quad \text{as } R \rightarrow 0 \ ,$$

where $R = (r^2 + z^2)^{\frac{1}{2}}$.

The solution of Laplace's equation can be achieved by the method of separation of variables. The procedure of solving the problem is outlined in Appendix B. We shall only state here the final form of the solution.

In Appendix B it is shown that the potential at any point on the surface of the n-layer earth is given by the expression

$$V_1(r,0) = \frac{I\rho_1}{2\pi} \int_0^\infty K_1(\lambda)\, J_0(\lambda r)\, d\lambda \qquad (2.12)$$

where $K_1(\lambda)$ is the 'kernel' which is expressed explicitly by (B.15a). It has been pointed out in Appendix B that the kernel $K_1(\lambda)$ is not identical with the Slichter's kernel. To avoid confusion we shall reserve the term, kernel, for the function $K_1(\lambda)$ only in all our following discussions. It may be noted that the kernel is a function dependent on the layer resistivities and thicknesses. Since the kernel embodies all the information concerning the layer resistivities and thicknesses it is of great interest to us in the interpretation of resistivity data.

Theoretical Apparent Resistivity Formula for The Wenner Electrode System

In Appendix A it has been shown that the apparent resistivity measured by the Wenner electrode system is defined by the equation

$$\rho_a = 2\pi t \frac{\Delta V}{I} .$$

If measurements are made over the surface of a layered earth,

then by making use of (2.12) one can easily show that the potential difference ΔV is given by the following expression:

$$\Delta V = \frac{I\rho_1}{\pi} \int_0^\infty K_1(\lambda) \{J_0(\lambda t) - J_0(2\lambda t)\} \, d\lambda \, .$$

It follows that the theoretical apparent resistivity function for an n-layer earth is given by

$$\rho_a(t) = 2t\rho_1 \int_0^\infty K_1(\lambda) \{J_0(\lambda t) - J_0(2\lambda t)\} \, d\lambda \, . \qquad (2.13)$$

Equation (2.13) forms the basis of the curve-matching methods of interpreting resistivity data obtained by using the Wenner electrode system. By assigning hypothetical values to the layer resistivities and thicknesses one can compute theoretical apparent resistivity curves from (2.13). Mooney and Wetzel (1956), for example, have prepared a set of about 2300 curves for the Wenner electrode system for one, two, and three layers over an infinite substratum. These curves are commonly employed for curve-matching purpose.

In practice the apparent resistivity function $\rho_a(t)$ is a known function determined by direct field measurements while the kernel $K_1(\lambda)$ appearing under the integral sign of (2.13) is an unknown function because the layer resistivities and thicknesses cannot be determined by direct observations. Thus (2.13) is essentially an integral equation. The

interpretation of the resistivity data amounts to the search for a suitable solution for this integral equation.

Solution of Integral Equation

A solution of the integral Equation (2.13) can be obtained by making use of the Hankel inversion theorem (Sneddon, 1951) which may be stated as follows: The Hankel transform of a function f(x) is defined by

$$H(u) = \int_0^\infty xf(x)J_\mu(ux)\ dx \qquad \mu \geq -\tfrac{1}{2}$$

which exists if f(x) is piecewise continuous in any finite interval and absolutely integrable. If, in addition, f(x) possesses piecewise continuous derivative in any finite interval the inversion integral

$$\tfrac{1}{2}\{f(x+0) + f(x-0)\} = \int_0^\infty uH(u)J_\mu(ux)\ du$$

exists.

If f(x) is continuous at the point x, then

$$f(x+0) = f(x-0) = f(x)$$

so that the theorem gives

$$f(x) = \int_0^\infty uH(u)J_\mu(ux)\ du.$$

In the special case $\mu = 0$ we have the Hankel transform pair,

$$H(u) = \int_0^\infty xf(x)J_0(ux)\ dx \tag{2.14a}$$

$$f(x) = \int_0^\infty uH(u)J_0(ux)\ du. \tag{2.14b}$$

To solve the integral Equation (2.13) we may proceed as follows: if both sides of (2.13) are multiplied by $J_0(\lambda' t)$ and then integrated with respect to t from 0 to ∞ we have

$$\int_0^\infty \rho_a(t)J_0(\lambda' t)\ dt = 2\rho_1\{\int_0^\infty tJ_0(\lambda' t) \int_0^\infty K_1(\lambda)J_0(\lambda t)\ d\lambda dt$$

$$- \int_0^\infty tJ_0(\lambda' t) \int_0^\infty K_1(\lambda)J_0(2\lambda t)\ d\lambda dt\} .$$

The application of the Hankel transform pair (2.14a) and (2.14b) to the right hand side of the above equation leads to

$$K_1(\lambda) - \tfrac{1}{2}K_1(\lambda/2) = \frac{\lambda}{2} \int_0^\infty \frac{\rho_a(t)}{\rho_1} J_0(\lambda t)\ dt \tag{2.15}$$

which is the desired solution of the integral equation. However, (2.15) is not an explicit expression for the kernel $K_1(\lambda)$. To derive such an expression we proceed in the

following manner. By setting λ equal to λ, $\lambda/2$, $\lambda/4$, $\lambda/8$,....., $\lambda/2^n$ ..... and then multiplying the resulting equations by 1, 1/2, 1/4, 1/8, ..., $1/2^n$,..... respectively, we obtain the following set of equations:

$$K_1(\lambda) - 1/2\ K_1(\lambda/2) = \lambda \int_0^\infty \frac{\rho_a(t)}{2\rho_1} J_0(\lambda t)\ dt$$

$$1/2\ K_1(\lambda) - 1/4\ K_1(\lambda/4) = \lambda/4 \int_0^\infty \frac{\rho_a(t)}{2\rho_1} J_0(\lambda t/2)\ dt \qquad (2.16)$$

$$1/4\ K_1(\lambda/4) - 1/8\ K_1(\lambda/8) = \lambda/16 \int_0^\infty \frac{\rho_a(t)}{2\rho_1} J_0(\lambda t/4)\ dt$$

.....

$$1/2^n\ K_1(\lambda/2^n) - 1/2^{n+1}\ K_1(\lambda/2^{n+1}) = \lambda/2^n \int_0^\infty \frac{\rho_a(t)}{2\rho_1} J_0(\lambda t/2^n)\ dt$$

.....

Summing up both sides of the above equations we obtain

$$K_1(\lambda) = \sum_{n=0}^{\infty} \frac{\lambda}{2^{2n}} \int_0^\infty \tfrac{1}{2} \frac{\rho_a(t)}{\rho_1} J_0(\lambda t/2^n)\ dt$$

By interchanging the order of summation and integration formally we have

$$K_1(\lambda) = \frac{\lambda}{2} \int_0^{\infty} \frac{\rho_a(t)}{\rho_1} \left\{ \sum_{n=0}^{\infty} \frac{1}{2^{2n}} J_0(\lambda t/2^n) \right\} \, dt \qquad (2.17)$$

By letting

$$F(\lambda t) = \sum_{n=0}^{\infty} \frac{1}{2^{2n}} J_0(\lambda t/2^n) \qquad (2.18)$$

(2.17) can be written as

$$K_1(\lambda) = \frac{\lambda}{2\rho_1} \int_0^{\infty} \rho_a(t) \, F(\lambda t) \, dt \qquad (2.19)$$

which is the desired expression for the kernel.

The infinite series (2.18) can be shown to converge uniformly and it behaves almost like the Bessel function $J_0(\lambda t)$. A brief discussion of the properties of $F(\lambda t)$ is given in Appendix C.

Though (2.15) is not an explicit expression for the kernel it serves to define a useful function from which one may determine the layer resistivities and thicknesses. By letting

$$B_1(\lambda) = K_1(\lambda) - \tfrac{1}{2} K_1(\lambda/2) \qquad (2.20)$$

(2.15) can be written as

$$B_1(\lambda) = \lambda/2 \int_0^{\infty} \frac{\rho_a(t)}{\rho_1} J_0(\lambda t) \, dt. \qquad (2.21)$$

For the ease of description we shall define $B_1(\lambda)$ as the 'associated kernel' for n-layer earth.

In conclusion we note that if the apparent resistivity function $\rho_a(t)$ is determined from field observations then (2.19) and (2.21) will enable us to compute the kernel and the associated kernel respectively from the observed resistivity data. Once the kernel and the associated kernel are known the layer resistivities and thicknesses may be obtained from these functions by some suitable methods of analysis. In Chapter III we shall consider the calculation of the kernel and the associated kernel from the observed apparent resistivity data. This is followed by the derivation of the methods used for analyzing $K_1(\lambda)$ and $B_1(\lambda)$ in Chapter IV.

CHAPTER III

NUMERICAL METHODS FOR CALCULATING THE KERNEL AND THE ASSOCIATED KERNEL

In Chapter II it has been shown that the solution of the integral equation for the Wenner electrode system leads to the following results:

$$K_1(\lambda) = \lambda/2 \int_0^\infty \frac{\rho_a(t)}{\rho_1} F(\lambda t) \, dt$$

and

$$B_1(\lambda) = \lambda/2 \int_0^\infty \frac{\rho_a(t)}{\rho_1} J_0(\lambda t) \, dt$$

where $K_1(\lambda)$ and $B_1(\lambda)$ are the kernel and the associated kernel respectively. The apparent resistivity function $\rho_a(t)$ which appears in the integrands of both the above integrals is, in practice, only known empirically from a finite number of measurements, but not known analytically. Consequently $K_1(\lambda)$ and $B_1(\lambda)$ cannot be determined by any method of direct integration. In order to obtain $K_1(\lambda)$ and $B_1(\lambda)$ from the observed apparent resistivity data one has to resort to the numerical techniques of integration. In this chapter we are going to develop the methods for evaluating the kernel and the associated kernel numerically.

Least-Squares Approximation of Apparent Resistivity Data

In the above introductory remarks we point out that the apparent resistivity is observed only at certain number of electrode spacings. For numerical evaluation of the integrals of $K_1(\lambda)$ and $B_1(\lambda)$ respectively, however, one needs to know the values of $\rho_a(t)$ at a large number of points along the t-axis; the set of field data is obviously inadequate for such purpose. Of course, it is highly impracticable and uneconomical to make a very large number of measurements in the field. The practical remedy to the problem is to interpolate the unknown values of $\rho_a(t)$ from the observed data. The interpolation can be achieved by approximating $\rho_a(t)$ with some suitable function. Since the field data usually contain a certain amount of noise the appropriate technique of approximation to be used would be the least-squares method.

The least-squares techniques of approximating function are well known and are described in many standard texts of numerical analysis (e.g. Hildebrand, 1956; Ralston, 1965). In the following we shall consider those facts which are pertinent to our problem.

Outline of least-squares method. Suppose that the values of the apparent resistivity function $\rho_a(t)$ is observed at a sequence of data points, namely $\{t_i\}$, $i = 1, 2, \ldots, n$. These observed values of $\rho_a(t)$ will generally be in error. Let $\rho_a(t_i)$ denote the true value of $\rho_a(t)$ at t_i and $\bar{\rho}_a(t_i)$ the observed value also at t_i. Next suppose that we have a

set of polynomials $\{P_j(t)\}$, j being the degree of the polynomials and j = 0, 1, 2,....., m, which are orthogonal over the set of points $\{t_i\}$. Our objective is to approximate $\bar{\rho}_a(t_i)$ by a linear combination of $\{P_j(t)\}$, that is,

$$\bar{\rho}_a(t_i) \simeq \sum_{j=o}^{m} c_j P_j(t_i) \quad \text{for } i = 1,2,.....,n \tag{3.1}$$

According to the principle of least-squares the coefficients c_j's must be determined in such a way that the function

$$H(c_0, c_1,....., c_m) = \sum_{i=1}^{n} \{\bar{\rho}_a(t_i) - \sum_{j=0}^{m} c_j P_j(t_i)\}^2 \tag{3.2}$$

is minimized. If H is minimum, then at the point in question

$$\frac{\partial H}{\partial c_k} = 2 \sum_{i=1}^{n} \{\bar{\rho}_a(t_i) - \sum_{j=0}^{m} c_j P_j(t_i)\} (-P_k(t_i)) = 0$$

or

$$\sum_{j=0}^{m} c_j \sum_{i=1}^{n} P_j(t_i)P_k(t_i) = \sum_{i=1}^{n} \bar{\rho}_a(t_i)P_k(t_i) \tag{3.3}$$

for k = 0, 1, 2, 3,....., m. The system (3.3) consists of m+1 linear equations for m+1 unknown c_j's. This system is called the normal equations. If the determinant of the coefficients does not vanish we can solve for the c_j's.

By making use of the orthogonal relation

$$\sum_{i=1}^{n} P_j(t_i)P_k(t_i) = 0 \quad \text{for } j = k$$

we find that the solution of (3.3) is given by

$$c_k = \frac{\sum_{i=1}^{n} \bar{\rho}_a(t_i)\, P_k(t_i)}{\sum_{i=1}^{n} \{P_k(t_i)\}^2} \tag{3.4}$$

A few words may be said about the selection of m, the degree of polynomial approximation, for a given value of n. One way of making the choice is to compute the function

$$\sigma_m^2 = E_m^2 \; / \; (n - m - 1) \tag{3.5}$$

where

$$E_m^2 = \sum_{i=1}^{n} \{\bar{\rho}_a(t_i) - \sum_{j=0}^{m} c_j P_j(t_i)\}^2 \; .$$

According to the statistical null hypothesis (Ralston, p. 234) the expected value of σ_m^2 is independent of m for m = M, M+1, ..., n-1. In practice, since we do not know M, we would wish to solve the normal Equations (3.3) for m = 1, 2, 3,..... and compute σ_m^2 and continue as long as σ_m^2 decreases significantly with increasing m. As soon as a value of m is reached after which there is no significant change in σ_m^2 then this value is that of the null hypothesis, and we have the desired least-squares approximation.

In the above discussion it is pointed out that the search for a suitable m would require one to solve the normal Equations (3.3) repeatedly. This is indeed a very tedious process. However, such a computational problem does not arise with the use of orthogonal polynomials since all the coefficients c_k can be calculated independently from (3.4). It may also be noted that the use of orthogonal polynomials avoids the problem of forming an ill-conditioned matrix of the coefficients in (3.3) when large values of m are used.

Generation of orthogonal polynomials. The set of orthogonal polynomials $\{P_j(t)\}$ which is used in the least-squares approximation may be generated in a number of ways. The writer finds that a method proposed by Forsythe (1957) is most suited for his purpose. Forsythe's method of generating orthogonal polynomials may be outlined as follows.

Suppose that $\{P_j(t)\}$ is any sequence of polynomials satisfying the orthogonal relationship

$$\sum_{i=1}^{n} P_j(t_i)P_k(t_i) = 0 \quad \text{for } j \neq k$$

with respect to a sequence of data point $\{t_i\}$, i = 1, 2, 3,....., n. This sequence of orthogonal polynomials can be generated by the following recursion formulas:

$$
\begin{aligned}
P_{-j}(t) &= 0 \\
P_0(t) &= 1 \\
P_1(t) &= (t - p_1)\, P_0(t) \\
P_2(t) &= (t - p_2)\, P_1(t) - q_1\, P_0(t) \\
&\cdots\cdots\cdots\cdots\cdots\cdots\cdots\cdots \\
P_m(t) &= (t - p_m)\, P_{m-1}(t) - q_{m-1}\, P_{m-2}(t)
\end{aligned}
\tag{3.6}
$$

where p_m and q_m are constants so chosen to make the orthogonal relations hold. It can be shown that

$$
p_m = \frac{\sum_{i=1}^{n} t_i \{P_{m-1}(t_i)\}^2}{\sum_{i=1}^{n} \{P_{m-2}(t_i)\}^2} \tag{3.7}
$$

and

$$
q_m = \frac{\sum_{i=1}^{n} t_i\, P_{m-1}(t_i)\, P_{m-2}(t_i)}{\sum_{i=1}^{n} P_{m-2}(t_i)^2} \tag{3.8}
$$

The range of the independent variable t may be normalized for range $0 < t_i' < 1$ by using the transformation

$$
t_i' = (t_i - t_1) / (t_n - t_1) \; . \tag{3.9}
$$

Some computational details. The Forsythe's method of generating orthogonal polynomials for data-fitting is well suited for cases in which the data points are not equally spaced. Also the computational works involved in this method

can be performed automatically by a digital computer. All the results presented in the following were computed by the IBM-360 MOD 50 system at the UMR computer center. Outline of the computational procedures is given in Appendix E.

It may be pointed out that our primary aim here is to obtain a single least-squares approximating function that can fit the apparent resistivity data in the entire range of electrode spacing concerned.

Two different approaches have been tried to fit the apparent resistivity data by the least-squares method outlined above. The first method consists of the fitting of the curve $\rho_a(t)$ vs. t, while in the second method attempt is made to fit the curve $\log \rho_a(t)$ vs. $\log t$. The use of the second method is due to the following reasons. In practice a typical sequence of electrode spacing used for field measurements is {1, 2, 4, 6, 8, 10, 15, 20, 30, 40, 60, 80, 100, etc}; the unit used may be meter or feet. It is evident that there will be more data points crowed into the lower range of the electrode spacing than in its upper range when one attempts to fit the curve $\rho_a(t)$ vs. t. Such a feature is undesirable if we were to fit all the data within the entire range with a single function. This crowding of data within a particular interval along the t-axis can be avoided if $\log \rho_a(t)$ is plotted against $\log t$. For instance, in Fig. 3.1 which shows a typical set of apparent resistivity data plotted on linear scales, the crowding phenomenon is clearly evident

within the interval $0 < t < 10$. When the same set of data is plotted on bilogarithmic scales (Fig. 3.2) a more uniform distribution of the data is obtained.

The advantage of using the second method of fitting compared to the use of the first method is clearly indicated by the results of actual calculations. Figs. 3.3 and 3.4 show the results of fitting a three-layer resistivity curve with least-squares approximations of different degrees using the first method. From these figures it is noted that the fitting is far from satisfaction when the degree m of the least-squares polynomial is less than 6. For larger values of m the fitting is quite satisfactory in the middle and upper range of t, but is relatively poor when $t < 10$. The results of fitting by the second method are shown in Fig. 3.5. Comparing the results of the two methods it is obvious that the second method of fitting is a more suitable procedure than the first one. The numerical values for the graphs shown in the above mentioned figures are given in Tables 3.1 and 3.2.

The next question of importance is how good is the approximation at points lying between the given data points? In other words, once the coefficients c_j are obtained, can (3.1) be used to interpolate values of $\rho_a(t)$ between the observed values? To seek an answer to this question calculations of the values of $\rho_a(t)$ spaced at an interval $\Delta t = 0.5$ apart were carried out using (3.1) with the appropriate

coefficients c_j. Table 3.3 illustrates some typical results. From these numerical values one can see that the resulting curve is quite smooth. Thus one may conclude that (3.1) can indeed be used for interpolating purpose. However, further calculations using a finer interval, say $\Delta t = 0.05$, produced some unexpected results. Fig. 3.6 illustrate a typical example of the irregularity encountered. The interpolated values tend to oscillate about the true curve of $\rho_a(t)$. Such behavior is, of course, undesirable because in the process of evaluating the integral of either $K_1(\lambda)$ or $B_1(\lambda)$ the values of $\rho_a(t)$ must be known at points which may be spaced at intervals much smaller than $\Delta t = 0.5$.

A remedy to the above mentioned difficulty is to avoid the use of (3.1) to compute the values of $\rho_a(t)$ at too fine an interval. Equation (3.1) may be used to generate values of $\rho_a(t)$ spaced at an interval, say $\Delta t = 0.5$ or larger. Then the other values of $\rho_a(t)$ that lie within each interval can be obtained by interpolation with the use of some suitable interpolating formulas. It was found that a three-point Lagrangian interpolating formula was adequate for our purpose when $\Delta t = 0.5$. Curve II shown in Fig. 3.6 was obtained by interpolation between points spaced at an interval $\Delta t = 0.5$ apart.

An outline of the Lagrangian interpolating formulas is given in Appendix D.

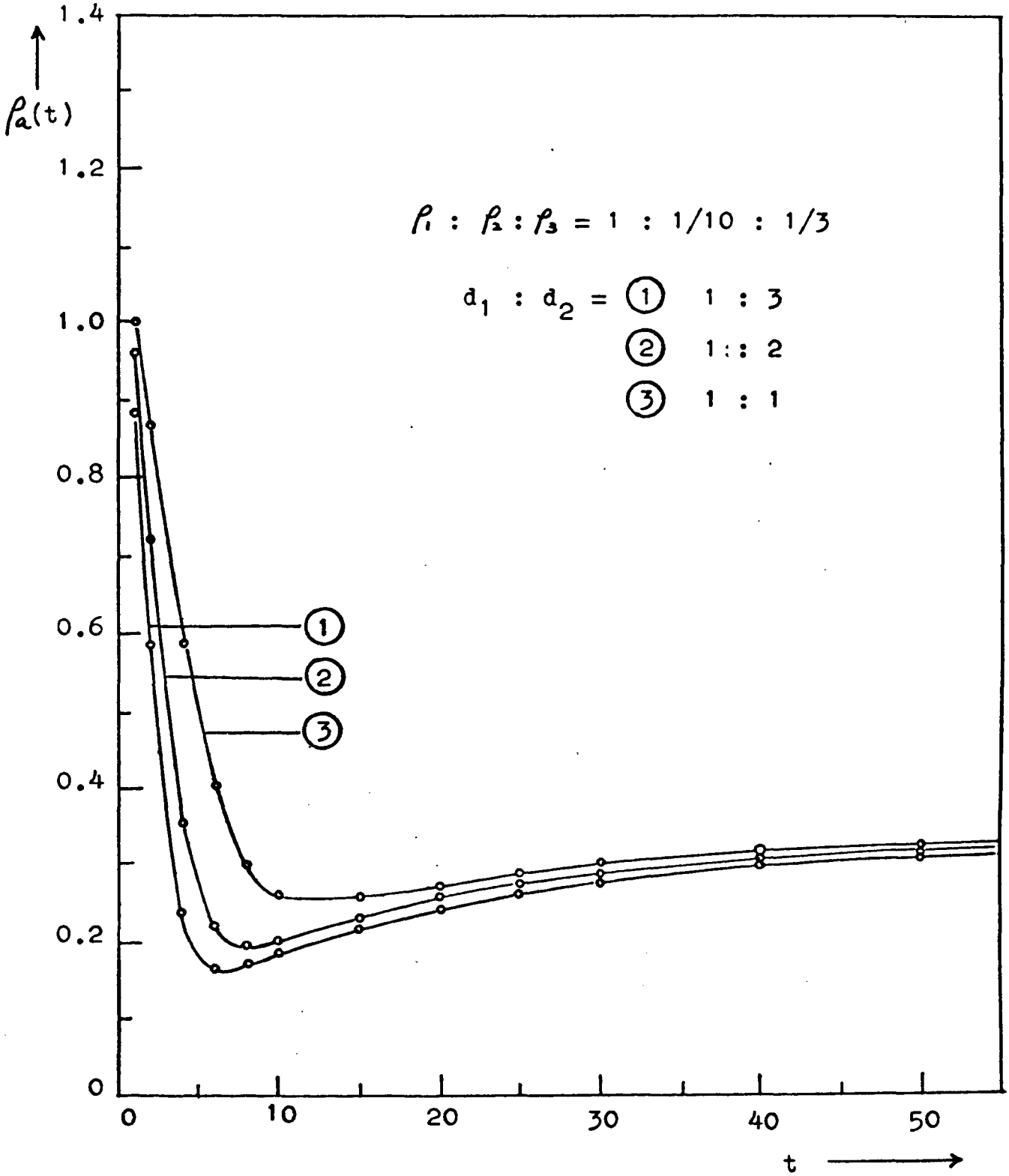

Fig. 3.1. Apparent resistivity curves which would be obtained with a Wenner electrode system over a three-layer earth.

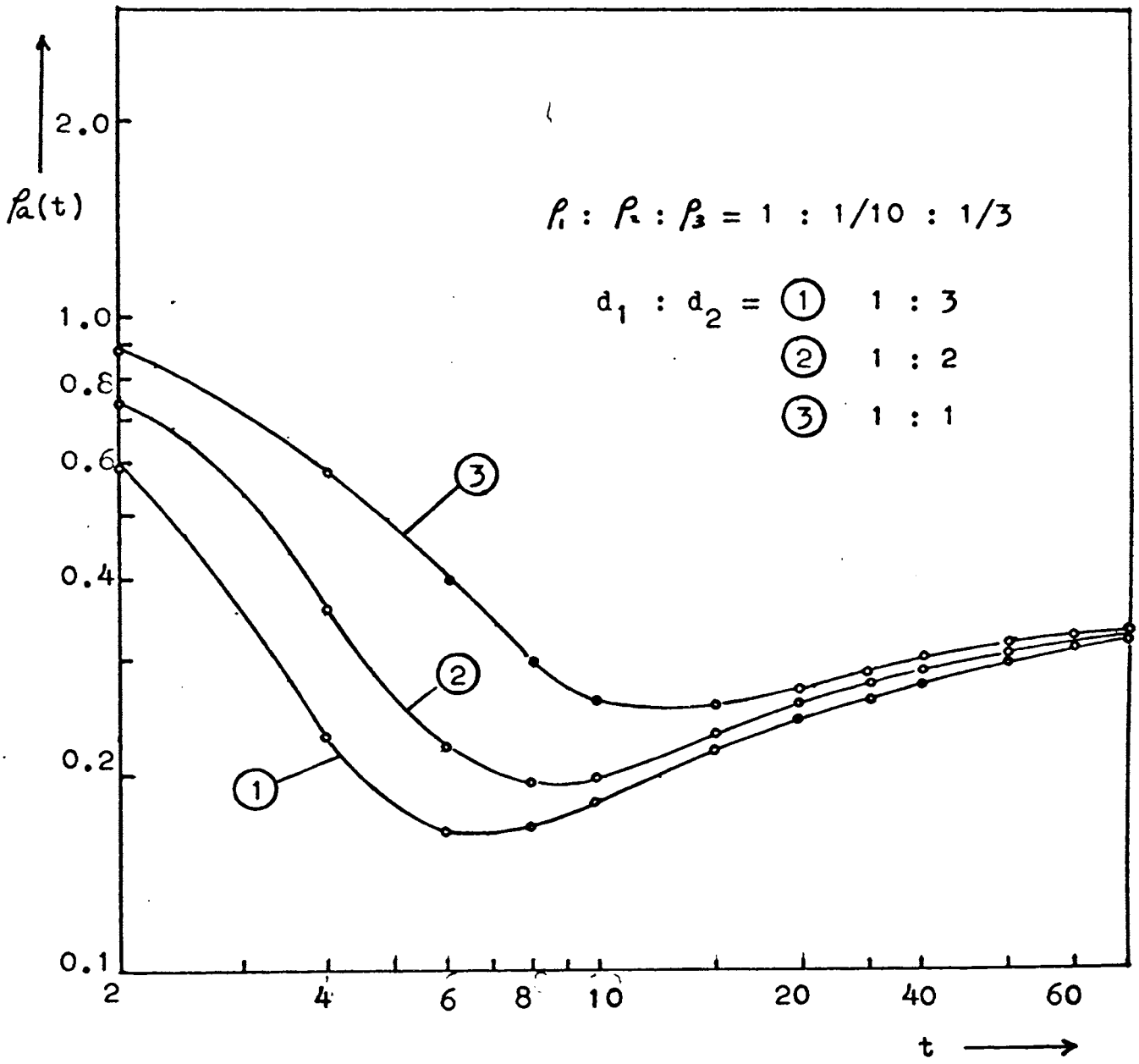

Fig. 3.2. Apparent resistivity curves which would be obtained with a Wenner electrode system over a three-layer earth, logarithmic plotting.

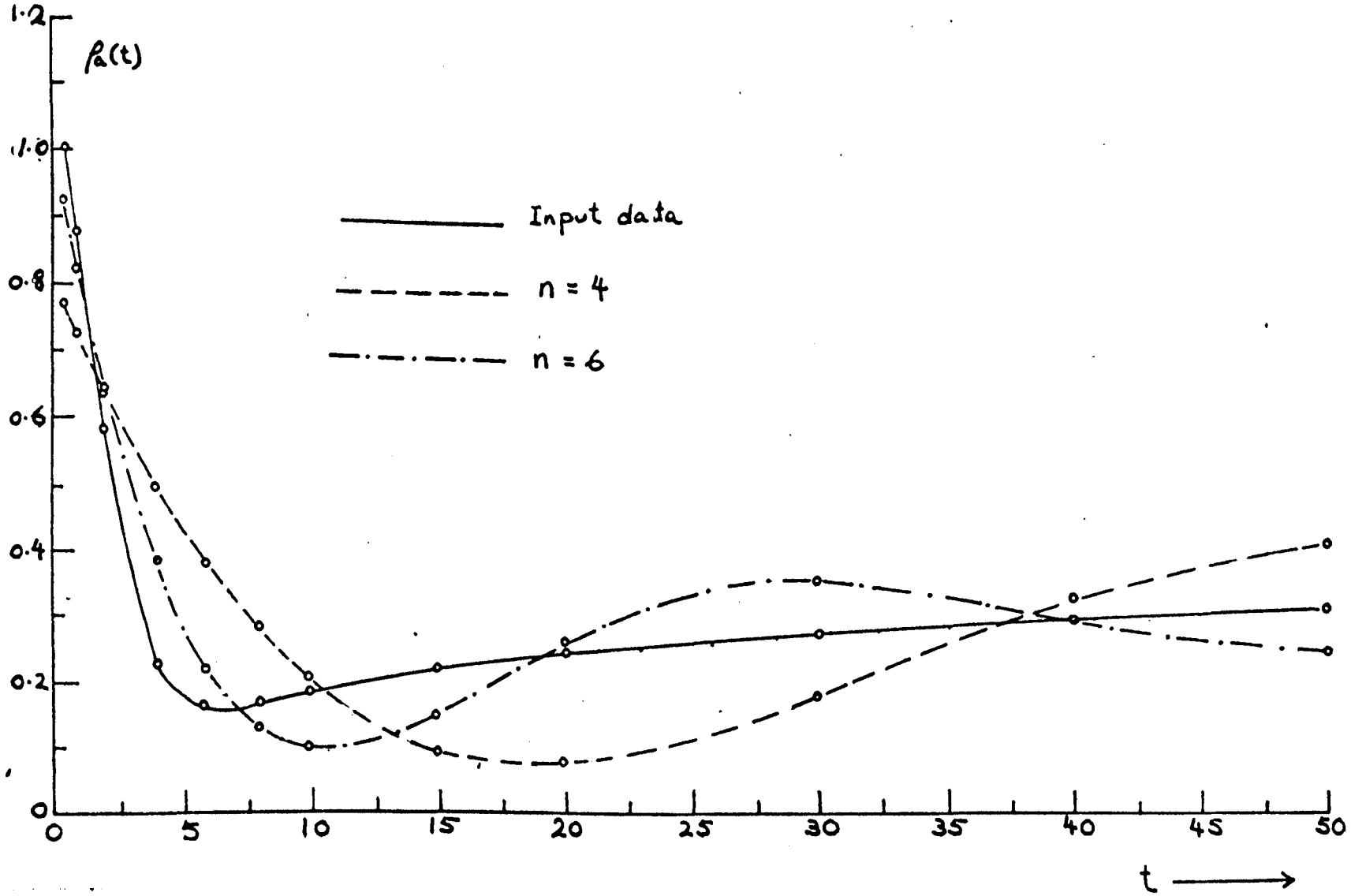

Fig. 3.3. Comparison of input data with least-squares approximations of degree 4 and 6 respectively, using the first approach of fitting. Case $\rho_1 : \rho_2 : \rho_3 = 1 : 1/10 : 1/3$, $d_1 : d_2 = 1 : 3$.

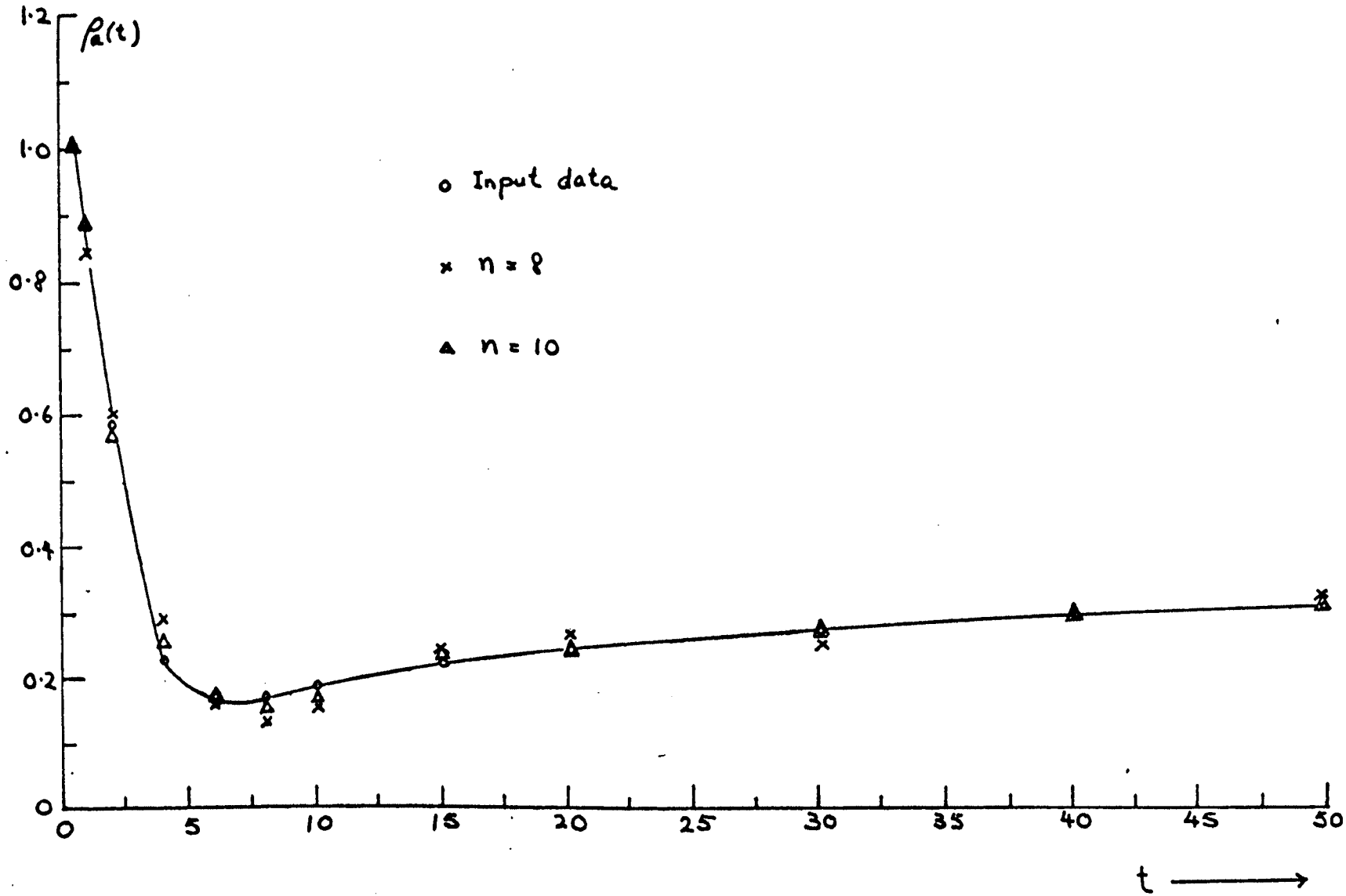

Fig. 3.4. Comparison of input data with least-squares approximations of degree 8 and 10 respectively, using the first approach of fitting. Case $\rho_1 : \rho_2 : \rho_3 = 1 : 1/10 : 1/3$, $d_1 : d_2 = 1 : 3$.

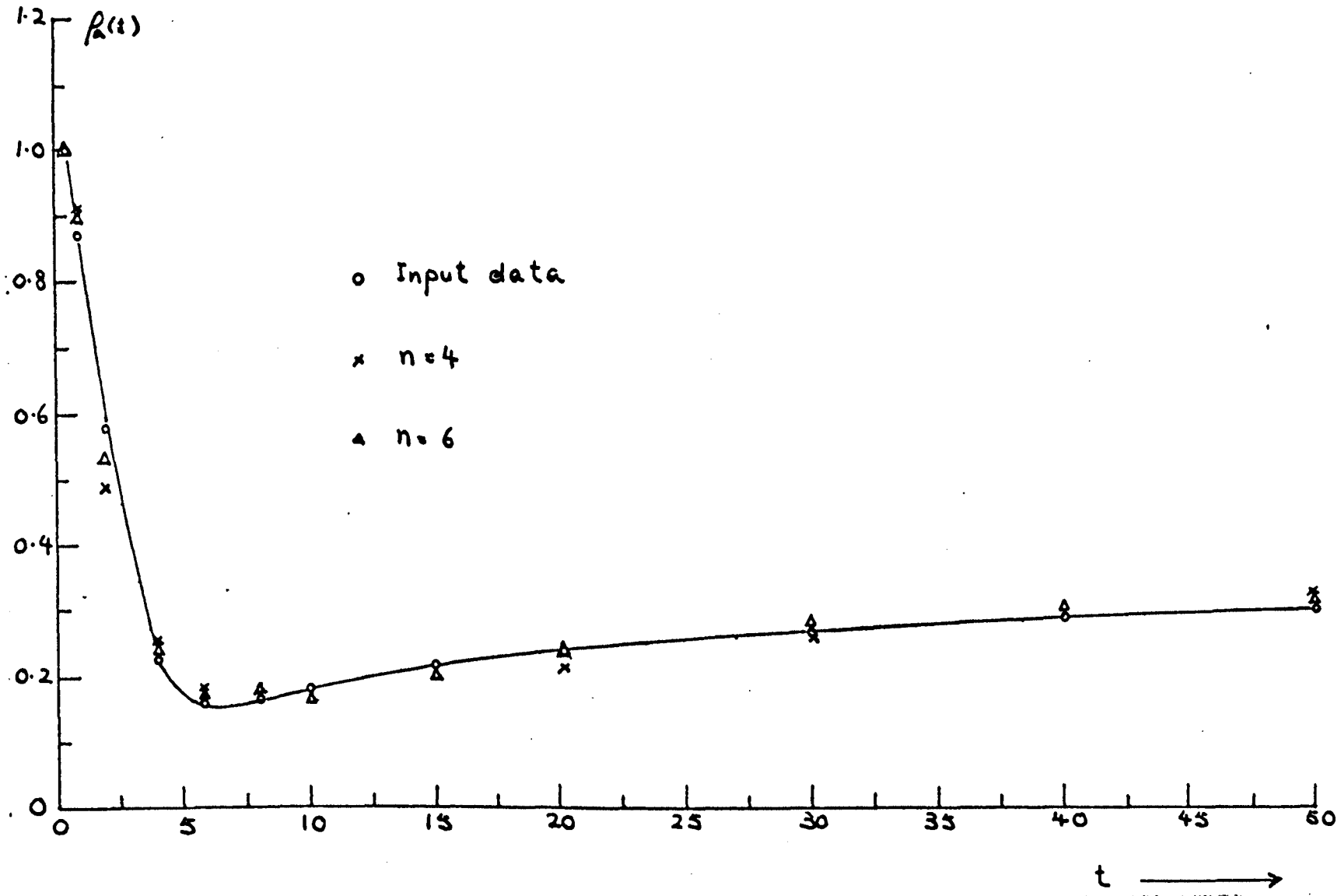

Fig. 3.5. Comparison of input data with least-squares approximations of degree 4 and 6 respectively, using the second approach of fitting. Case $\rho_1 : \rho_2 : \rho_3 = 1 : 1/10 : 1/3$, $d_1 : d_2 = 1 : 3$.

TABLE 3.1 Example of the fitting of the curve $\rho_a(t)$ vs. t by least-squares approximations of different degrees. Case $\rho_1 : \rho_2 : \rho_3 = 1 : 1/10 : 1/3$, $d_1 : d_2 = 1 : 3$

t	Input data	n=4	n=6	n=8	n=10
0.5	1.000	0.762	0.923	1.002	1.031
1.0	0.880	0.718	0.821	0.842	0.845
2.0	0.580	0.634	0.643	0.595	0.563
4.0	0.226	0.489	0.379	0.288	0.260
6.0	0.163	0.370	0.216	0.157	0.160
8.0	0.164	0.275	0.127	0.127	0.152
10.0	0.180	0.201	0.093	0.147	0.175
15.0	0.215	0.096	0.143	0.238	0.225
20.0	0.237	0.076	0.253	0.268	0.234
30.0	0.268	0.177	0.354	0.236	0.267
40.0	0.289	0.323	0.282	0.293	0.291
50.0	0.302	0.404	0.239	0.325	0.301
60.0	0.313	0.380	0.317	0.286	0.314
70.0	0.327	0.286	0.386	0.342	0.327
80.0	0.330	0.229	0.288	0.326	0.330
90.0	0.333	0.388	0.342	0.334	0.333

These relations are illustrated graphically in Figs. 3.3 and 3.4.
n = degree of least-squares approximation

TABLE 3.2 Example of the fitting of the curve log $\rho_a(t)$ vs. log t by least-squares approximations of different degrees. Case $\rho_1 : \rho_2 : \rho_3 = 1 : 1/10 : 1/3$, $d_1 : d_2 = 1 : 3$

t	Input data	n=4	n=6	n=8	n=10
0.5	1.000	1.002	0.993	1.000	1.000
1.0	0.880	0.927	0.918	0.879	0.880
2.0	0.580	0.480	0.528	0.583	0.580
4.0	0.226	0.247	0.238	0.221	0.226
6.0	0.163	0.193	0.177	0.168	0.163
8.0	0.164	0.176	0.165	0.165	0.165
10.0	0.180	0.173	0.168	0.176	0.179
15.0	0.215	0.186	0.199	0.212	0.215
20.0	0.237	0.210	0.236	0.241	0.238
30.0	0.268	0.261	0.286	0.271	0.267
40.0	0.289	0.302	0.304	0.286	0.289
50.0	0.302	0.329	0.305	0.300	0.303
60.0	0.313	0.340	0.304	0.314	0.314
70.0	0.327	0.337	0.308	0.326	0.324
80.0	0.330	0.325	0.322	0.333	0.333
90.0	0.333	0.304	0.351	0.332	0.332

These relations are shown graphically in Fig. 3.5.

n = degree of least-squares approximation

TABLE 3.3 Values of $\rho_a(t)$ generated by least-squares approximation of degree 10. These values are spaced at an interval $\Delta t = 0.5$. Case $\rho_1 : \rho_2 : \rho_3 = 1 : 1/10 : 1/3$, $d_1 : d_2 = 1 : 3$

t	Input data	Gener-ated value	t	Input data	Gener-ated value
0.5	1.000	1.000	10.5		0.184
1.0	0.880	0.880	11.0		0.188
1.5		0.732	11.5		0.191
2.0	0.580	0.580	12.0		0.195
2.5		0.468	12.5		0.199
3.0		0.354	13.0		0.202
3.5		0.276	13.5		0.206
4.0	0.226	0.226	14.0		0.209
4.5		0.196	14,5		0.212
5.0		0.178	15.0	0.215	0.215
5.5		0.168	15.5		0.217
6.0	0.163	0.165	16.0		0.220
6.5		0.161	16.5		0.223
7.0		0.161	17.0		0.225
7.5		0.162	17.5		0.227
8.0	0.164	0.165	18.0		0.230
8.5		0.168	18.5		0.232
9.0		0.172	19.0		0.234
9.5		0.176	19.5		0.236
10.0	0.180	0.180	20.0	0.237	0.238

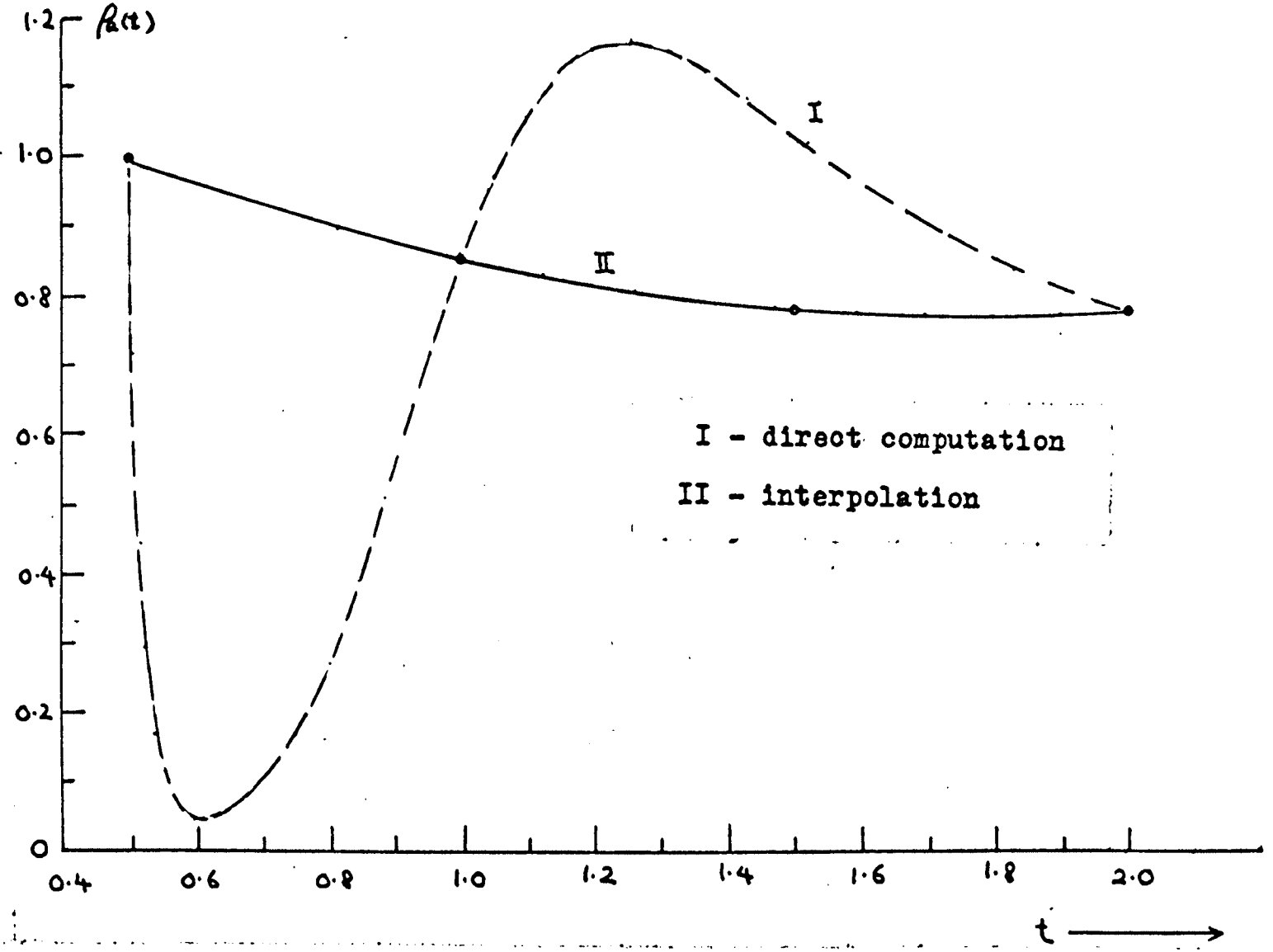

Fig. 3.6. Apparent resistivity obtained by direct computation from least-squares polynomial using an interval $\Delta t = 0.05$ and by interpolation between values generated at an interval $\Delta t = 0.5$.

Numerical Calculation of the Kernel

As it stands (2.19) is not suitable for numerical calculation. Some manipulations are necessary in order to reduce the infinite integral to some suitable form for computation. Equation (2.19) may be rewritten in the following form:

$$K_1(\lambda) = \frac{\lambda \rho_n}{2\rho_1} \int_0^\infty F(\lambda t)dt + \frac{\lambda}{2\rho_1} \int_0^\infty (\rho_a(t) - \rho_n)F(\lambda t) \quad dt \tag{3.10}$$

The explicit form of the first integral on the right hand side of (3.10) is given by

$$\int_0^\infty F(\lambda t)dt = \int_0^\infty \sum_{k=0}^{\infty} \frac{1}{2^{2k}} J_0(\lambda t/2^k) \quad dt$$

$$= \sum_{k=0}^{\infty} \frac{1}{2^{2k}} \int_0^\infty J_0(\lambda t/2^k) \quad dt.$$

By noting the fact that

$$\int_0^\infty J_0(px)\, dx = 1/p$$

the above expression is reduced to

$$\int_0^{\infty} F(\lambda t)\, dt = \frac{1}{\lambda} \sum_{k=0}^{\infty} \frac{1}{2^k} = 2/\lambda \qquad (3.11)$$

The second integral on the right hand side of (3.10) can be reduced to a definite integral with finite upper limit by considering the asymptotic behavior of the apparent resistivity function $\rho_a(t)$ at large t. It can be shown that when the electrode spacing t is large compared to the thickness the apparent resistivity curve will approach asymptotically to the line $\rho_a(t) = \rho_n$, that is, the value of $\rho_a(t)$ approaches the value of the resistivity of the bottom layer (Keller and Frischknecht, 1966). Such asymptotic property of the apparent resistivity function is, however, not observed in either one of the following cases: (1) the bottom layer is a perfect conductor, and (2) the bottom layer has an infinite resistance. Since these two exceptional cases are seldom encountered in practice we shall not include them in our discussions. This asymptotic property of the apparent resistivity function is best illustrated by the curves of the two-layer structures as shown in Fig. 3.7. It may be noted that $\rho_a(t)$ approaches the value of the resistivity of the bottom layer faster in the case $\rho_2 < \rho_1$ than in the case $\rho_2 > \rho_1$.

Suppose that $\rho_a(t) \to \rho_n$ for $t \geq b$. Then we have

$$\int_0^{\infty} (\rho_a(t) - \rho_n)F(\lambda t)\, dt \simeq \int_0^{b} (\rho_a(t) - \rho_n)F(\lambda t)\, dt.$$

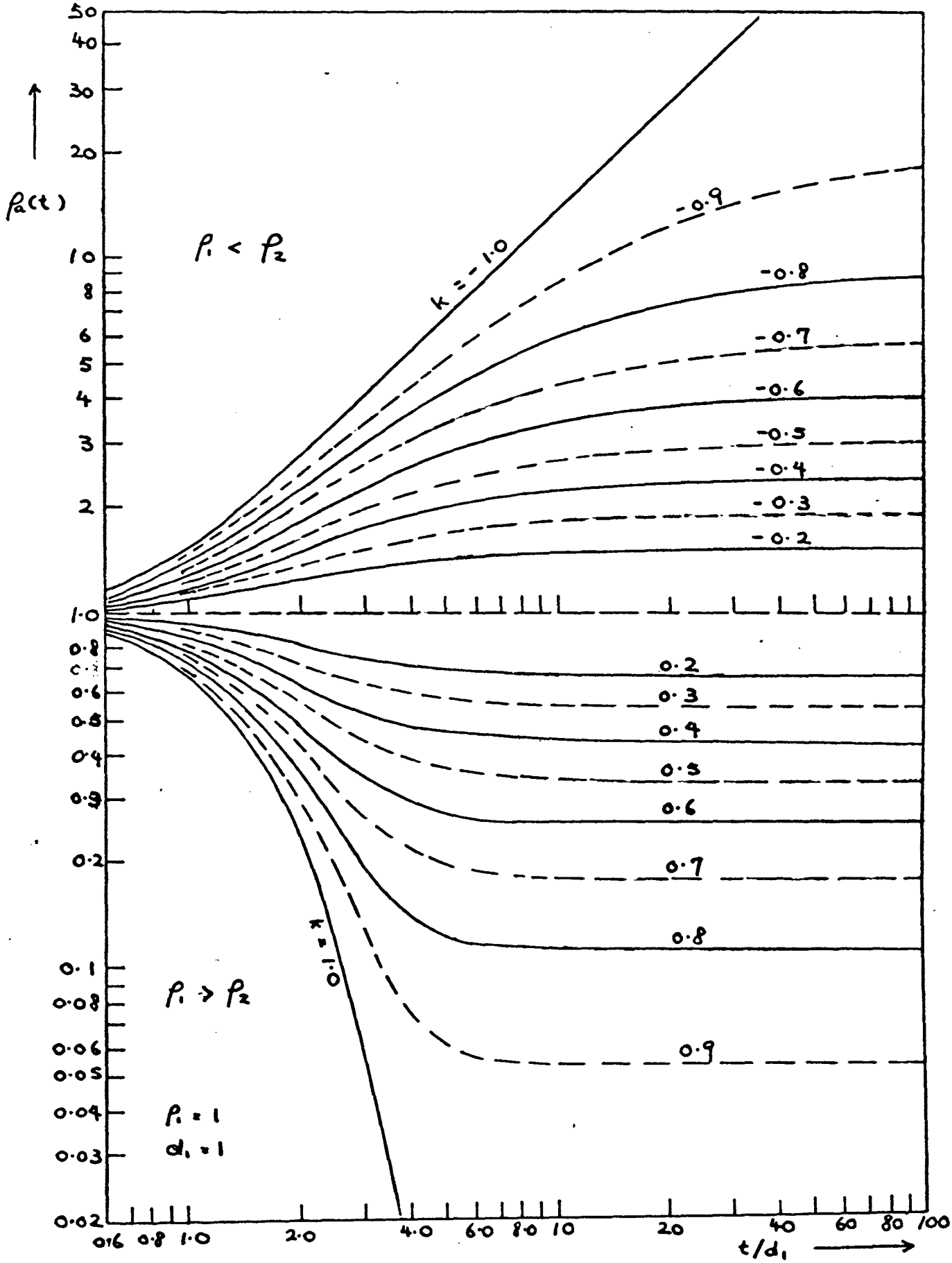

Fig. 3.7. Apparent resistivity curves for two-layer case, logarithmic plotting.

Furthermore we note that when the electrode spacing t is small compared to the thickness of the top layer $\rho_a(t)$ will approach ρ_1, the resistivity of the top layer. As a matter of fact this property of the apparent resistivity function is utilized in practice; the determination of the resistivity of the surface layer of the ground is often achieved by making measurements with very small electrode spacings. So, if we make a further assumption that $\rho_a(t) \to \rho_1$ for $t \leq a$ then the above integral is reduced to

$$\int_0^b (\rho_a(t) - \rho_n)F(\lambda t)dt \simeq (\rho_1 - \rho_n) \int_0^a F(\lambda t)\ dt + \int_0^b (\rho_a(t) - \rho_n)F(\lambda t)\ dt \qquad (3.12)$$

By making use of (3.11) and (3.12), (3.10) may be written in the form

$$K_1(\lambda) = \rho_n/\rho_1 + \lambda/2\ (1 - \rho_n/\rho_1) \int_0^a F(\lambda t)\ dt + \lambda/2\rho_1 \int_a^b (\rho_a(t) - \rho_n)F(\lambda t)\ dt \qquad (3.13)$$

which is the final form of the kernel that is suitable for numerical calculation. For the ease of discussion let

$$K_1'(\lambda) = \int_0^a F(\lambda t)\ dt \tag{3.14}$$

and

$$K_1''(\lambda) = \int_a^b (\rho_a(t) - \rho_n)F(\lambda t)\ dt \tag{3.15}$$

Then (3.13) becomes

$$K_1(\lambda) = \rho_n/\rho_1 + \lambda/2\ (1 - \rho_n/\rho_1)K_1'(\lambda) + \lambda/2\ _1\ K''_1(\lambda) \tag{3.16}$$

Integration of $K_1'(\lambda)$. $K_1'(\lambda)$ can be evaluated quite readily by approximating the integral with a Legendre-Gauss quadrature formula after some suitable change of variable to convert the interval of integration from (0,a) to (-1,1). Thus in (3.14) if we make the change of variable

$$t = a\ (y + 1)\ /2$$

we get

$$K_1'(\lambda) = \tfrac{1}{2}\ a \int_{-1}^{1} F(\tfrac{1}{2}\ a\lambda\{y + 1\})\ dy \tag{3.17}$$

By applying the Legendre-Gauss formula to (3.17) we obtain

$$K_1'(\lambda) = \tfrac{1}{2}\ a \sum_{j=1}^{m} F(\tfrac{1}{2}\ a\lambda\{y_j + 1\})\ W_j \tag{3.18}$$

where the abscissas $\dot{y}_j$ are the zeros of the Legendre polynomials and W_j are the corresponding weights (Ralston, 1965). It may be noted that a very complete and detailed listing of y_j and the associated W_j is given by Stroud and Secrest (1966) in their book on Gaussian quadrature formulas.

It is to be pointed out that the magnitude of the upper limit a of the integral (3.14) is in general quite small. Consequently the use of a single quadrature formula of relatively low order, say about 10, will give reasonably accurate values of $K_1'(\lambda)$. However, should larger values of a be encountered, accurate evaluation of $K_1'(\lambda)$ can be achieved either by using a single quadrature formula of higher order or by using the composite quadrature formula which will be discussed in the following section.

Integration of $K_1''(\lambda)$. The calculation of $K_1''(\lambda)$ is not so straightforward as in the case of $K_1'(\lambda)$. In this case the upper limit of the integral (3.15) is generally quite large, say greater than 50, and consequently the oscillating nature of the integrand due to the presence of the function $F(\lambda t)$ is going to influence the accuracy of our result. Because of the oscillation of the integrand we have to sample the integrand at a finer interval than in the case in which the integrand is not an oscillating function, in order to achieve the same degree of accuracy. The application of a single quadrature formula of very high order is very inconvenient

because a large number of y_j's and W_j's are needed to be stored. The writer found that the following two methods gave satisfactory results.

(i) Method of composite rule (Ralston, 1965) — In this method a composite quadrature formula is obtained as follows: 1. Break up the interval of integration, (a,b), into a number, say N, of subintervals. 2. On each subinterval apply a quadrature and sum the results. The quadrature formula to be used in each subinterval is generally one of low order.

By applying step 1 of the above composite rule to (3.15) we obtain

$$K_1''(\lambda) = \sum_{k=1}^{N} \int_{t_{k-1}}^{t_k} (\rho_a(t) - \rho_n) F(\lambda t) \, dt \tag{3.19}$$

in which $t_0 = a$ and $t_N = b$. Next, if we make a change of variable

$$t = \tfrac{1}{2} \{(t_k - t_{k-1})\, y + t_k + t_{k-1}\}$$

(3.19) is transformed into the following form

$$K_1''(\lambda) = \sum_{k=1}^{N} \tfrac{1}{2} (t_k - t_{k-1}) \int_{-1}^{1} g(y) \, dy \tag{3.20}$$

where

$$g(y) = \{\rho_a(\tfrac{1}{2}[(t_k - t_{k-1})y + t_k + t_{k-1}]) - \rho_n\} \; x$$

$$F(\tfrac{1}{2}\lambda[(t_k - t_{k-1})y + t_k + t_{k-1}]) \qquad (3.21)$$

The integral in (3.20) can now be replaced by a quadrature formula. Thus

$$K_1''(\lambda) = \tfrac{1}{2} \sum_{k=1}^{N} \sum_{j=1}^{M} (t_k - t_{k-1}) g(y_j) \; W_j \qquad (3.22)$$

which is the final form suitable for numerical calculation.

If the subintervals are of equal size, say h, where $h = (b - a)/N$, (3.22) can be reduced to a simpler form

$$K_1''(\lambda) = h/2 \sum_{k=1}^{N} \sum_{j=1}^{M} g(y_j) \; W_j \qquad (3.23)$$

where

$$g(y_j) = \{\rho_a(\tfrac{1}{2}[2a + h\,(y_j + 2k - 1)]) - \rho_n\} \; x$$

$$F(\tfrac{1}{2}\lambda[2a + h\,(y_j + 2k - 1)]) \qquad (3.24)$$

In deriving the above equation we have made use of the fact that $t_k = a + kh$ and $t_{k-1} = a + (k - 1)\,h$.

(ii) Method of approximating part of the integrand by a parabolic arc — One of the techniques used for the evaluation of integral transform involves the approximation of one of the two functions forming the integrand by a parabolic arc

over a small interval (Sneddon, 1955). This technique can be adopted here for the evaluation of (3.15). The procedure may be outlined as follows: The interval (a,b) is divided into N equal intervals, each of size h. Equation can be written as

$$K_1''(\lambda) = \sum_{k=1}^{N} \int_{a+(k-1)h}^{a+kh} G(t)\ F(\lambda t)\ dt \qquad (3.25)$$

where $G(t) = \rho_a(t) - \rho_n$. Suppose that within each subinterval the function G(t) may be fitted with sufficient accuracy by the parabolic arc

$$G(t) = A_k + B_k\, t + C_k\, t^2 \qquad (3.26)$$

where A_k, B_k, and C_k are constants. The constants A_k, B_k, and C_k can be determined by requiring the parabolic arc to pass through three points, namely $t = a + (k-1)h$, $t = a + (k-\frac{1}{2})h$, and $t = a + kh$, respectively within the interval. This requirement leads to a system of three linear equations, namely

$$G(a+[k-1]h) = A_k + B_k\{a + [k-1]h\} + C_k\{a + [k-1]h\}^2$$

$$G(a+[k-\tfrac{1}{2}]h) = A_k + B_k\{a + [k-\tfrac{1}{2}]h\} + C_k\{a + [k-\tfrac{1}{2}]h\}^2$$

$$G(a + kh) = A_k + B_k\{a + kh\} + C_k\{a + kh\}^2$$

Solving this system of equations we get

$$A_k = G(a+[k-1]h)\ \{1 + \frac{3(a + (k-1)h)}{h} + \frac{2(a + (k-1)h)^2}{h^2}\}$$

$$- 4G(a+[k-\tfrac{1}{2}]h)\ \frac{(a + (k-1)k)}{h}\ \{1 + \frac{(a + (k-1)h)}{h}\}$$

$$+ G(a+kh)\ \frac{(a + (k-1)h)}{h}\ \{1 + \frac{2(a + (k-1)h)}{h}\}$$

$$B_k = -G(a+[k-1]h)\ \{3 + \frac{4(a + (k-1)h)}{h}\}\ \frac{1}{h} \qquad (3.27)$$

$$+ 4G(a+[k-\tfrac{1}{2}]h)\ \{1 + \frac{2(a + (k-1)h)}{h}\}\ \frac{1}{h}$$

$$- G(a+kh)\ \{1 + \frac{2(a + (k-1)h}{h}\}\ \frac{1}{h}$$

$$C_k = \frac{2}{h^2}\ \{G(A+[k-1]h) - 2G(a+[k-\tfrac{1}{2}]h) + G(a+kh)\}$$

By substituting (3.26 into (3.25) we get

$$K_1''(\lambda) = \sum_{k=1}^{N} \{A_k \int_{a+(k-1)h}^{a+kh} F(\lambda t)dt +$$

$$B_k \int_{a+(k-1)h}^{a+kh} t\ F(\lambda t)dt + \qquad (3.28)$$

$$C_k \int_{a+(k-1)h}^{a+kh} t^2\ F(\lambda t)dt\}$$

The second and third integrals on the right hand side of (3.28) may be integrated directly. However, there is no advantage of performing the direct integration because this will lead to divergent infinite series. So instead the integration can be carried out numerically. Each of the above integral can be approximated by a Legendre-Gauss quadrature formula. Thus

$$K_1''(\lambda) = h/2 \sum_{k=1}^{N} \sum_{j=1}^{M} \{A_k g_1(y_j) + B_k g_2(y_j) + C_k g_3(y_j)\} \qquad (3.29)$$

where

$$g_1(y_j) = F(\tfrac{1}{2}\lambda[2a + h(y_j + 2k - 1)]),$$

$$g_2(y_j) = \tfrac{1}{2}\{2a + h(y_j + 2k - 1)\}\, g_1(y_j), \qquad (3.30)$$

$$g_3(y_j) = \tfrac{1}{4}\{2a + h(y_j + 2k - 1)\}^2\, g_1(y_j) .$$

Some details of computation. In the process of computing the kernel the first thing which one may have to consider is the apparent resistivity function. It has already been pointed out that the apparent resistivity function is known only at a certain number of electrode spacings by direct field observations and that the values of this function not determined by field measurement but required for the numerical

integration of the kernel have to be interpolated from the observed data. The question of how to generate the unknown values of the apparent resistivity function has been discussed in great details at the beginning of this chapter.

The next thing of importance is the behavior of the integrands associated with the integrals of $K_1'(\lambda)$ and $K_1''(\lambda)$ respectively. In the case of $K_1'(\lambda)$ the integrand is simply the function $F(\lambda t)$. It has been shown that the function $F(\lambda t)$ is an oscillating function and behaves almost like the Bessel function $J_0(\lambda t)$. The spacing between any two consecutive zeros of $F(\lambda t)$ along the t-axis is obviously governed by the parameter λ; it decreases as λ increases. This would imply that in the process of evaluating $K_1'(\lambda)$ one may have to use a larger number of ordinates in the quadrature formula when the values of λ are large than in the case when smaller values of λ are used, in order to obtain an accurate sampling of the function $F(\lambda t)$. It is quite fortunate that in the case of $K_1'(\lambda)$ the interval of integration (0,a) is not large because a is generally quite small, say less than 5, and that the range of λ in which the kernel is of interest for the determination of the layer resistivities and thicknesses, is also not large and lies approximately in the interval (0,5). In all the computations which had been carried out it was found that the results of integrating $K_1'(\lambda)$ with the use of a single quadrature formula stabilized when the order of the quadrature formula was greater than 8 with $0 < \lambda < 5$ and $0.5 \leq a \leq 2.0$.

The integrand of the integral of $K_1''(\lambda)$ is the function $G(t)F(\lambda t)$ which behaves almost like $F(\lambda t)$ excepting that the amplitude is now being modulated by the function $G(t)$. Since the zeros of $G(t)F(\lambda t)$ are dependent on both the component functions, they are different from those of $F(\lambda t)$. Under the condition that $\rho_a(t) > \rho_n$ or $\rho_a(t) < \rho_n$, that is, $|\rho_a(t) - \rho_n| \neq 0$, throughout the entire range of integration the zeros of $G(t)F(\lambda t)$ will be identical with those of $F(\lambda t)$. Fig. 3.8 illustrates a typical example of the function $G(t)F(\lambda t)$. It may also be noted that the integrand should approach to zero at the upper limit b because $\rho_a(t) \to \rho_n$.

In the calculation of $K_1''(\lambda)$ by either the method of composite rule or the method of approximation by a parabolic arc, the number N of subintervals into which the range of intergration is going to be divided is dependent on the parameter λ. Generally speaking the larger the value of λ the finer the subdivision will have to be. In our calculations a sequence of 40, 60, 80, 100, 150, 200, 250, 300 subintervals was used with the upper limit b lying between 50 and 100, and the integral associated with each subinterval was approximated by a quadrature formula of order 2. It may be noted that when an integral is approximated by a composite quadrature formula the round-off error may become a significant factor that affects the accuracy of the final results. Since the expected round-off error will be minimized when the coefficients are most nearly equal (Ralston, p. 119) the

composite rule using a quadrature formula of order 2 has ideal round-off properties. It may be pointed out that both the weights in the Legendre-Gauss quadrature formula of order 2 are equal to unity.

Table 3.4 illustrates an example of the values of $K_1''(\lambda)$ computed by the use of the method of composite rule. It is a remarkable fact that these results agree with those computed by the alternative method up to at least the fifth place of decimal. From Table 3.4 we can see that the values of $K_1''(\lambda)$ associated with the smaller values of λ tend to stabilize more rapidly than those associated with the larger values of λ. For instance, for $0.01 \leq \lambda \leq 0.20$ the third decimal place of each value of $K_1''(\lambda)$ remains unchanged in two successive approximations when the number of subintervals is greater than 60, whereas for larger values of λ the results will not stabilize until larger number of subintervals are used. For all the values of λ shown on the table the corresponding values of $K_1''(\lambda)$ stabilize up to their fourth decimal place when N is greater than 250.

Figs. 3.9, 3.10, 3.11 and 3.12 are some typical examples of the values of the kernel computed from the apparent resistivity data, compared with those values of the kernel calculated from the analytical expressions of the kernel. The numerical values corresponding to each of the curves shown in these figures are given in Tables 3.5 and 3.6. From these examples we can see that the results of numerical

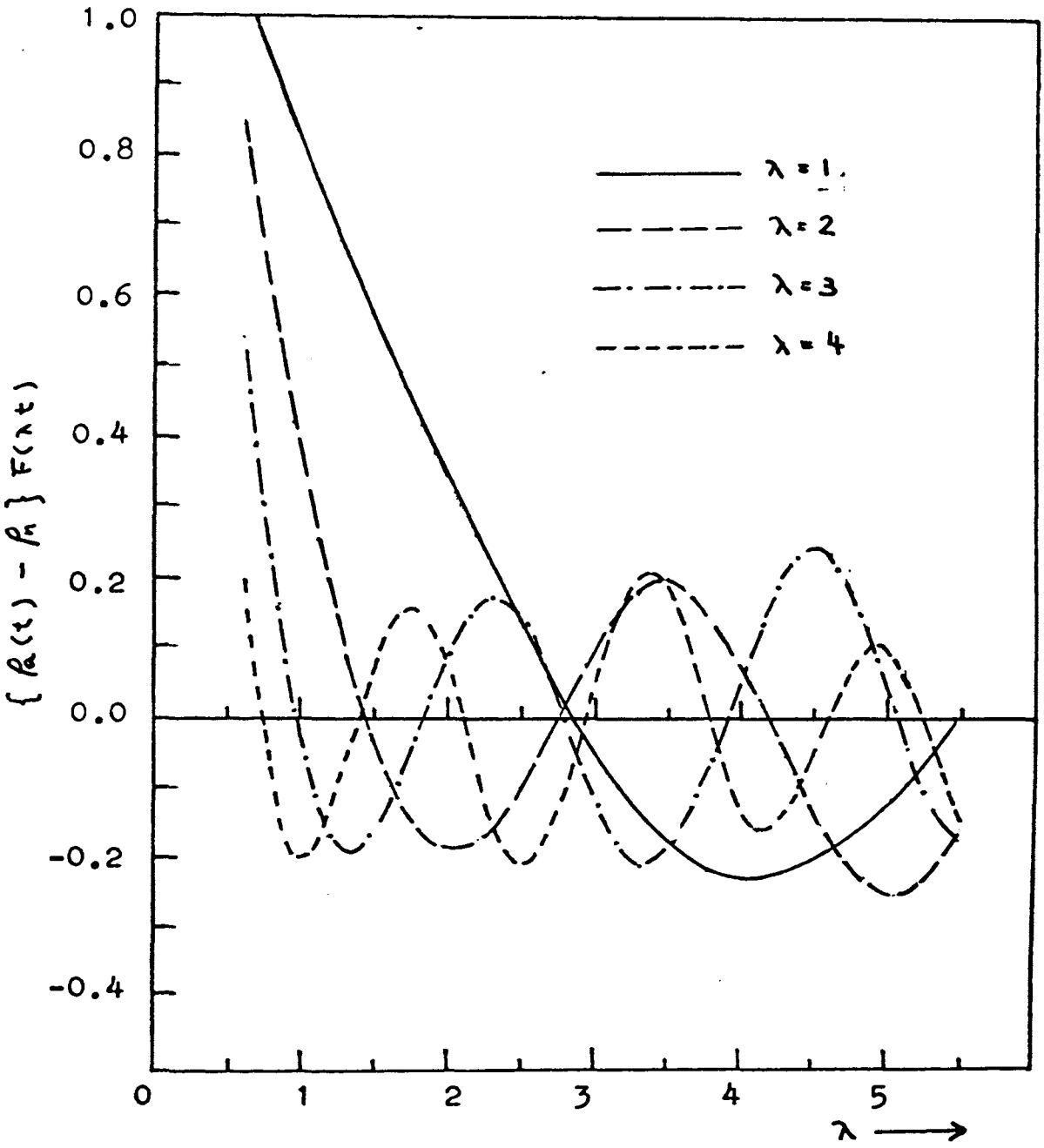

Fig. 3.8. Examples of the curves of the function $\{\rho_a(t) - \rho_n\} F(\lambda t)$ for different values of λ.

TABLE 3.4 An example of the numerical values of $K_1''(\lambda)$ obtained by the method of composite rule. n is the number of subintervals used. Case $\rho_1 : \rho_2 : \rho_3 : \rho_4 = 1 : 1/3 : 3 : 1/10$, $d_1 : d_2 : d_3 = 1 : 4 : 1$

λ	n=40	n=60	n=80	n=100
0.01	0.45128	0.45171	0.45185	0.45170
0.02	0.88866	0.88951	0.88979	0.88950
0.04	0.16758	0.16775	0.16780	0.16775
0.06	0.23032	0.23058	0.23066	0.23058
0.08	0.27692	0.27726	0.27737	0.27725
0.10	0.31068	0.31110	0.31124	0.31110
0.20	0.38070	0.38153	0.38180	0.38152
0.40	0.42365	0.42516	0.42564	0.42514
0.60	0.46288	0.46418	0.46475	0.46414
0.80	0.48441	0.48631	0.48684	0.48623
1.00	0.49112	0.49253	0.49288	0.49237
1.20	0.48273	0.48307	0.48314	0.48278
1.40	0.46098	0.45952	0.45928	0.45908
1.60	0.42903	0.42490	0.42437	0.42428
1.80	0.39092	0.38319	0.38245	0.38238
2.00	0.35009	0.33787	0.33698	0.33686

TABLE 3.4 (cont.)

λ	n=150	n=200	n=250	n=300
0.01	0.45175	0.45174	0.45174	0.45173
0.02	0.88960	0.88957	0.88957	0.88956
0.04	0.16777	0.16776	0.16776	0.16776
0.06	0.23061	0.23058	0.23060	0.23059
0.08	0.27729	0.27728	0.27728	0.27728
0.10	0.31115	0.31113	0.31113	0.31113
0.20	0.38161	0.38159	0.38159	0.38157
0.40	0.42531	0.42526	0.42526	0.42524
0.60	0.46436	0.46430	0.46431	0.46427
0.80	0.48645	0.48641	0.48641	0.48637
1.00	0.49246	0.49254	0.49254	0.49250
1.20	0.48291	0.48290	0.48290	0.48287
1.40	0.45911	0.45912	0.45912	0.45911
1.60	0.42422	0.42423	0.42423	0.42424
1.80	0.38224	0.38224	0.38224	0.38226
2.00	0.33665	0.33663	0.33663	0.33665

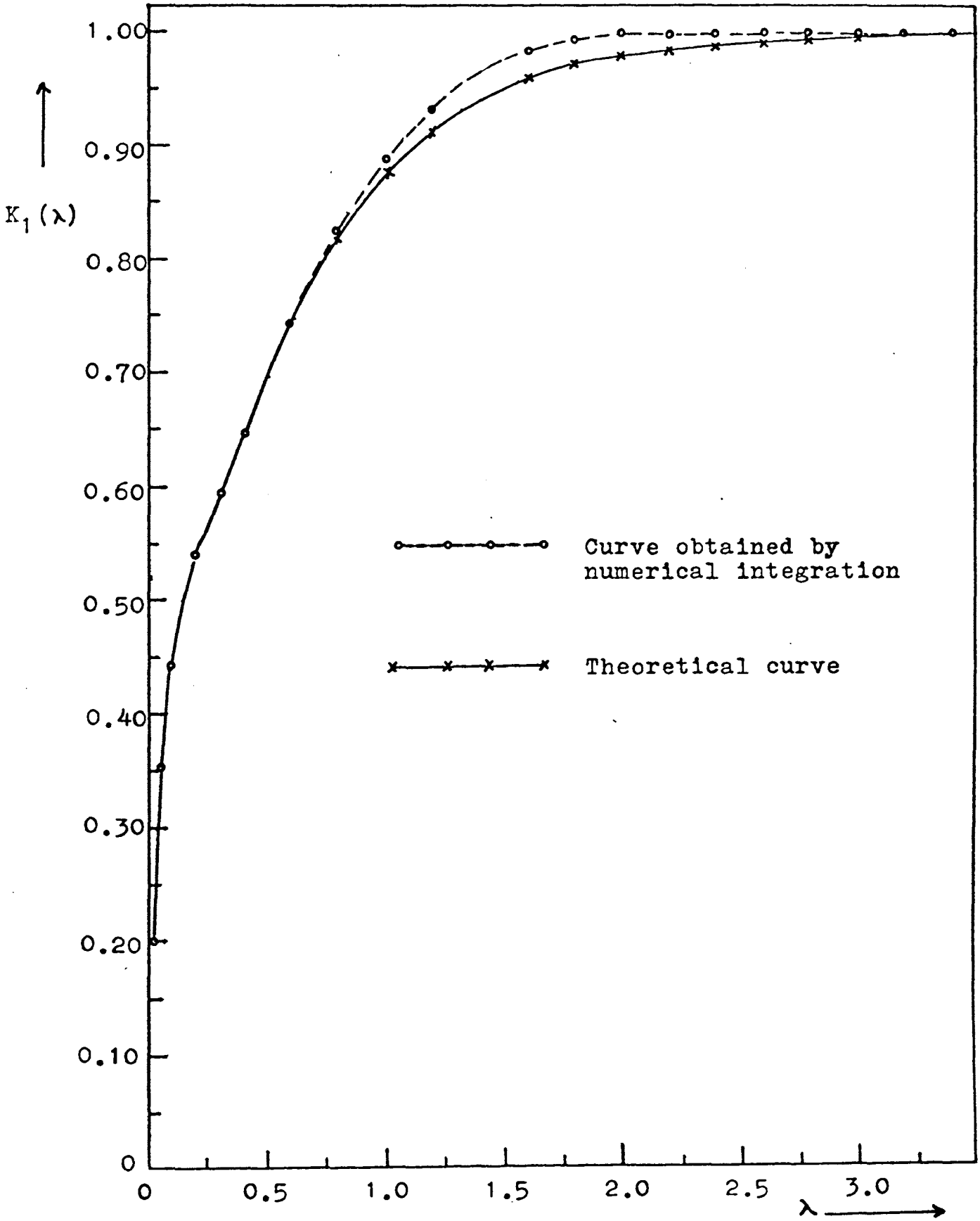

Fig. 3.9. Kernel obtained by numerical integration and from theoretical formula. Case $\rho_1 : \rho_2 : \rho_3 : \rho_4 = 1 : 1/3 : 3 : 1/10$, $d_1 : d_2 : d_3 = 1 : 4 : 1$.

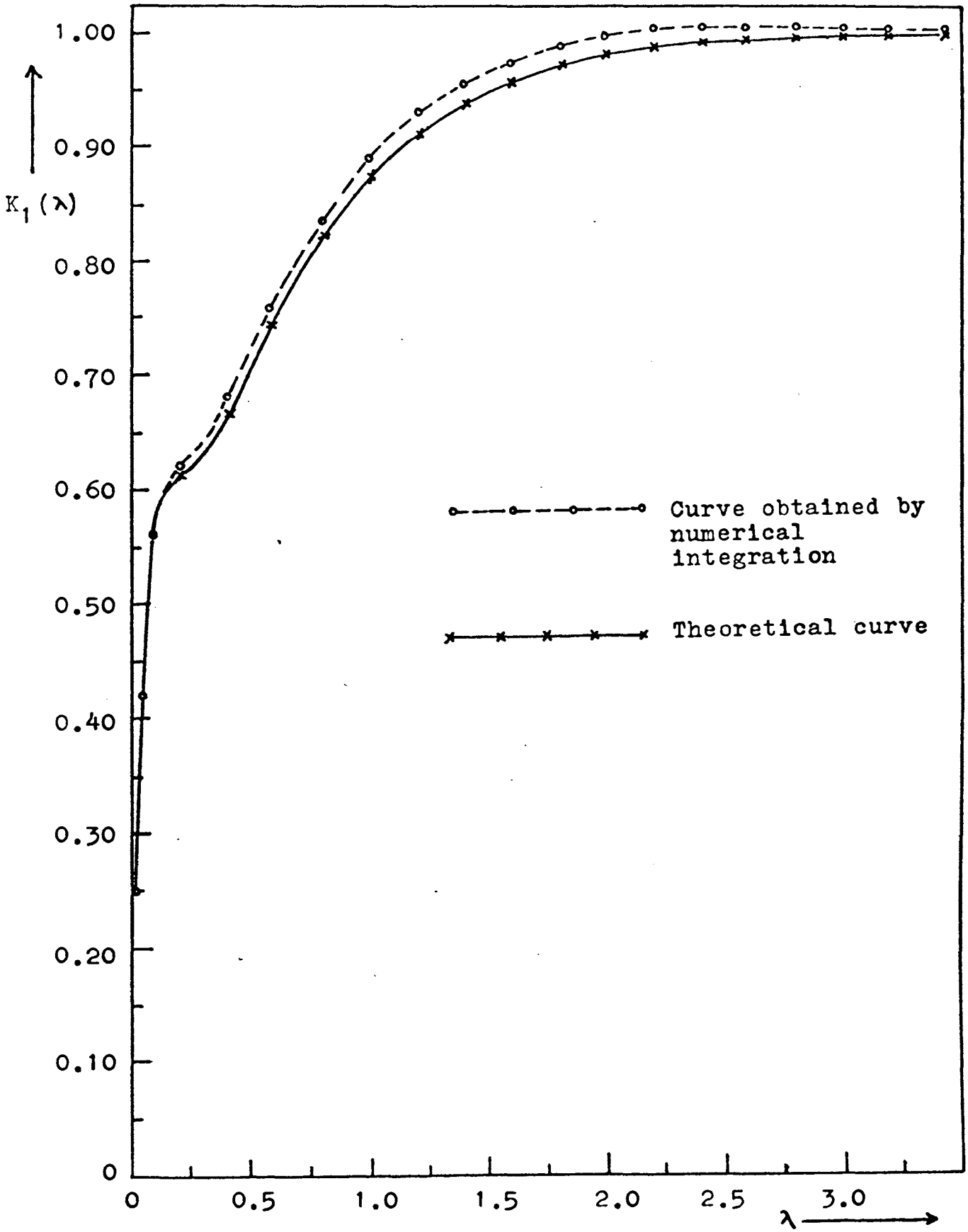

Fig. 3.10. Kernel obtained by numerical integration and from theoretical formula. Case $\rho_1 : \rho_2 : \rho_3 : \rho_4 = 1 : 1/3 : 3 : 1/10$, $d_1 : d_2 : d_3 = 1 : 3 : 2$

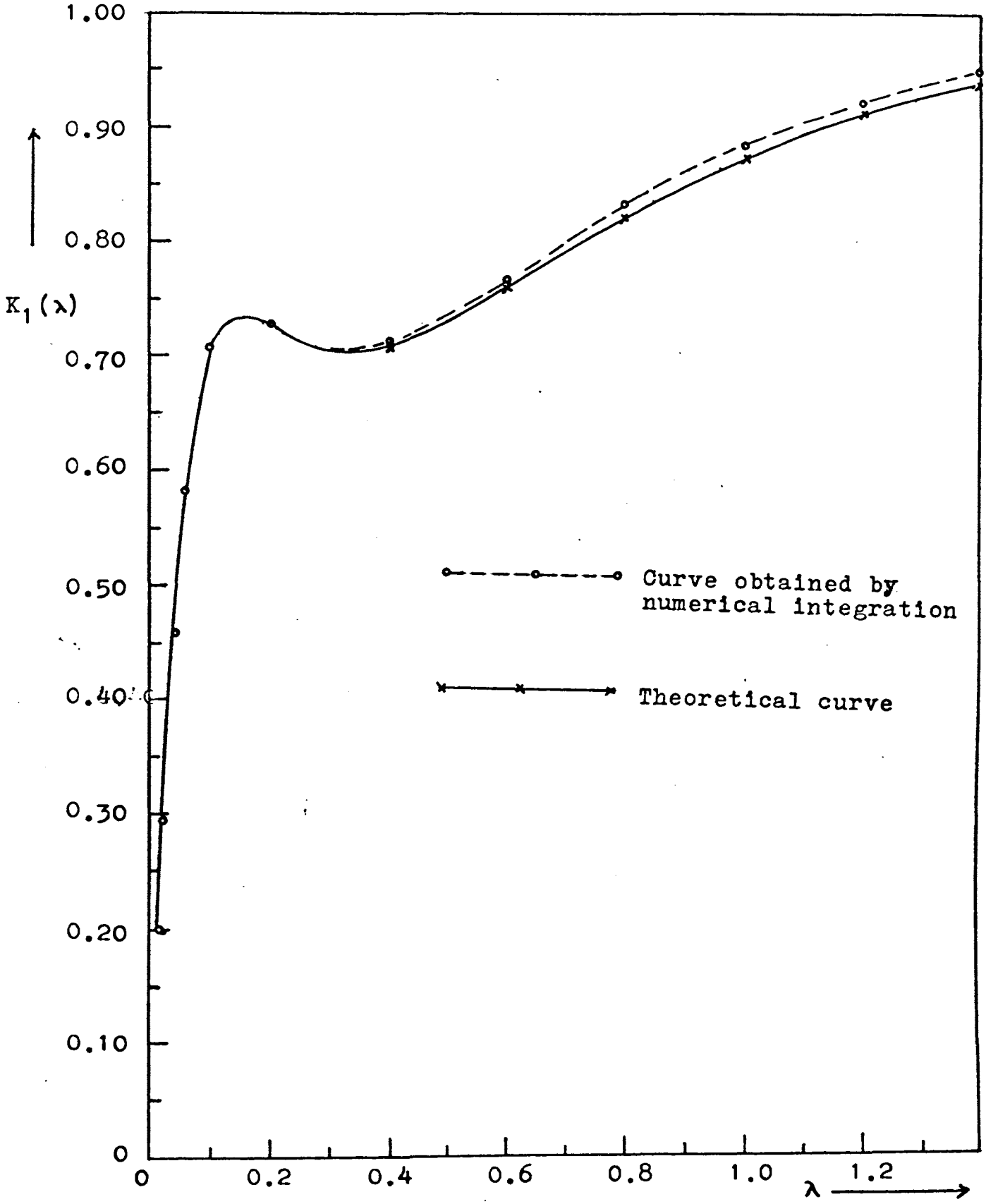

Fig. 3.11. Kernel obtained by numerical integration and from theoretical formula. Case $\rho_1 : \rho_2 : \rho_3 : \rho_4 = 1 : 1/3 : 3 : 1/10$, $d_1 : d_2 : d_3 = 1 : 2 : 3$.

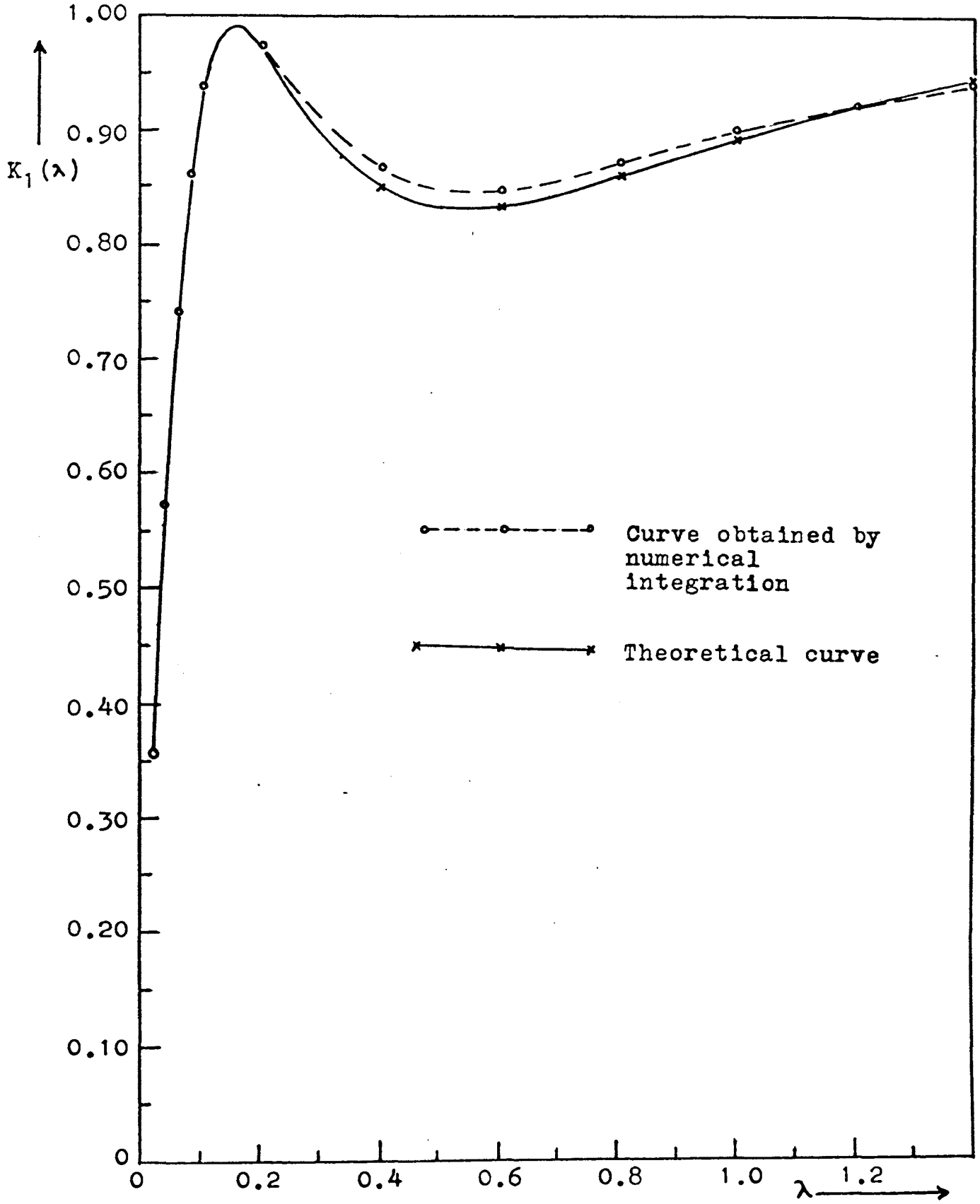

Fig. 3.12. Kernel obtained by numerical integration and from theoretical formula. Case $\rho_1 : \rho_2 : \rho_3 : \rho_4 =$ 1 : 1/3 : 3 : 1/10, $d_1 : d_2 : d_3 = 1 : 1 : 4$.

TABLE 3.5 Numerical values of the kernel obtained by integration of apparent resistivity data and from theoretical formula. Case $\rho_1 : \rho_2 : \rho_3 : \rho_4 = 1 : 1/3 : 3 : 1/10$.

λ	$d_1:d_2:d_3 = 1 : 4 : 1$		$d_1:d_2:d_3 = 1 : 3 : 2$	
	I	II	I	II
0.01	0.151	0.148	0.177	0.175
0.02	0.199	0.195	0.249	0.247
0.04	0.284	0.280	0.372	0.372
0.06	0.352	0.349	0.463	0.465
0.08	0.405	0.401	0.524	0.526
0.10	0.444	0.441	0.562	0.563
0.20	0.540	0.542	0.612	0.621
0.40	0.644	0.645	0.664	0.680
0.60	0.740	0.743	0.745	0.764
0.80	0.817	0.824	0.818	0.836
1.00	0.873	0.888	0.874	0.889
1.20	0.913	0.934	0.913	0.928
1.40	0.941	0.966	0.941	0.955
1.60	0.960	0.984	0.960	0.975
1.80	0.973	0.994	0.973	0.989
2.00	0.982	0.998	0.982	0.998
2.20	0.988	0.999	0.987	1.003
2.40	0.992	1.000	0.992	1.006
2.60	0.995	1.001	0.995	1.007
2.80	0.996	1.002	0.996	1.007

I = theoretical values II = integrated values

TABLE 3.6 Numerical values of the kernel obtained by integration of apparent resistivity data and from theoretical formula. Case $\rho_1 : \rho_2 : \rho_3 : \rho_4 =$ 1 : 1/3 : 3 : 1/10

λ	$d_1:d_2:d_3 = 1:2:3$		$d_1:d_2:d_3 = 1:1:4$	
	I	II	I	II
0.01	0.204	0.196	0.231	0.229
0.02	0.301	0.289	0.356	0.353
0.04	0.467	0.454	0.576	0.574
0.06	0.587	0.577	0.745	0.744
0.08	0.665	0.659	0.862	0.862
0.10	0.709	0.707	0.934	0.937
0.20	0.728	0.732	0.969	0.974
0.40	0.712	0.721	0.851	0.867
0.60	0.764	0.769	0.836	0.846
0.80	0.825	0.834	0.861	0.872
1.00	0.876	0.887	0.984	0.899
1.20	0.914	0.925	0.923	0.919
1.40	0.941	0.952	0.945	0.937
1.60	0.960	0.972	0.962	0.953
1.80	0.973	0.987	0.974	0.970
2.00	0.982	0.997	0.982	0.985
2.20	0.988	1.003	0.988	0.997
2.40	0.992	1.007	0.992	1.005
2.60	0.995	1.008	0.995	1.010
2.80	0.996	1.007	0.996	1.011

I = theoretical values II = integrated values

integration compare favorably with the theoretical values of the kernel. The range of differences between the integrated values and the theoretical values varies from less than one percent to a maximum of about two and a half percent of the theoretical values. It may be noted that the input data, namely values of the apparent resistivity function, which were obtained from the tables of potential data given by Mooney and Wetzel (1956), are accurate only up to the third place of decimal. So we expect that the accuracy of the integrated values of the kernel cannot be greater than that of the input data.

All the calculations mentioned above were carried out by the IBM-360 system at the UMR computer center. Details of the computational procedures are outlined in Appendix E.

Numerical Calculation of the Associated Kernel

Following an approach similar to that used for the reduction of the integral of the kernel, the integral of the associated kernel can be reduced to the form

$$B_1(\lambda) = \tfrac{1}{2}\,\rho_n/\rho_1 + \tfrac{1}{2}\lambda(1 - \rho_n/\rho_1)\,B_1'(\lambda) + \lambda/2\rho_1\,B_1''(\lambda) \tag{3.31}$$

where

$$B_1'(\lambda) = \int_0^a J_0(\lambda t)\ dt \tag{3.32}$$

and

$$B_1''(\lambda) = \int_a^b (\rho_a(t) - \rho_n)\, J_0(\lambda t)\, dt \qquad (3.33)$$

In the following we shall derive the formulas for the evaluation of $B_1'(\lambda)$ and $B_1''(\lambda)$ respectively.

Integration of $B_1'(\lambda)$. The calculation of $B_1'(\lambda)$ is quite straightforward and can be achieved by the use of a single Legendre-Gauss quadrature formula. By making the change of variable,

$$t = a(y + 1)/2,$$

and then approximating the resulting integral with the Legendre-Gauss formula (3.32) is transformed into

$$B_1'(\lambda) = a/2 \sum_{j=1}^{M} J_0(\tfrac{1}{2} a\lambda[y_j + 1])\, W_j \qquad (3.34)$$

where y_j and W_j again denote the abscissas and weights of the quadrature formula.

Integration of $B_1''(\lambda)$. As in the case of $K_1''(\lambda)$, $B_1''(\lambda)$ can be calculated either by (i) the method of composite rule or (ii) the method of approximating $G(t) = \rho_a(t) - \rho_n$ by a parabolic arc. In this case the oscillating behavior of the integrand is due to the Bessel function $J_0(\lambda t)$.

In method (i) the interval of integration is subdivided into N small intervals, each of size h = (b - a)/N. After making the appropriate change of variable and approximating the integral in each subinterval with a quadrature formula the result is

$$B_1''(\lambda) = h/2 \sum_{k=1}^{N} \sum_{j=1}^{M} f(y_j) \quad W_j \tag{3.35}$$

where

$$f(y_j) = \{\rho_a(\tfrac{1}{2}[2a + h\,(y_j + 2k - 1)]) \leftarrow \rho_n\}$$

$$J_0(\tfrac{1}{2}\lambda[2a + h\,(y_j + 2k - 1)]) \tag{3.36}$$

In method (ii) we make the same assumption as in the case of $K_1''(\lambda)$ that G(t) can be approximated by the parabolic arc (3.26). By substituting (3.26) into (3.33) we obtain the following expression:

$$\begin{aligned} B_1''(\lambda) = \sum_{k=1}^{N} & A_k \int_{a+(k-1)h}^{a+kh} J_0(\lambda t)\ dt \\ & + B_k \int_{a+(k-1)}^{a+kh} t\, J_0(\lambda t)\ dt \\ & + C_k \int_{a+(k-1)}^{a+kh} t^2\, J_0(\lambda t)\ dt \end{aligned} \tag{3.37}$$

where the constants A_k, B_k, and C_k are given by (3.27). The second and third integrals of the above expression may be integrated directly by noting that

$$\int x\, J_0(x)\, dx = x\, J_1(x)$$

and

$$\int x^2\, J_0(x)\, dx = x^2 J_1(x) + x\, J_0(x) - \int J_0(x)\, dx.$$

(Bowman, 1958). By carrying out the integrations with the aid of these two formulas (3.37) is reduced to

$$\begin{aligned} B_1''(\lambda) = \sum_{k=1}^{N} \{ & (A_k - C_k/\lambda) \int_{a+(k-1)h}^{a+kh} J_0(\lambda t)\, dt \\ & + (a+kh)(B_k + C_k(a+kh))\, J_1(\lambda[a+kh])/\lambda \\ & - (a+(k-1)h)(B_k + C_k[a+(k-1)])\, J_1(\lambda[a+(k-1)])/\lambda \\ & + C_k/\lambda^2\, (a+kh)\, J_0(\lambda[a+kh]) \\ & - (a+(k-1)h)\, J_0(\lambda[a+(k-1)h])\}. \end{aligned} \tag{3.38}$$

The integral which appears in the first term of (3.38) can, of course, be evaluated by means of a quadrature formula.

Some details of computation. From the equations derived above one can see that the process for calculating the associated kernel does not differ much from that for calculating the kernel, with the exception that the function $F(\lambda t)$ is now replaced by the Bessel function $J_0(\lambda t)$. So most of the remarks made earlier concerning the calculation of $K_1(\lambda)$ can equally be applied here. Consequently the following discussions will be quite brief.

In the calculation of $B_1'(\lambda)$ it was found that a single quadrature formula of order between 10 and 20 was adequate for all calculations in which $0 < \lambda < 10$ and $0.5 \leq a \leq 2.0$.

Fig. 3.13 illustrates an example of the integrand $G(t)J_0(\lambda t)$ associated with the integral of $B_1''(\lambda)$. Like in the case of $G(t)F(\lambda t)$ the zeros of $G(t)J_0(\lambda t)$ are more closely spaced when the values of λ are large than when the values of λ are small. Hence the number N of subintervals into which the interval (a,b) of integration is going to be divided is dependent on the value of λ. Table 3.7 shows a set of values of $B_1''(\lambda)$ computed for a sequence of 40, 60, 80, 100, 150, 200, 250, 300 subintervals by the method of approximation by a parabolic arc. One can see from this table that the values of $B_1''(\lambda)$ stabilize to the fourth place of decimal when N is equal or greater than 250; these values associated with small values of λ tend to stabilize more quickly. Values computed by the method of composite rule agree very closely with these values shown here.

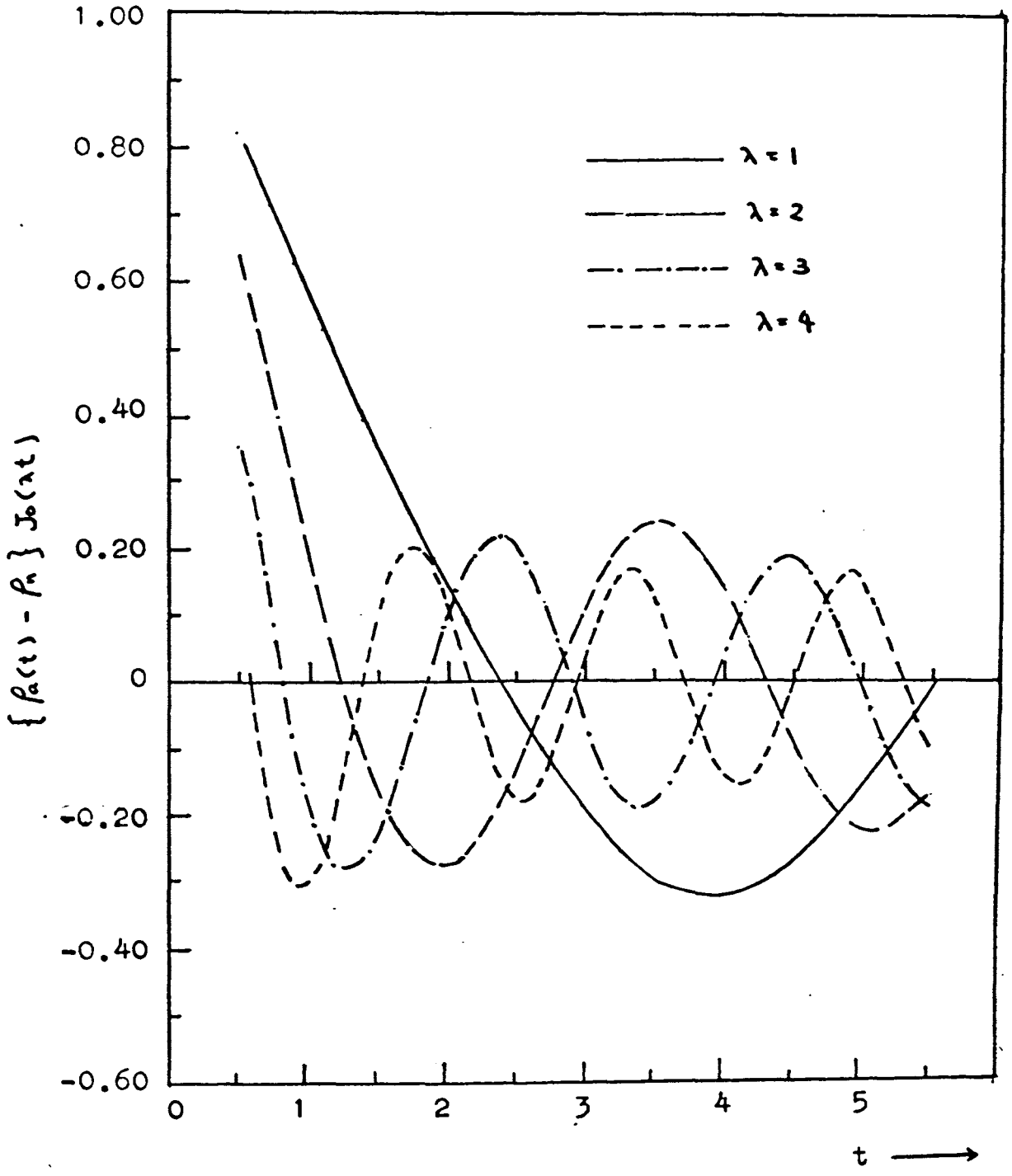

Fig. 3.13. Examples of the curves of the function $\{\rho_a(t) - \rho_n\} J_0(\lambda t)$ for different values of λ.

TABLE 3.7 An example of the numerical values of $B_1''(\lambda)$ obtained by the method of partial approximation of the integrand by a parabolic arc. n is the number of subintervals used.
Case $\rho_1 : \rho_2 : \rho_3 : \rho_4 = 1 : 1/3 : 3 : 1/10$, $d_1 : d_2 : d_3 = 1 : 1 : 4$.

λ	n=40	n=60	n=80	n=100
0.01	0.09369	0.09375	0.09371	0.09372
0.02	0.18333	0.18344	0.18337	0.18339
0.04	0.33704	0.33726	0.33711	0.33716
0.06	0.44420	0.44453	0.44431	0.44437
0.08	0.50434	0.50478	0.50449	0.50457
0.10	0.52742	0.52797	0.52761	0.52771
0.20	0.40291	0.40395	0.40327	0.42345
0.40	0.22735	0.22910	0.22803	0.22823
0.60	0.19450	0.19644	0.19544	0.19542
0.80	0.20058	0.20211	0.20170	0.20122
1.00	0.21317	0.21357	0.21412	0.21306
1.20	0.21045	0.20895	0.21057	0.20895
1.40	0.18872	0.18493	0.18746	0.18549
1.60	0.15312	0.14760	0.15060	0.14867
1.80	0.11050	0.10487	0.10756	0.10622
2.00	0.06638	0.06304	0.06444	0.06426

TABLE 3.7 (cont.)

λ	n=150	n=200	n=250	n=300
0.01	0.09372	0.09373	0.09373	0.09373
0.02	0.18340	0.18340	0.18340	0.18340
0.04	0.33717	0.33718	0.33718	0.33717
0.06	0.44440	0.44441	0.44441	0.44440
0.08	0.50460	0.50462	0.50462	0.50461
0.10	0.52775	0.52777	0.52777	0.52776
0.20	0.40353	0.40358	0.40357	0.40355
0.40	0.22839	0.22848	0.22844	0.22841
0.60	0.19567	0.19576	0.19571	0.19568
0.80	0.20157	0.20161	0.20157	0.20154
1.00	0.21350	0.21347	0.21344	0.21342
1.20	0.20944	0.20932	0.20933	0.20931
1.40	0.18596	0.18576	0.18580	0.18578
1.60	0.14902	0.14877	0.14883	0.14881
1.80	0.10635	0.10609	0.10617	0.10616
2.00	0.06405	0.06383	0.06391	0.06392

Typical examples of the curves of the associated kernel obtained from the integration of the apparent resistivity data are shown in Figs. 3.14, 3.15, 3.16, and 3.17. On these figures are shown also the corresponding theoretical curves of the associated kernel. The numerical values for these curves are given in Talbs 3.8 and 3.9. These examples show that there is a general close agreement between the theoretical and the integrated values of the associated kernel. Again, it may be noted that the input resistivity data were obtained from the tables of potential data given by Mooney and Wetzel.

The computational procedures are outlined in Appendix E.

Some Possible Sources of Error

Apart from the errors that are inherent in the integration formulas there are several other factors which may influence the results of integration of both the kernel and the associated kernel. Since the apparent resistivity function is only known empirically the accuracy of the input values of the apparent resistivity function is obviously one of the influencing factors. Because of the fact that a unique correspondence exists between the apparent resistivity function and the kernel (or the associated kernel) one may expect that the result of the numerical integration will be sensitive to any variations in the input apparent resistivity data. The closeness of fit between the least-squares

polynomial and apparent resistivity data would be another influencing factor. Generally speaking the greater the number of data points the better the least-squares approximation will be. In all our calculations sixteen data points were used and the results were satisfactory.

In the derivation of the integration formulas we made the assumption that the resistivity of the top and bottom layers could be determined if measurements were made with very short or very long electrode separation. In practice some uncertainty may exist in the determination of the values of a and b, and also that of ρ_1 and ρ_n. Thus this is another factor that may influence the result of integration. Under normal field conditions a can be determined with a high degree of precision while b can only be determined approximately. This is indeed quite fortunate in the sense that error in the measurement of a will have a greater influence on the result of integration than that in the measurement of b because the terms in the quadrature formulas near the upper limit of the integral generally have negligible contribution to the total sum owing to the fact that both the functions $G(t)$ and $J_0(\lambda t)$ (or $F(\lambda t)$) are very small in magnitude near the upper limit of the integral. With regard to the resistivity of the top and bottom layers, information on them is often available from other external sources. If this information is available it will be of great help in our computation.

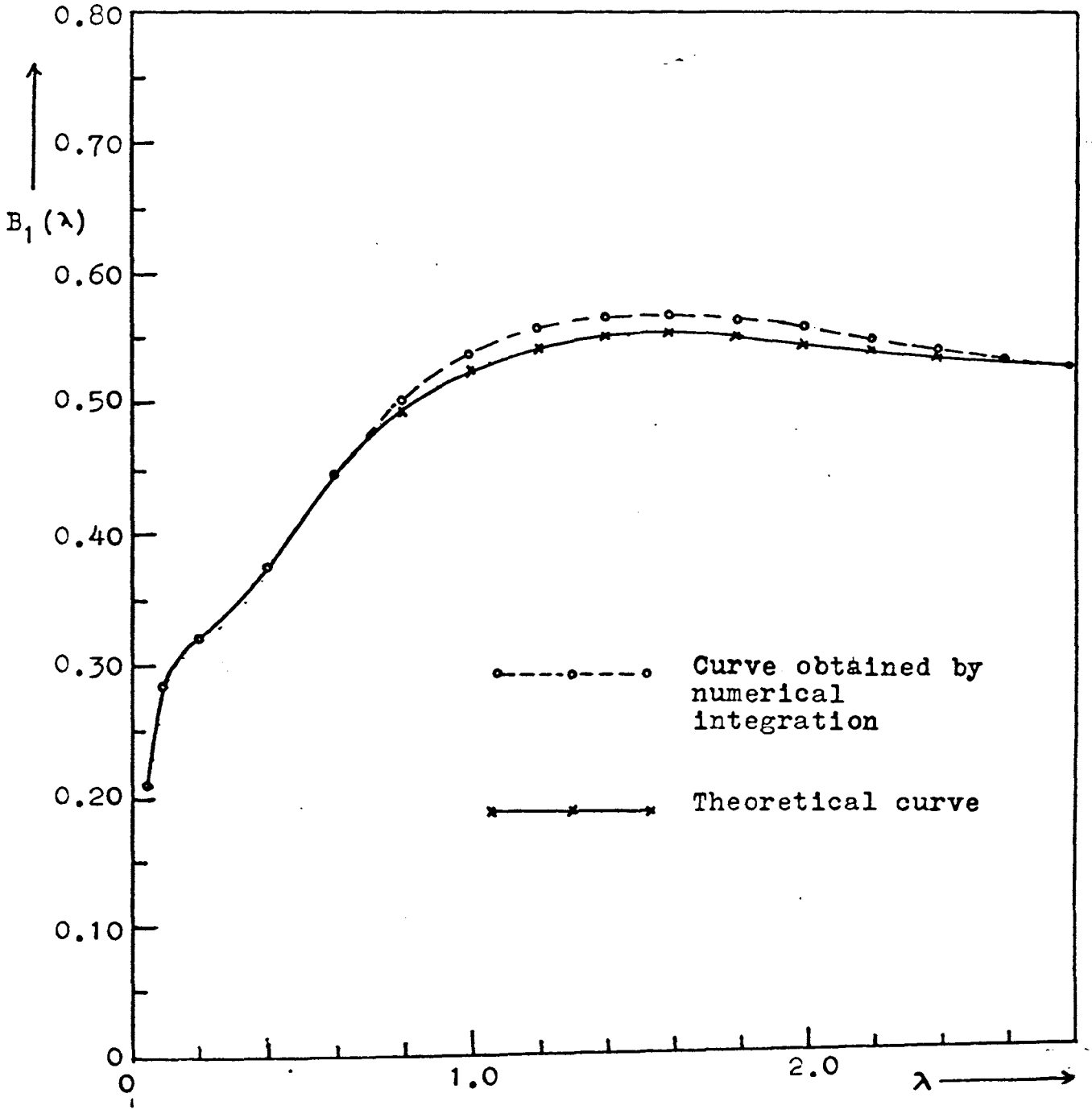

Fig. 3.14. Associated kernel obtained by numerical integration and from theoretical formula. Case $p_1 : p_2 : p_3 : p_4 = 1 : 1/3 : 3 : 1/10, d_1 : d_2 : d_3 = 1 : 4 : 1$.

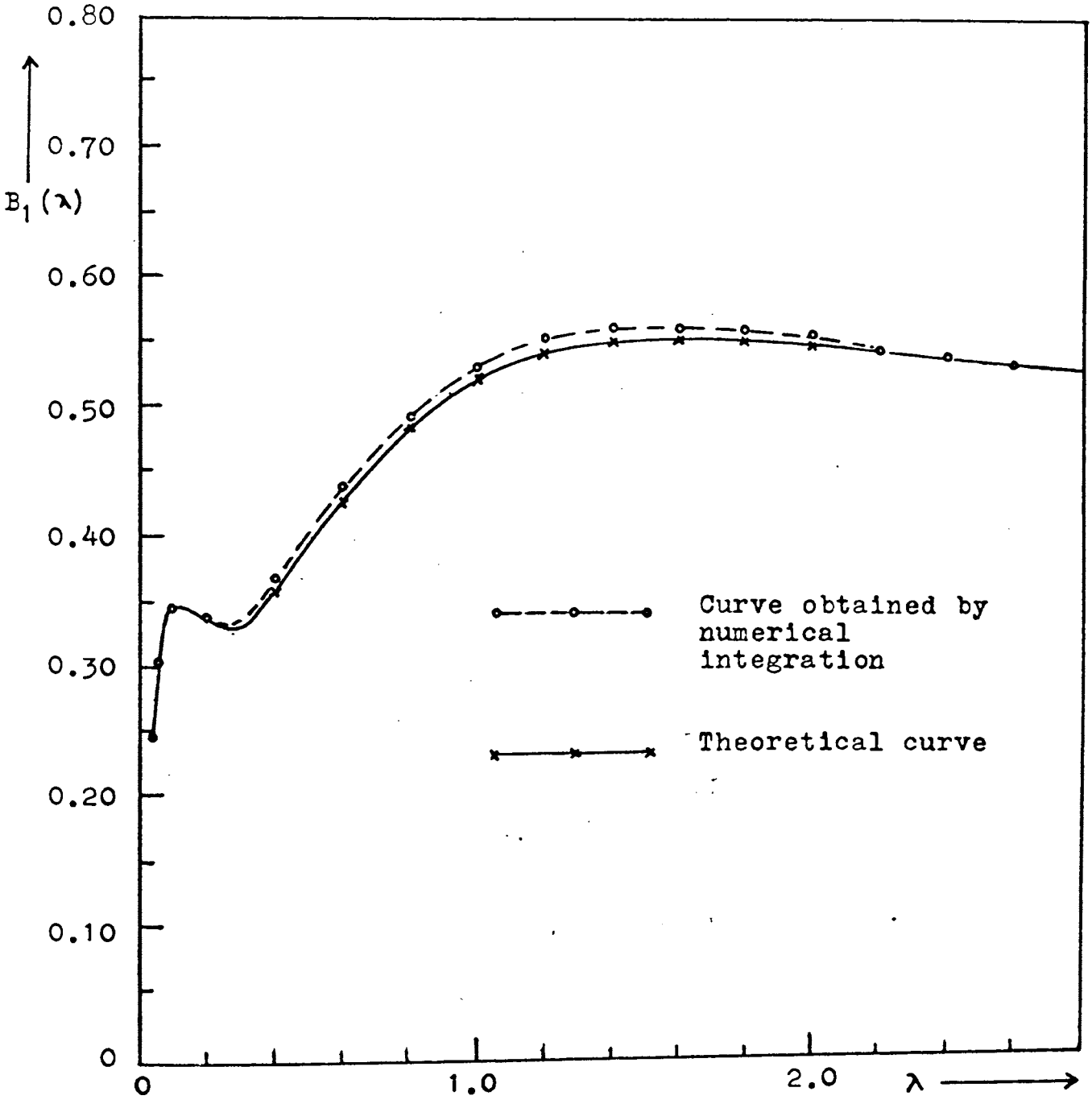

Fig. 3.15. Associated kernel obtained by numerical integration and from theoretical formula. Case $p_1 : p_2 : p_3 : p_4 = 1 : 1/3 : 3 : 1/10$, $d_1 : d_2 : d_3 = 1 : 3 : 2$.

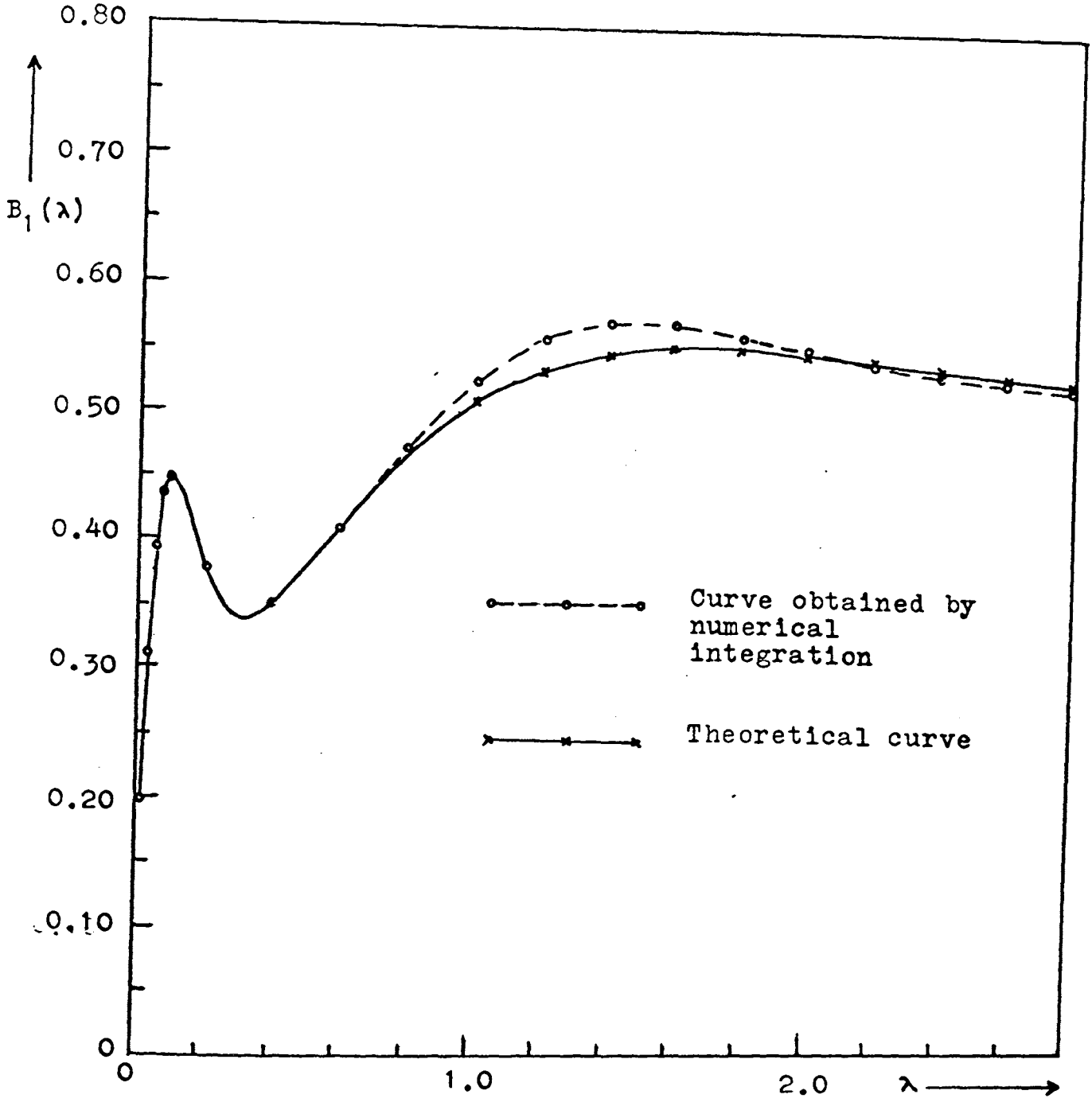

Fig. 3.16. Associated kernel obtained by numerical integration and from theoretical formula. Case $p_1 : p_2 : p_3 : p_4 = 1 : 1/3 : 3 : 1/10$, $d_1 : d_2 : d_3 = 1 : 2 : 3$.

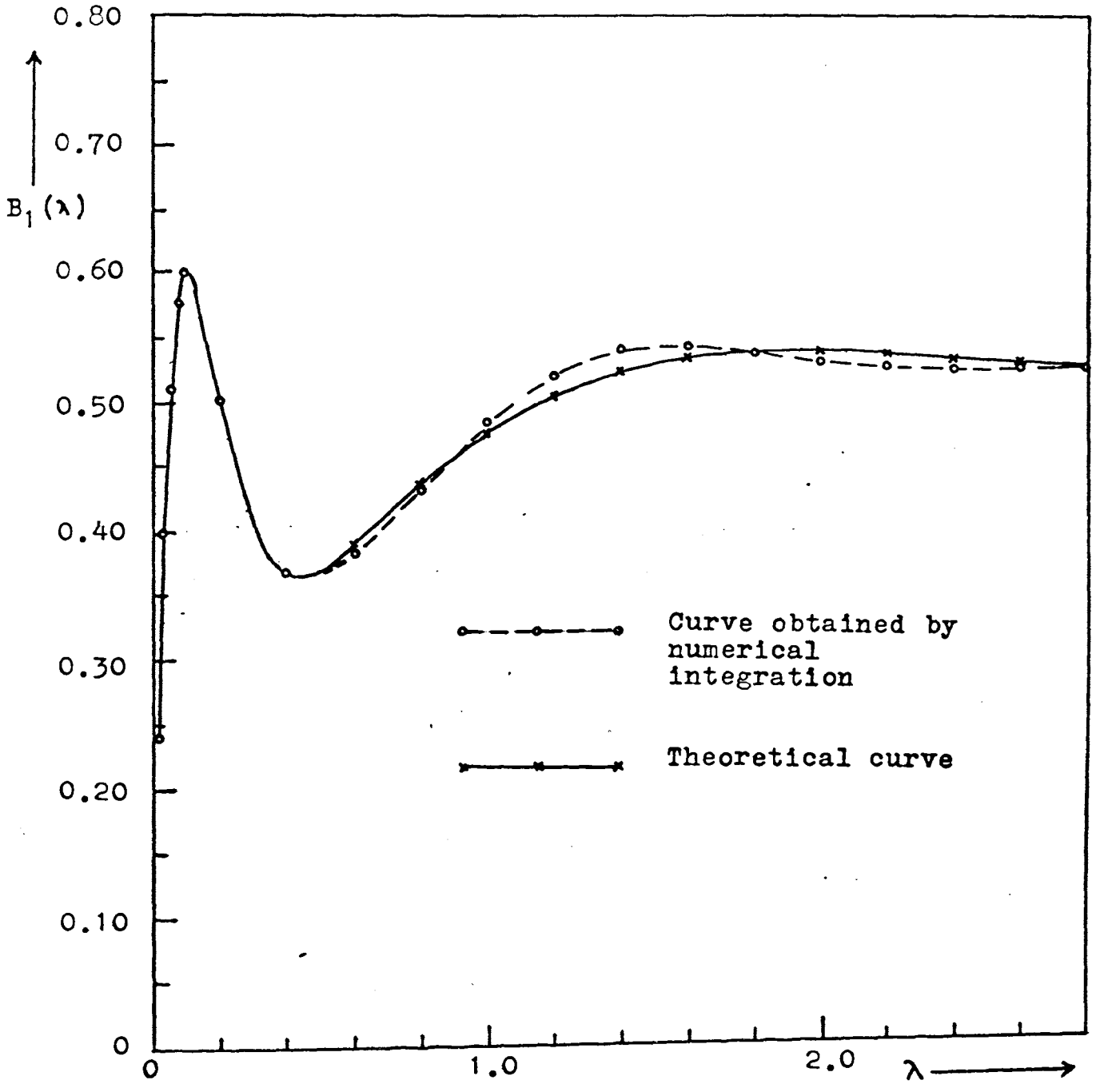

Fig. 3.17. Associated kernel obtained by numerical integration and from theoretical formula. Case $p_1 : p_2 : p_3 : p_4 = 1 : 1/3 : 3 : 1/10$, $d_1 : d_2 : d_3 = 1 : 1 : 4$.

TABLE 3.8 Numerical values of the associated kernel obtained by integration of apparent resistivity data and from theoretical formula. Case $\rho_1 : \rho_2 : \rho_3 : \rho_4 = 1 : 1/3 : 3 : 1/10$

λ	$d_1:d_2:d_3 = 1:4:1$		$d_1:d_2:d_3 = 1:3:2$	
	I	II	I	II
0.01	0.088	0.086	0.108	0.106
0.02	0.123	0.121	0.161	0.159
0.04	0.184	0.183	0.248	0.248
0.06	0.231	0.230	0.306	0.308
0.08	0.263	0.262	0.338	0.339
0.10	0.284	0.284	0.351	0.351
0.20	0.318	0.323	0.331	0.337
0.40	0.374	0.377	0.358	0.368
0.60	0.444	0.449	0.430	0.439
0.80	0.495	0.503	0.486	0.493
1.00	0.526	0.538	0.521	0.530
1.20	0.543	0.557	0.541	0.551
1.40	0.550	0.566	0.549	0.561
1.60	0.552	0.567	0.551	0.562
1.80	0.549	0.563	0.549	0.558
2.00	0.545	0.556	0.545	0.552
2.20	0.540	0.547	0.540	0.544
2.40	0.535	0.539	0.535	0.537
2.60	0.530	0.531	0.530	0.530
2.80	0.526	0.524	0.526	0.525

I = theoretical values II = integrated values

TABLE 3.9 Numerical values of the associated kernel obtained by integration of apparent resistivity data and from theoretical formula. Case $\rho_1 : \rho_2 : \rho_3 : \rho_4$ = 1 : 1/3 : 3 : 1/10

λ	$d_1:d_2:d_3 = 1:2:3$		$d_1:d_2:d_3 = 1:1:4$	
	I	II	I	II
0.01	0.128	0.122	0.148	0.146
0.02	0.199	0.191	0.241	0.238
0.04	0.317	0.308	0.397	0.396
0.06	0.393	0.388	0.509	0.508
0.08	0.431	0.431	0.574	0.574
0.10	0.442	0.445	0.601	0.600
0.20	0.373	0.374	0.502	0.499
0.40	0.348	0.348	0.367	0.368
0.60	0.411	0.405	0.389	0.380
0.80	0.469	0.469	0.436	0.436
1.00	0.509	0.522	0.476	0.483
1.20	0.532	0.554	0.504	0.521
1.40	0.544	0.568	0.522	0.538
1.60	0.548	0.568	0.531	0.540
1.80	0.548	0.560	0.535	0.535
2.00	0.544	0.549	0.535	0.528
2.20	0.540	0.539	0.534	0.523
2.40	0.535	0.531	0.531	0.522
2.60	0.530	0.525	0.527	0.523
2.80	0.526	0.522	0.524	0.527

I = theoretical values II = integrated values

CHAPTER IV

ANALYSIS OF THE KERNEL AND THE ASSOCIATED KERNEL

In Chapter III we have shown that under certain conditions the kernel and the associated kernel may be computed from the apparent resistivity data. Since both the kernel and the associated kernel are dependent on the layer resistivities and thicknesses, a knowledge of the values of these functions may provide us valuable information concerning the subsurface physical and geological conditions. Having determined the values of the kernel and the associated kernel the next problem confronting us will be the determination of the layer parameters from the known values of both of these functions. In the following the answer to this problem will be discussed.

Analysis of the Kernel: Numerical-Graphical Method

The analytical expression of the kernel as derived in Appendix B may be rewritten as

$$K_1(\lambda) = (1 - U_1 e^{-2\lambda d_1})/(1 + U_1 e^{-2\lambda d_1}) \qquad (4.1)$$

where

$$U_1 = (\rho_1 - \rho_2 K_2)/(\rho_1 + \rho_2 K_2)$$

$$K_2 = (1 - U_2 e^{-2\lambda d_2})/(1 + U_2 e^{-2\lambda d_2})$$

$$U_2 = (\rho_2 - \rho_3 K_3)/(\rho_2 + \rho_3 K_3)$$

.....

.....

$$K_i = (1 - U_i e^{-2\lambda d_i})/(1 + U_i e^{-2\lambda d_i})$$

$$U_i = (\rho_i - \rho_{i+1} K_{i+1})/(\rho_i + \rho_{i+1} K_{i+1})$$

.....

.....

$$K_{n-1} = (1 - U_{n-1} e^{-2\lambda d_{n-1}})/(1 + U_{n-1} e^{-2\lambda d_{n-1}})$$

$$U_{n-1} = k_{n-1,n} = (\rho_{n-1} - \rho_n)/(\rho_{n-1} + \rho_n).$$

To analyze this function we begin with the simplest case, namely the two-layer case, and then proceed to the three-layer case, after which the analysis will be generalized to the n-layer problem. The general procedure of the analysis presented here is quite similar to that of Pekeris (1940) in the sense that our method is also a numerical-graphical method which depends on the behavior of the kernel at large λ. However, the details of our analysis are totally different from those of Pekeris's method and also the kernel defined here is not identical with that employed by Pekeris in his analysis.

Two-layer case. In (4.1) if we put n = 2, we obtain the kernel for the two-layer case:

$$K_1(\lambda) = (1 - k_{12}e^{-2\lambda d_1})/(1 + k_{12}e^{-2\lambda d_1}) \qquad (4.2)$$

where $K_{12} = (\rho_1 - \rho_2)/(\rho_1 + \rho_2)$. To analyze the kernel let us define a function T_1 by the equation

$$T_1 = (1 + K_1(\lambda))/(1 - K_1(\lambda)). \qquad (4.3)$$

By rearranging (4.2) one can easily show that

$$T_1 = e^{2\lambda d_1}/k_{12} \qquad (4.4)$$

from which

$$\log|T_1| = 2\lambda d_1 \log e + \log|(1/k_{12})| \qquad (4.5)$$

where $|T_1|$ and $|(1/k_{12})|$ denote the absolute values of T_1 and $1/k_{12}$ respectively. From (4.5) it is immediately obvious that if $\log |T_1|$ is plotted against λ the resulting graph will be a straight line which has a slope of $2d_1 \log e$ and an intercept on the ordinate equal to $\log|(1/k_{12})|$. Thus (4.5) provides us with a very convenient graphical method for determining the layer parameters d_1 and k_{12}. Let s_1 and c_1 denote the slope and the intercept respectively. Then we have

$$d_1 = s_1 / 2 \log e \qquad (4.6)$$

and

$$|k_{12}| = 10^{-c} \qquad (4.7)$$

It may be noted that the reflection factor k_{12} may take on any value lying in the interval (-1,1). The result given by (4.7) does not indicate whether k_{12} is positive or negative. But it will be shown later that the sign of the reflection factor is related to the sign of the function T_1. Assuming that the sign of the reflection factor is known then ρ_2 can be calculated from

$$\rho_2 = \rho_1 (1 - k_{12})/(1 + k_{12}) \tag{4.8}$$

since ρ_1 is already known from direct field observations.

Three-layer case. By putting n = 3 one gets the three-layer kernel:

$$K_1(\lambda) = (1 - U_1 e^{-2\lambda d_1})/(1 + U_1 e^{-2\lambda d_1}) \tag{4.9a}$$

where

$$U_1 = (\rho_1 - \rho_2 K_2)/(\rho_1 + \rho_2 K_2) \tag{4.9b}$$

$$K_2 = (1 - k_{23} e^{-2\lambda d_2})/(1 + k_{23} e^{-2\lambda d_2}) \tag{4.9c}$$

$$k_{23} = (\rho_2 - \rho_3)/(\rho_2 + \rho_3) \ . \tag{4.9d}$$

The procedure for analyzing this three-layer kernel may be outlined as follows:

(i) Determination of d_1 and k_{12} — Again using (4.3) as the

definition of T_1 one can show from (4.9a) that

$$T_1 = e^{2\lambda d_1}/U_1 \tag{4.10}$$

from which one gets

$$\log |T_1| = 2\lambda d_1 \log e + \log |(1/U_1)| \tag{4.11}$$

We note that in this case $\log |T_1|$ is no longer a linear function of λ because the function U_1 is also dependent on λ, but it will approach a linear function when λ becomes large. At large values of λ, since the function $e^{-2\lambda d_2}$ whose magnitude decreases rather rapidly with the increase of λ becomes negligible we may make the following approximations: $k_{23}e^{-2\lambda d_2} \to 0 \Rightarrow K_2 \to 1 \Rightarrow U_1 \to k_{12}$. It follows that when becomes large the function $\log |T_1|$ should approach asymptotically to the straight line

$$Y_1 = \lambda s_1 + c_1$$

where $s_1 = 2d_1 \log e$ and $c_1 = \log |(1/k_{12})|$. Hence d_1 and k_{12} can be determined from the slope and the intercept of the asymptotic straight line respectively.

(ii) Determination of d_2 and k_{23} — Since d_1 is known from the result of step (i) U_1 can be computed from (4.10), that is,

$$U_1 = e^{2\lambda d_1}/T_1 \tag{4.12}$$

From (4.9b) we obtain

$$K_2 = \rho_1 (1 - U_1)/\rho_2(1 + U_1) \tag{4.13}$$

from which K_2 can be calculated. The rearrangement of (4.9c) leads to the equation

$$(1+K_2)/(1-K_2) = e^{2\lambda d_2/k_{23}} = T_2 \tag{4.14}$$

It follows that

$$\log |T_2| = 2\lambda d_2 \log e + \log |(1/k_{23})|. \tag{4.15}$$

Equation (4.15) represents a straight line with slope $s_2 = 2d_2 \log e$ and intercept $c_2 = \log|(1/k_{23})|$. Thus the layer parameters of the three-layer problem are completely determined.

Generalization to n-layer case. The kernel for the n-layer case is given by (4.1). To determine the layer parameters from this kernel we merely extend the procedure employed for the decomposition of the three-layer kernel as follows: (i) Determination of d_1 and k_{12} — In this case d_1 and k_{12} can be determined in exactly the same manner as in the three-layer problem. Using similar arguments as before we can show that the function

$$\log T_1 = 2\lambda d_1 \log e + \log |(1/U_1)| \tag{4.16}$$

should approach asymtotically to the straight line

$$Y_1 = \lambda s_1 + c_1$$

where $s_1 = 2d_1 \log e$ and $c_1 = \log (1/k_{12})$. Thus d_1 and k_{12} are determined.

(ii) Determination of d_2 and k_{23} — By letting T_2 to denote $(1 + K_2)/(1 - K_2)$ one can show that

$$\log |T_2| = 2\lambda d_2 \log e + \log |(1/U_2)| \qquad (4.17)$$

Since U_2 approaches k_{23} at large λ (4.17) will approach the straight line

$$Y_2 = \lambda s_2 + c_2$$

where $s_2 = 2d_2 \log e$ and $c_2 = \log |(1/k_{23})|$. From s_2 and c_2 d_2 and k_{23} can be determined.

(iii) Determination of $k_{i,i+1}$ and d_i — By repeating the process described in step (ii) the layer parameters for each successive deeper layer can be obtained. Assuming that the parameters of the first i-1 layers have been determined we wish to solve for $k_{i,i+1}$ and d_i now. To do this we make use of the following equations:

$$U_{i-1} = e^{2\lambda d_{i-1}/T_{i-1}} \qquad (4.18)$$

$$K_i = \rho_{i-1} (1 - U_{i-1})/\rho_i (1 + U_{i-1}) \qquad (4.19)$$

$$\log |T_i| = 2\lambda d_i \log e + \log |(1/U_i)| \qquad (4.20)$$

where $T_i = (1 + K_i)/(1 - K_i)$. Since U_i approaches $K_{i,i+1}$ at large λ the function $\log|T_i|$ will approach its asymptote

$$Y_i = \lambda s_i + c_i \qquad (4.21)$$

where $s_i = 2d_i \log e$ and $c_i = \log (1/k_{i,i+1})$. It follows that

$$d_i = s_i / 2 \log e, \qquad (4.22a)$$

$$|k_{i,i+1}| = 10^{-c}, \qquad (4.22b)$$

and $$\rho_{i+1} = \rho_i (1 - k_{i,i+1})/(1 + k_{i,i+1}). \qquad (4.22c)$$

where i = 2, 3, 4,.....,n-2.

(iv) Determination of $k_{n-1,n}$ and d_{n-1} — U_{n-2} and K_{n-1} can be obtained from (4.18) and (4.19) respectively by putting i = n-1. Since $U_{n-1} = k_{n-1,n} = (\rho_{n-1} - \rho_n)/(\rho_{n-1} + \rho_n)$, it is clear from (4.20) that

$$\log |T_{n-1}| = 2\lambda d_{n-1} \log e + \log |(1/k_{n-1,n})| \qquad (4.23)$$

Equation (4.23) represents a straight line with slope $s_{n-1} = 2d_{n-1} \log e$ and intercept $c_{n-1} = \log (1/k_{n-1,n})$. It follows that

$$d_{n-1} = s_{n-1}/2 \log e \qquad (4.24a)$$

$$|k_{n-1,n}| = 10^{-c} \tag{4.24b}$$

$$\rho_n = \rho_{n-1}\,(1-k_{n-1,n})/(1 + k_{n-1,n}). \tag{4.24c}$$

Discussion of examples. In order to illustrate the procedure of analysis discussed above we shall consider some examples. Again we shall begin our discussion with the two-layer case.

The two-layer case comprises a top layer of resistivity ρ_1 and thickness d_1, and a substratum of resistivity ρ_2 and infinite thickness. Examples of the kernels associated with two-layer structures are given in Figs. 4.1 and 4.2. In Fig. 4.1 are shown the kernels associated with these cases in which the reflection factors are positive while those kernels shown in Fig. 4.2 are associated with two-layer structures with negative reflection factors. It may be noted that all these curves of the kernel were computed from the analytical expression (4.2).

The first step in the analysis of a two-layer kernel involves the calculation of T_1 from (4.3). The general relationship between T_1 and $K_1(\lambda)$ as defined by (4.3) is illustrated in Fig. 4.3. There are two things to be noted from Fig. 4.3. First, the function T_1 possesses an infinite discontinuity when $K_1(\lambda)$ takes on the value of unity. The next thing to be noted is that $T_1 > 0$ if $K_1(\lambda) < 1$ and $T_1 < 0$ if $K_1(\lambda) < 1$. Thus from Figs. 4.1 and 4.2 it is evident that

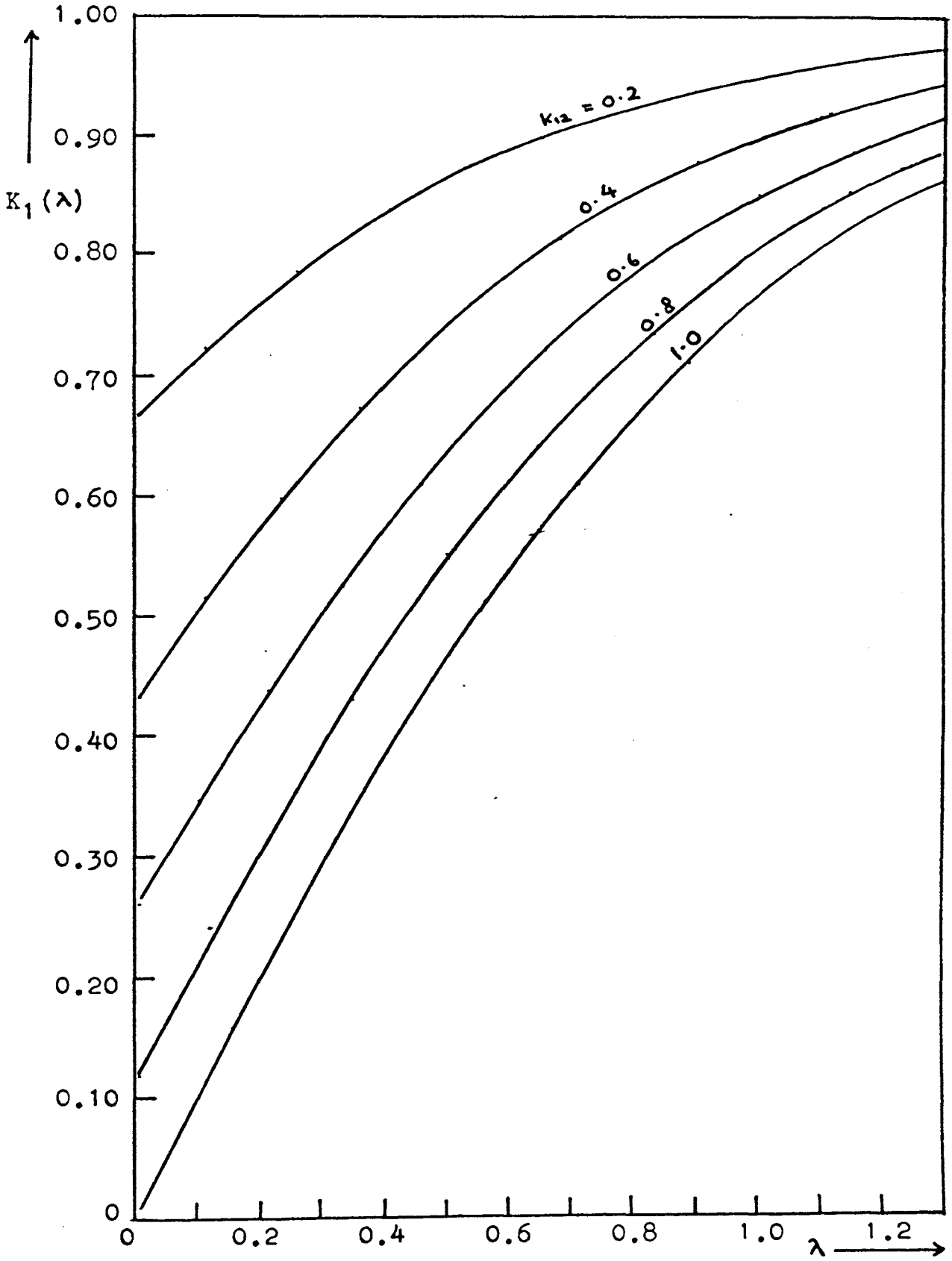

Fig. 4.1. Curves of two-layer kernels with positive reflection factors

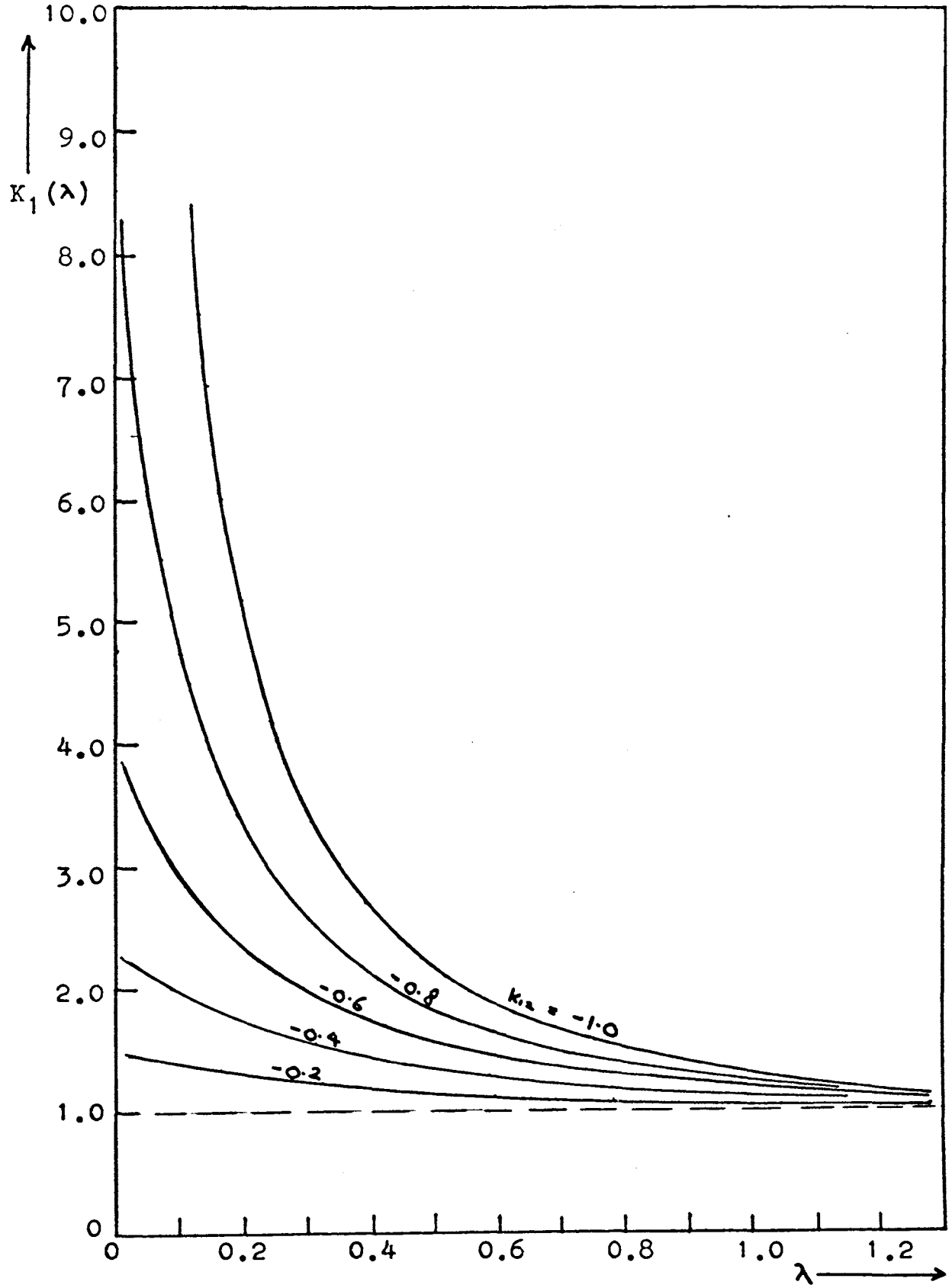

Fig. 4.2. Curves of two-layer kernels with negative reflection factors.

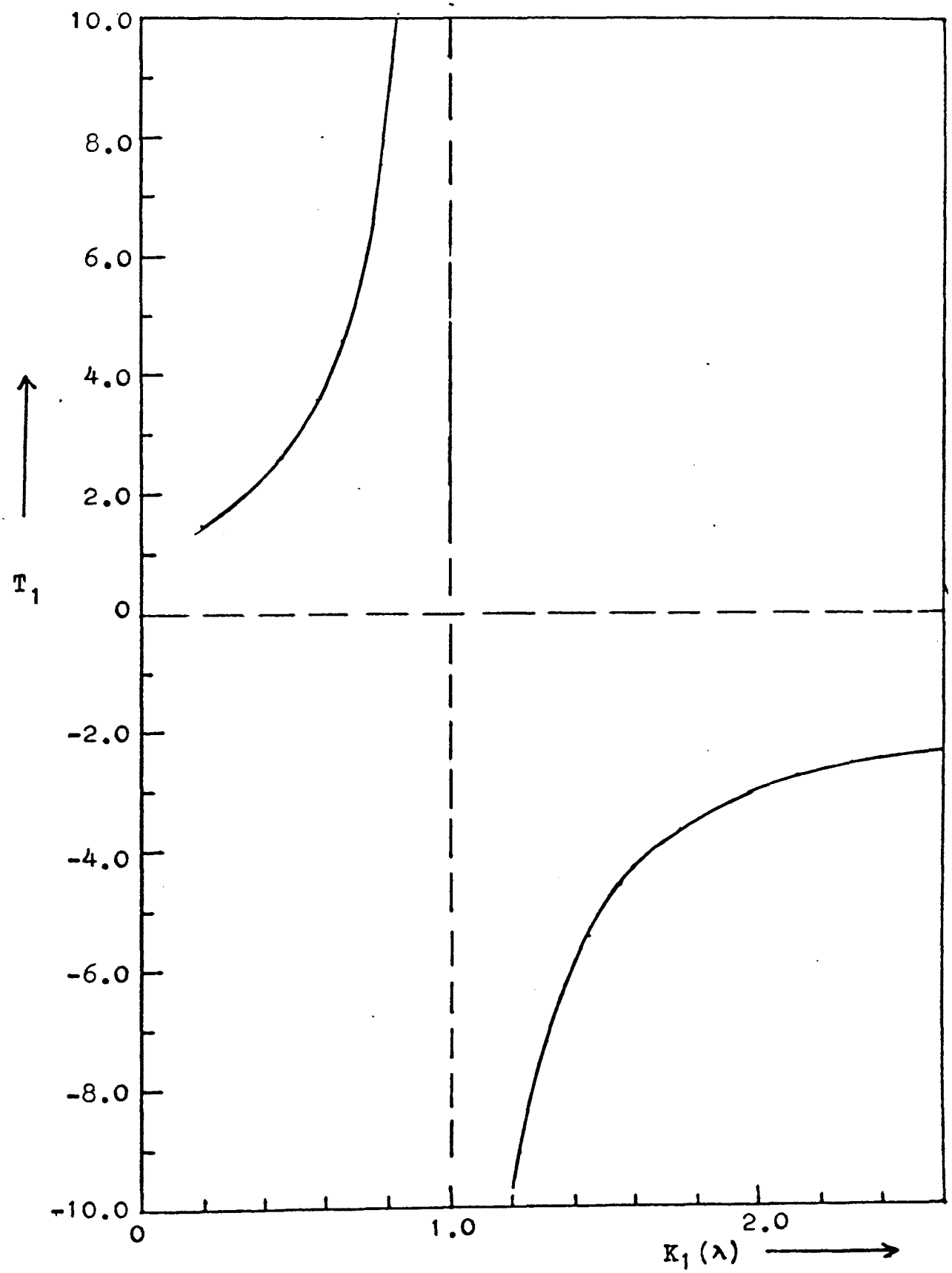

Fig. 4.3. Relation between $K_1(\lambda)$ and T_1.

the positive values of T_1 will be associated with positive reflection factors because in such cases $K_1(\lambda) < 1$, while the negative values of T_1 will be associated with negative reflection factors because $K_1(\lambda) > 1$ for such cases. Furthermore one may note that in any two cases in which the reflection factors are of the same magnitude but of opposite signs the T_1's will have the same absolute values, providing that d_1 is the same for both cases. Thus the graphs of log $|T_1|$ plotted against λ are identical in all cases which have the same absolute value for k_{12} and the same thickness d_1. Examples of the graphs of log $|T_1|$ plotted against λ corresponding to the kernels shown in Figs. 4.1 and 4.2 are illustrated in Fig. 4.4. The fact that all the graphs are straight lines is clear from (4.5).

From each of the graphs shown in Fig. 4.4 one can determine the absolute value of k_{12} and d_1. One can easily estimate that the slope s_1 is equal to 0.8686. By substituting this value of s_1 into (4.6) one gets $d_1 = 1.0$. To determine the absolute value of k_{12} one merely extends each graph to intercept the vertical axis. The value of each intercept on the vertical axis is shown in Fig. 4.4. The absolute value of k_{12} is given by the reciprocal of the value of the intercept shown in the figure. The correct sign of each reflection factor has to be determined from the sign of T_1 associated with each case as it has been pointed out in the previous paragraph.

In practice it may not be necessary to carry out the calculation of the slope s_1. d_1 can easily be determined graphically. Let us consider the equation

$$\log Y = \lambda d \log e \qquad Y > 0$$

If d is considered to be a parameter, then by assigning different values of d to the above equation we can construct a master diagram which consists of a series of straight lines, each line corresponding to one of the values of d. Fig. 4.5 is an example of such master diagram. With the aid of a master diagram of some suitable scale one can determine d_1 as follows: Plot the graph of $\log |T_1|$ vs. λ on a tracing paper using a scale identical with that of the master diagram. Then superimpose the tracing on the master diagram with the vertical axes coinciding with each other. The tracing is moved until the plot on it fits one of the straight lines on the master diagram. Then the value of d_1 will be given by one-half the value of d associated the line that fits the graph on the tracing.

Next, let us consider the analysis of the three-layer kernels. The three-layer case comprises a top layer of thickness d_1, a middle layer of thickness d_2, and a bottom layer that is theoretically assumed to extend to infinity. There are an infinite number of permutations and combinations of resistivity contrasts of the three beds. However, there are only three main groups of possibilities concerning the resistivity of the middle layer in relation to that of the

others: it may be higher than, lower than, or intermediate between the resistivities of the top and bottom layers. Accordingly the resistivity curves are conveniently divided into four categories; (i) $\rho_1 > \rho_2 < \rho_3$, (ii) $\rho_1 < \rho_2 > \rho_3$, (iii) $\rho_1 < \rho_2 < \rho_3$, and (iv) $\rho_1 > \rho_2 > \rho_3$. Generally the sounding curves belonging to each category have a characteristic shape (see Fig. 4.6). This property of the sounding curves has often been utilized qualitatively for interpretative purposes. The curves of the kernels corresponding to these four categories of three-layer situations also exhibit similar characteristics. Figs. 4.7, 4.8, 4.9, and 4.10 are typical examples of the three-layer kernels.

Since the procedure for analyzing the three-layer kernels is identical for all cases, it is sufficient for us to consider the case shown in Fig. 4.7. The values of the layer resistivities and thicknesses assumed for the computation of these curves are $\rho_1 = 1$, $\rho_2 = 10$, $\rho_3 = 1/10$, $d_1 = 1$, and $d_2 = 4$, $1\frac{1}{2}$, $2/3$, and $\frac{1}{4}$ respectively. The reflection factors corresponding to the given values of the resistivities are $k_{12} = -0.82$ and $k_{23} = 0.98$. These kernels are analyzed according to the procedure discussed in the previous section; the results of the analyses are shown in Figs. 4.11, 4.12, 4.13, and 4.14.

Refering to the results of analyses shown in Figs. 4.11, 4.12, 4.13, and 4.14 one can see that for small values of the function $\log |T_1|$ is not linearly related to λ but it approaches

the linear relation

$$Y_1 = 2\lambda d_1 \log e + \log (1/k_{12})$$

rather rapidly at large values of λ. This behavior of $\log |T_1|$ is in accordance with that predicted by (4.11). The parameters d_1 and $|k_{12}|$ can easily be determined from the asymptotic portion of the curve of $\log |T_1|$ with the aid of a master diagram similar to the one shown in Fig. 415, but plotted with some suitable scales. It is of interest to note that in practice the non-linear relationship between $\log |T_1|$ and λ at small values of λ could serve as a useful guide to the fact that the problem under consideration is one involving more than two layers. So when this type of relationship is observed further decomposition is necessary in order to determine the parameters of the lower layer (or layers).

In the second stage of decomposition (4.12) and (4.13) are used to compute the function T_2. The resulting graphs of $\log |T_2|$ plotted against λ for all the four cases are straight lines, thus indicating that no further discontinuity exists beneath the second layer. The layer parameters d_2 and k_{23} can again be determined with the aid of a master diagram of some suitable scales.

As in the two-layer case the study of the behavior of the function T_1 may throw some light on the nature of the reflection factor k_{12}. Fig. 4.15 illustrates curve 4 of Fig. 4.7 together with the curve of the associated T_1.

The curve of T_1 shows the presence of a discontinuity in the neighbourhood of the point $\lambda = 3.6$ at which the curve of $K_1(\lambda)$ intersects the line $K_1(\lambda) = 1$. One may also note that the sign of T_1 changes from positive to negative as one crosses the discontinuity from the left to the right. This change in sign of T_1 is related to the fact that $K_1(\lambda) < 1$ when $\lambda < 3.6$ and $K_1(\lambda) > 1$ when $\lambda > 3.6$. It is clear that the T_1's associated with the kernels of the remaining three cases shown in Fig. 4.7 will behave in a similar manner. On the other hand one may expect that the T_1's associated with the kernels of the case $\rho_1 : \rho_2 : \rho_3 = 1 : 1/10 : 10$ shown in Fig. 4.8 will behave in an opposite manner, that is, the sign of T_1 changes from negative to positive as the discontinuity is crossed from the left to the right. The reason is simply that $K_1(\lambda) > 1$ to the left of the discontinuity and $K_1(\lambda) < 1$ to its right. Fig. 4.16, for instance, shows the function T_1 associated with the case $d_1 = 0.25$ of Fig. 4.8. For the cases $\rho_1 : \rho_2 : \rho_3 = 1 : 3 : 10$ and $\rho_1 : \rho_2 : \rho_3 = 1 : 1/3 : 1/10$ (Fig. 4.9 and Fig. 4.10 respectively) the function T_1 does not possess any discontinuity because $K_1(\lambda)$ is either greater or smaller than unity throughout the entire range of λ.

From the above observations we note that in the first cases, namely $\rho_1 : \rho_2 : \rho_3 = 1 : 10 : 1/10$ and $\rho_1 : \rho_2 : \rho_3 = 1 : 1/10 : 10$, T_1 is positive beyond the point of discontinuity if the reflection factor k_{12} is positive and is negative if k_{12} is negative. In the remaining two cases, similar relationships

exist between T_1 and k_{12}. Thus by noting the sign of the values of T_1 one can determine the correct sign of k_{12}.

Actually the above conclusion can be predicted from (4.9), the analytical expression for the kernel. It has already been pointed out that when λ is large U_1 approaches k_{12} and thus the kernel of a three-layer case is reduced essentially to that of a two-layer case. In the analysis of the two-layer kernels we observe that positive values of T_1 are related to positive reflection factors and negative values of T_1 are related to the negative reflection factors. Thus we expect that the T_1's of the three-layer cases will behave in a similar manner at large values of λ.

Refering to (4.9c) we can see that the expression for K_2 is actually the kernel function for a two-layer structure with a reflection factor equal to k_{23}, the thickness of its top layer being equal to d_2. It is, therefore, clear that T_2 will be related to k_{23} in exactly the same way as T_1 is related to k_{12}. In other words, T_2 is positive if k_{23} is positive and T_2 is negative if k_{23} is negative.

Since the analysis of the kernels of other multilayer problems is identical to that of the kernels of the three-layer case, we shall not consider any further examples. An example of the analysis of the four-layer kernels is given in Appendix F.

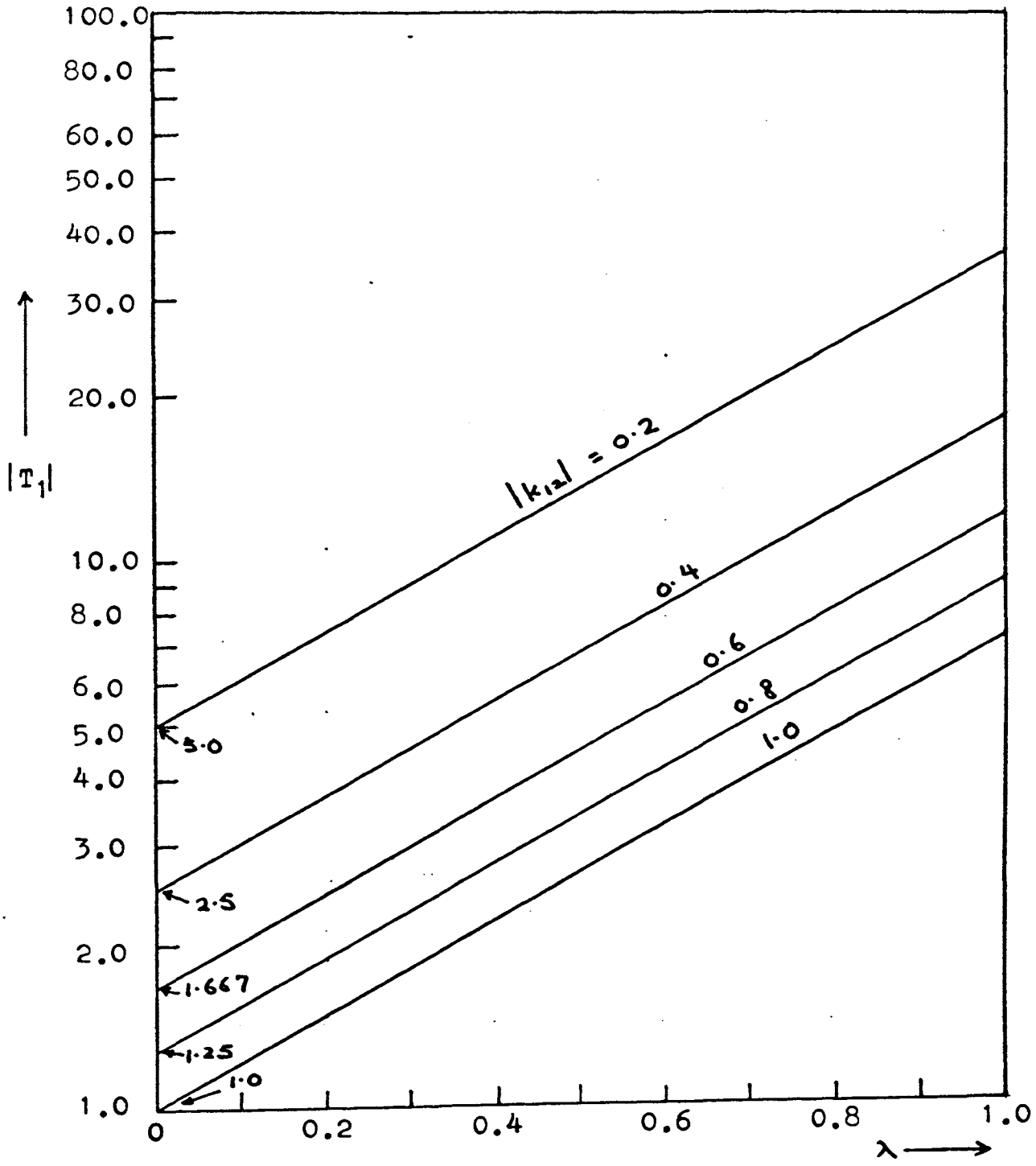

Fig. 4.4. Log $|T_1|$ vs. λ . Analysis of two-layer kernels.

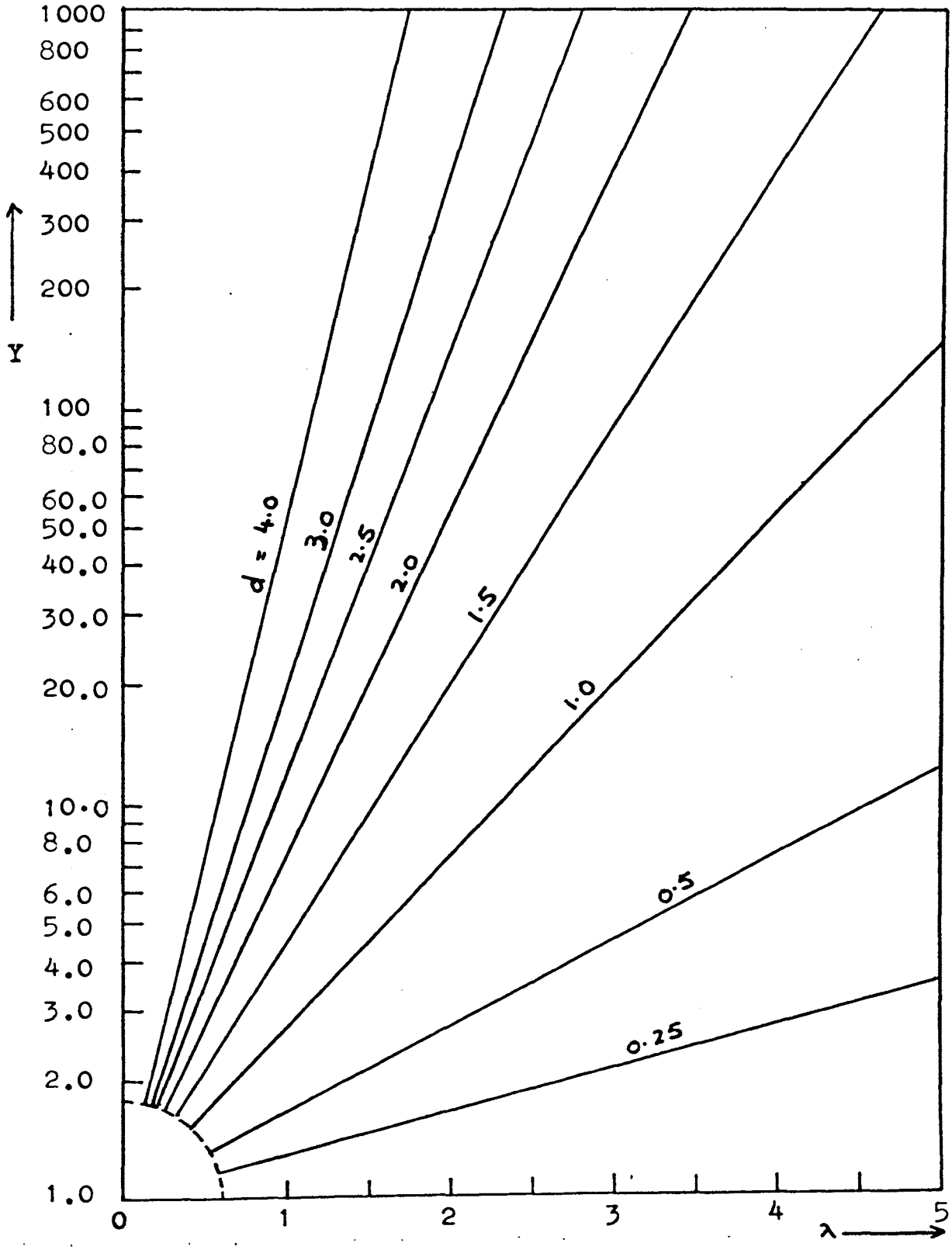

Fig. 4.5. Master diagram of the asymptotic straight line $\log Y = \lambda d \log e$

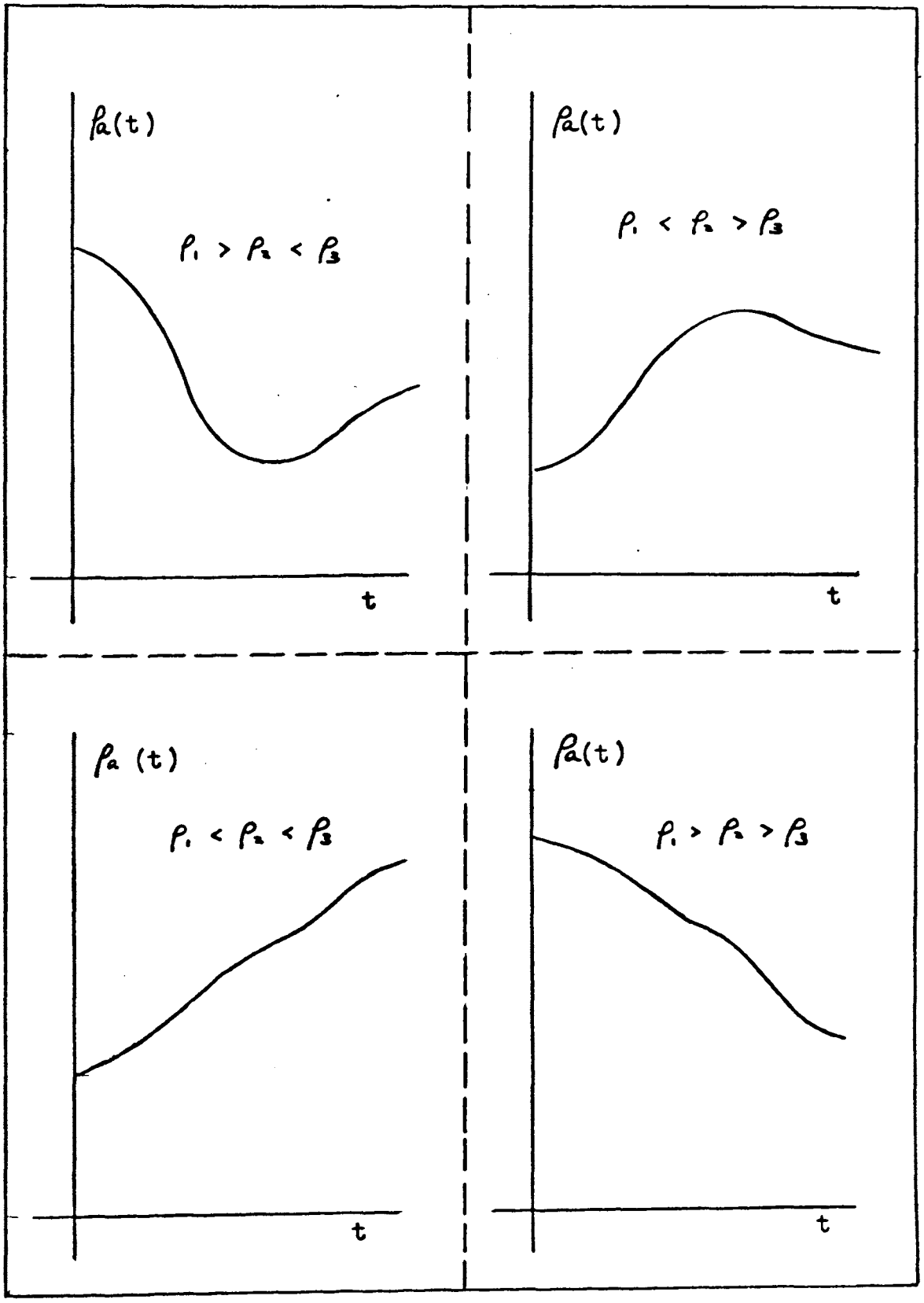

Fig. 4.6. Classification of three-layer apparent resistivity curves according to their characteristic shapes.

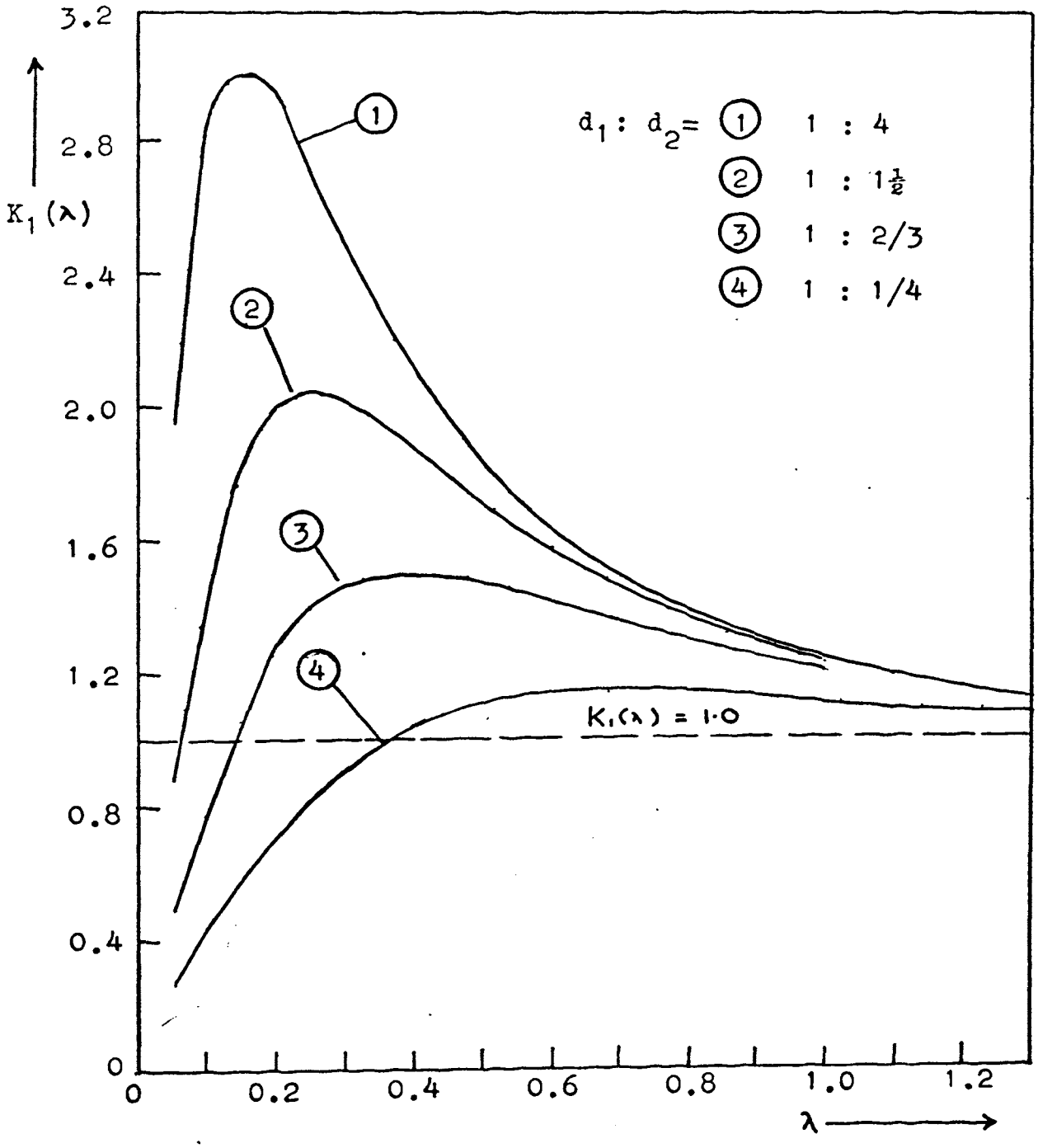

Fig. 4.7. Curves of three-layer kernels for the case $\rho_1 : \rho_2 : \rho_3 = 1 : 10 : 1/10$

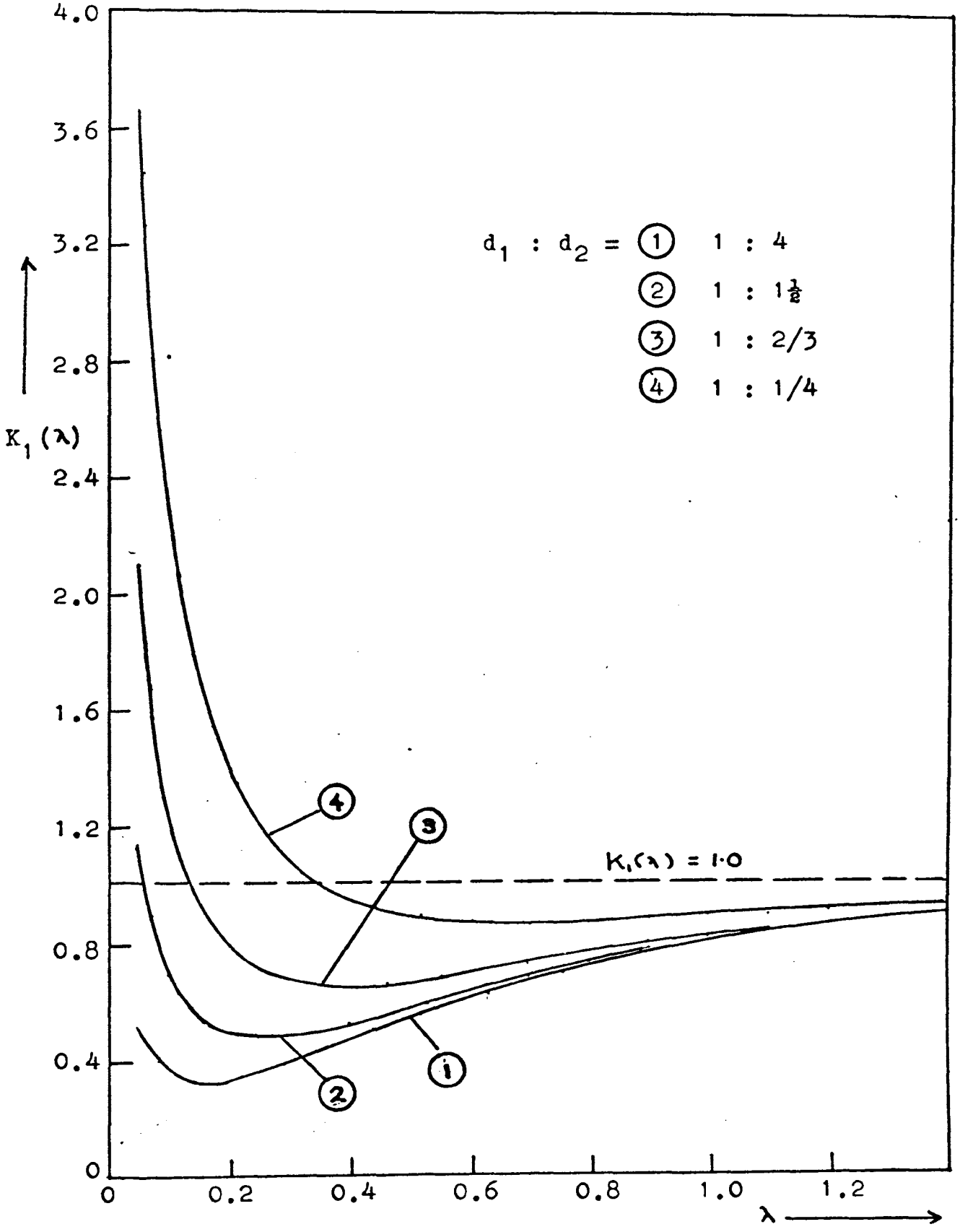

Fig. 4.8. Curves of three-layer kernels for the case $\rho_1 : \rho_2 : \rho_3 = 1 : 1/10 : 10$.

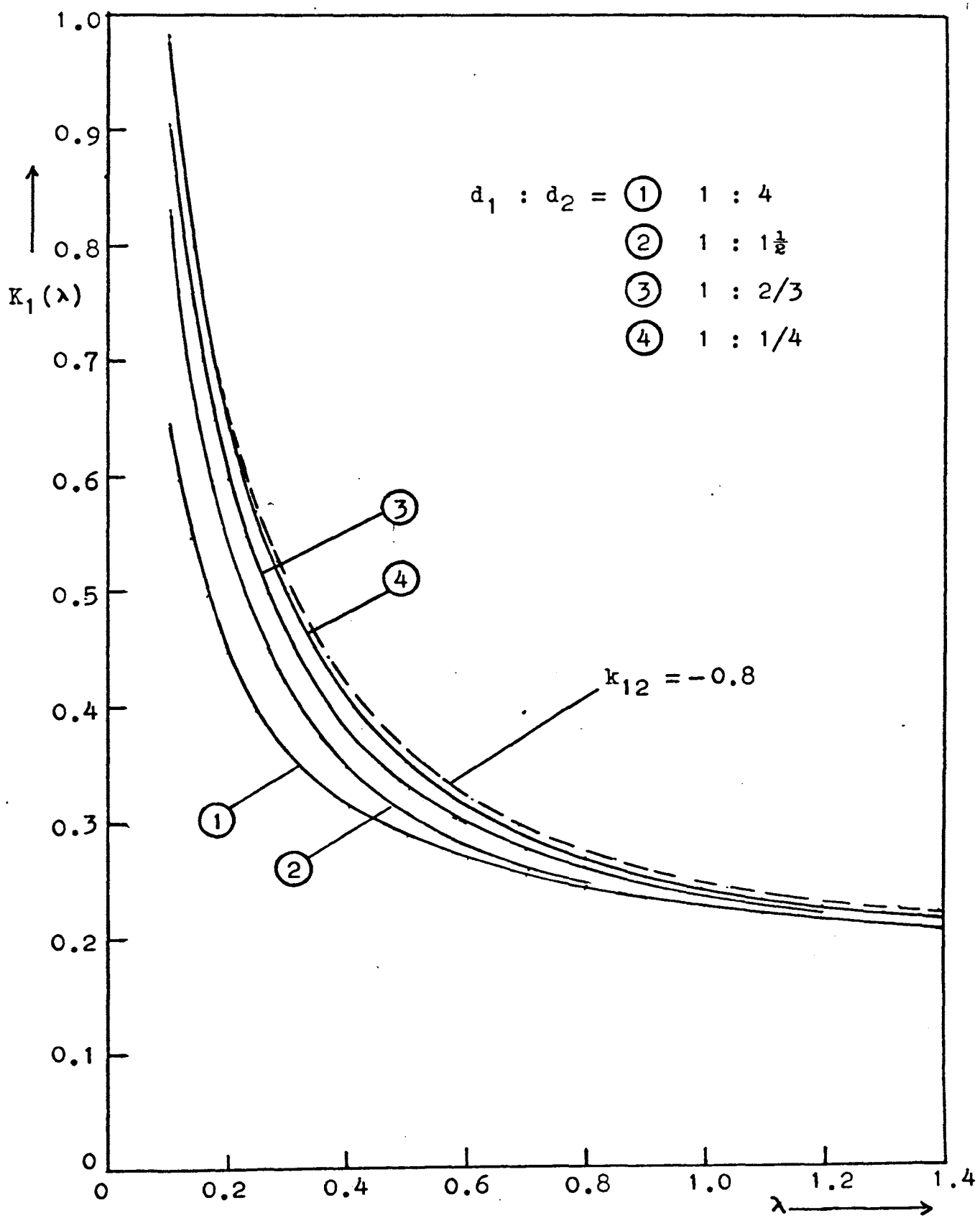

Fig. 4.9. Curves of three-layer kernels for the case $\rho_1 : \rho_2 : \rho_3 = 1 : 3 : 10$.

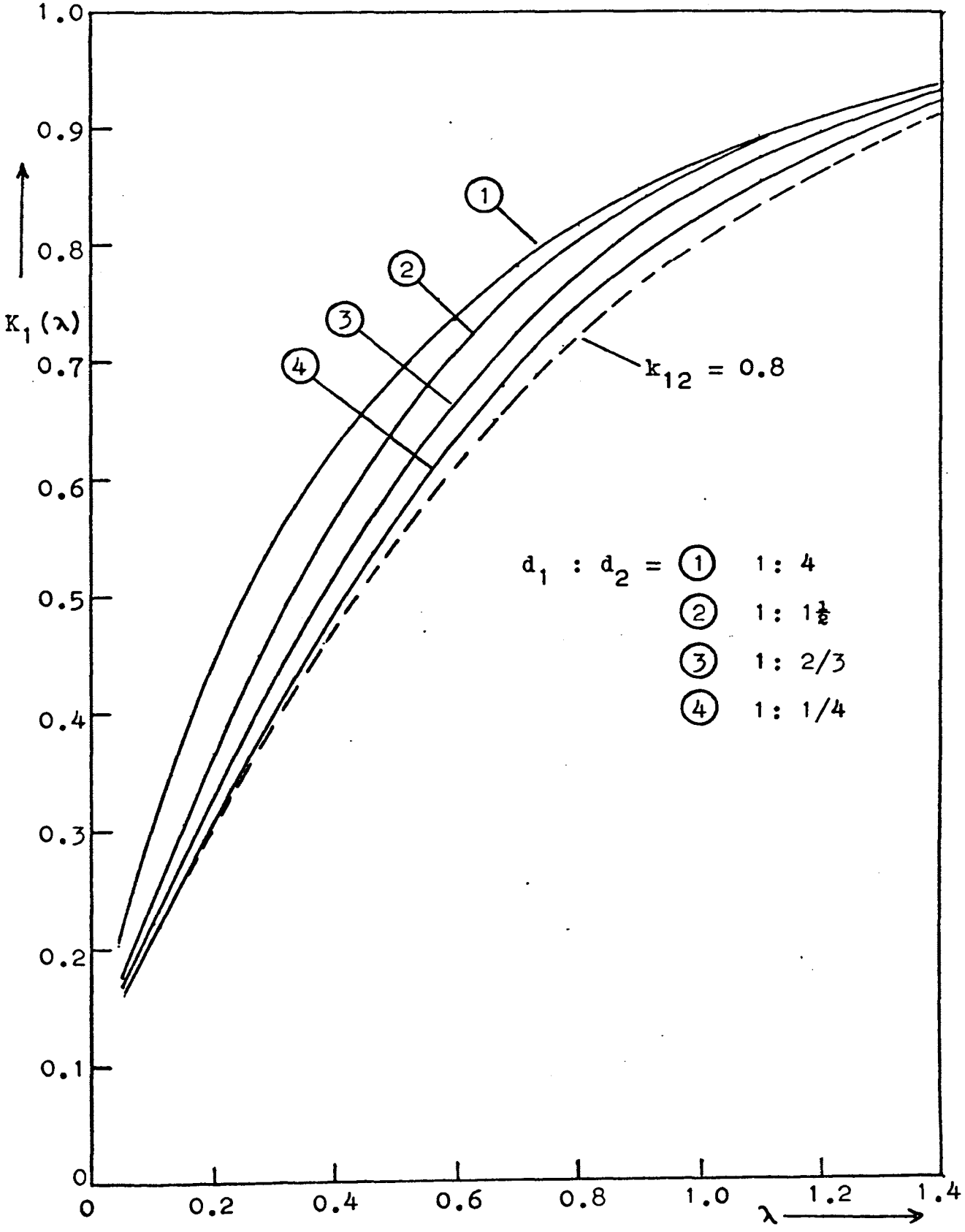

Fig. 4.10. Curves of three-layer kernels for the case $\rho_1 : \rho_2 : \rho_3 = 1 : 1/3 : 1/10$.

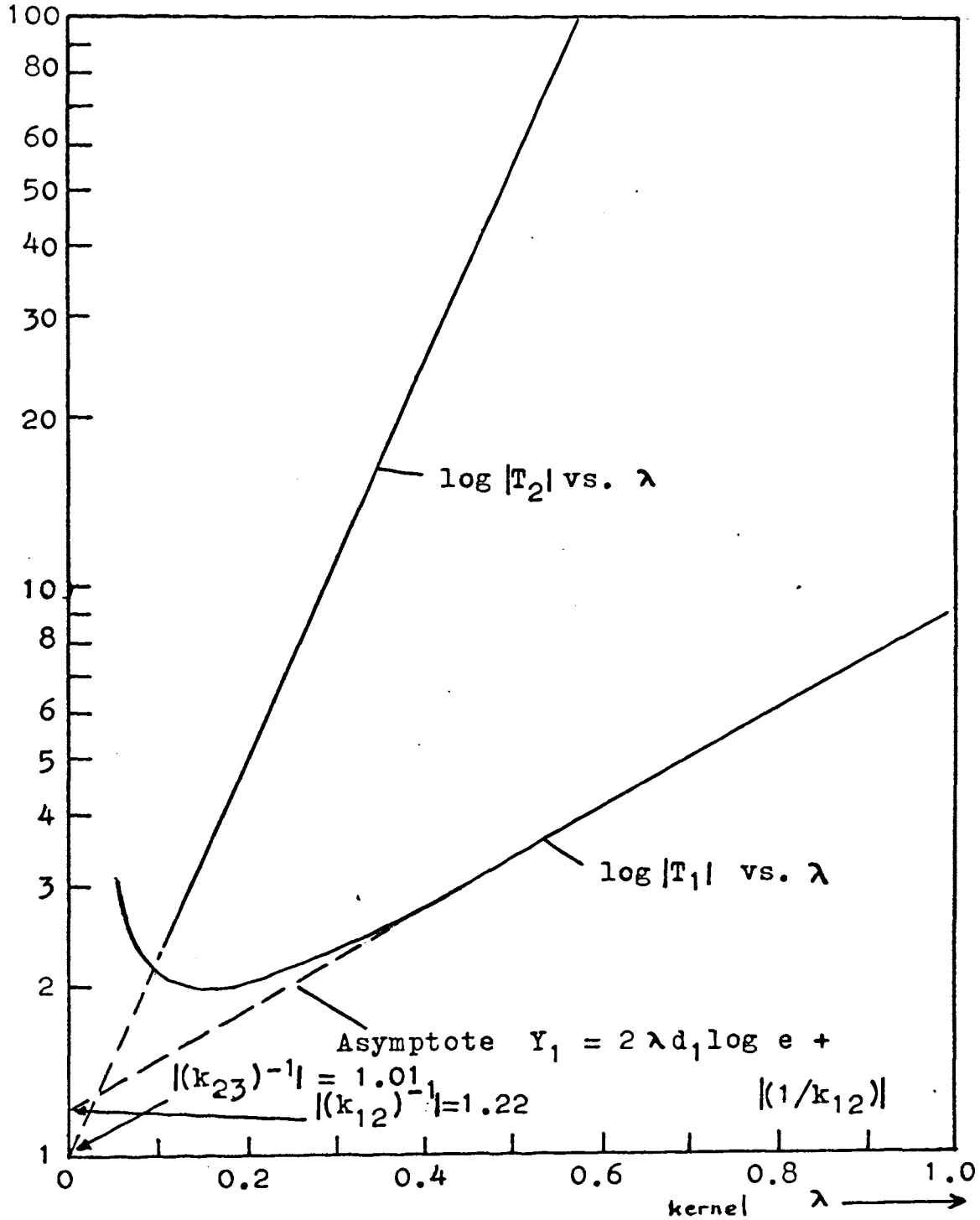

Fig. 4.11. Analysis of three-layer case of the case $\rho_1 : \rho_2 : \rho_3 = 1 : 10 : 1/10$, $d_1 : d_2 = 1 : 4$.

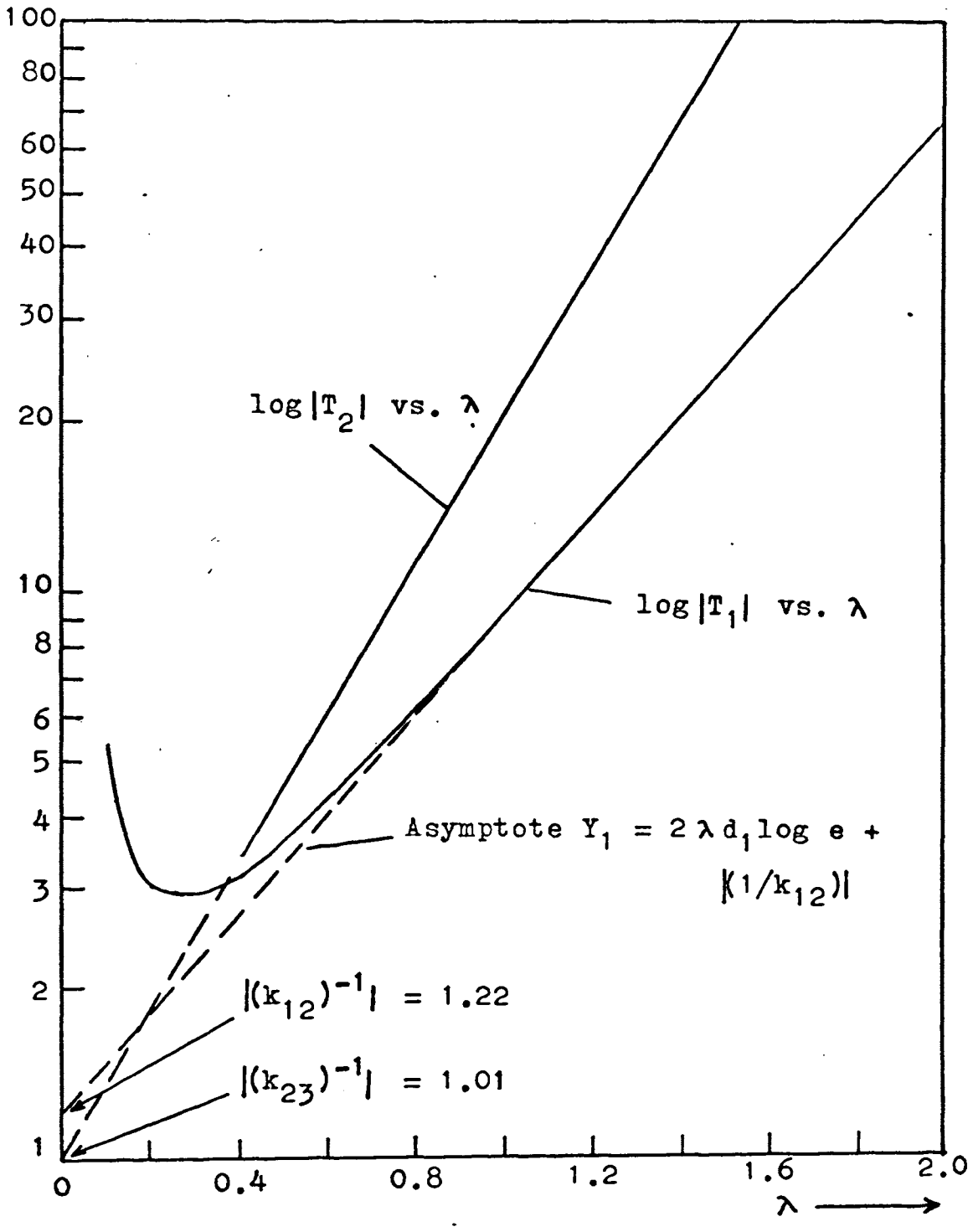

Fig. 4.12 Analysis of three-layer kernel of the case $\rho_1 : \rho_2 : \rho_3 = 1 : 10 : 1/10$, $d_1 : d_2 = 1 : 1\frac{1}{2}$.

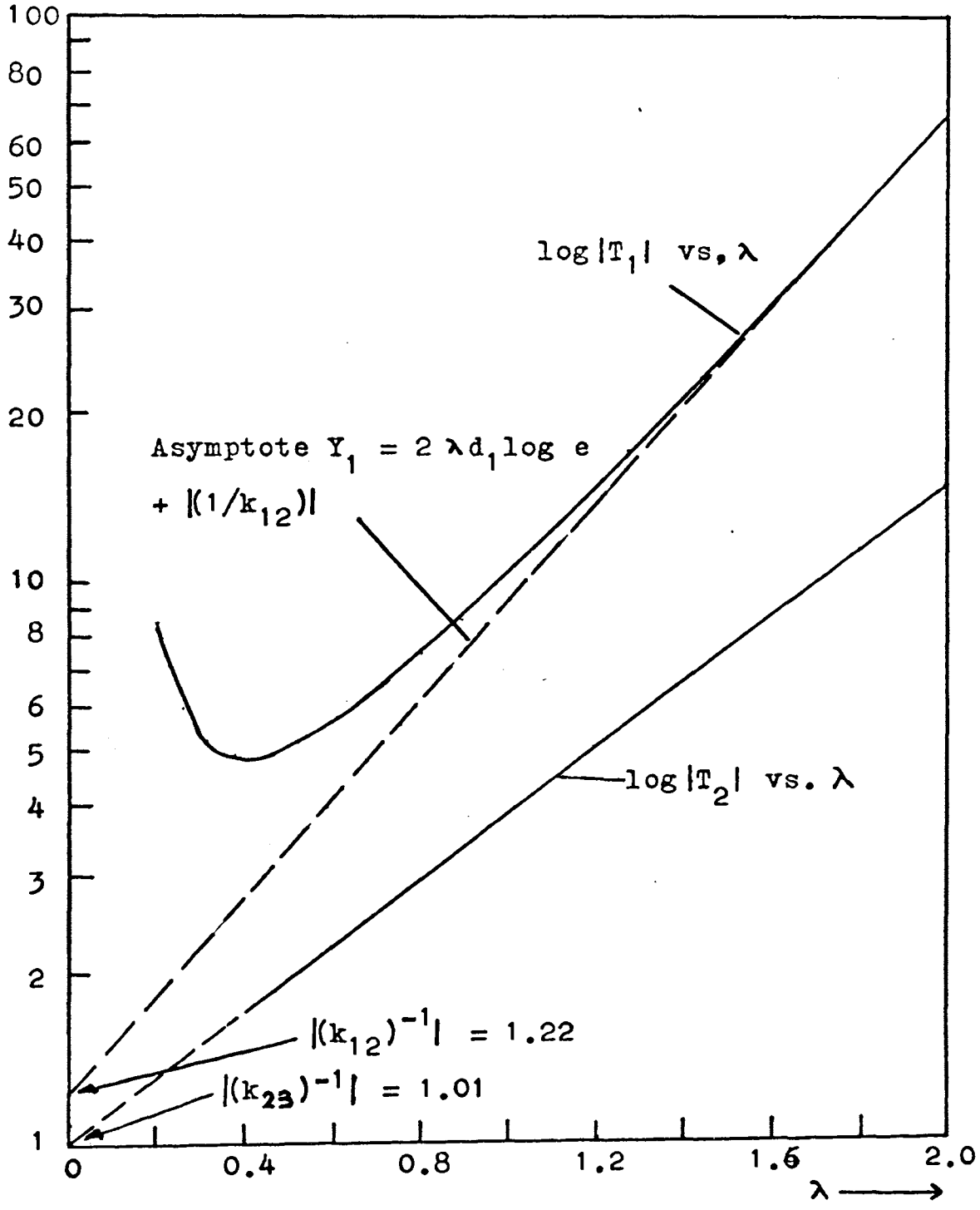

Fig. 4.13. Analysis of three-layer kernel of the case $\rho_1 : \rho_2 : \rho_3 = 1 : 10 : 1/10$, $d_1 : d_2 = 1 : 2/3$.

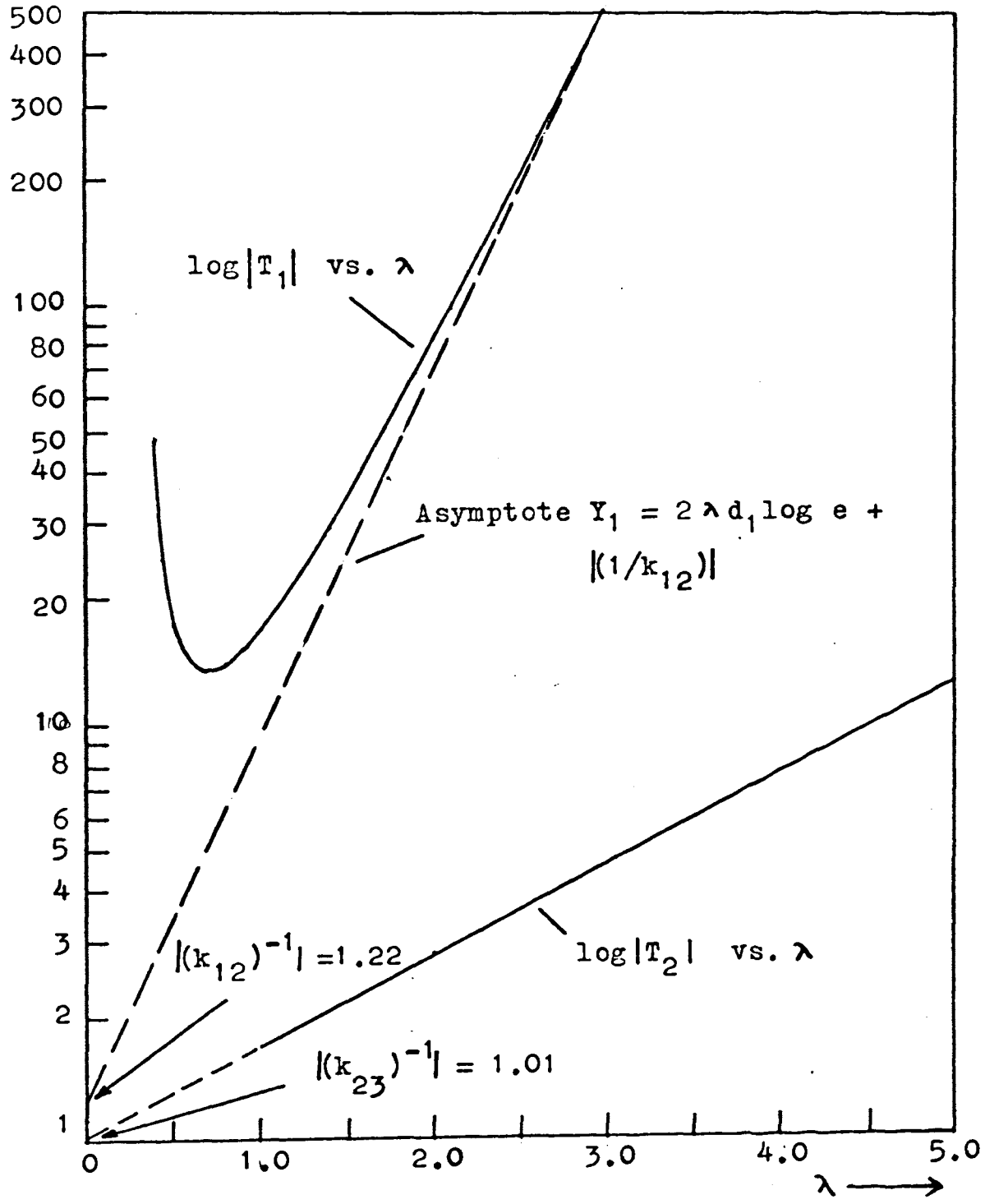

Fig. 4.14. Analysis of three-layer kernel of the case $\rho_1 : \rho_2 : \rho_3 = 1 : 10 : 1/10$, $d_1 : d_2 = 1 : 1/4$.

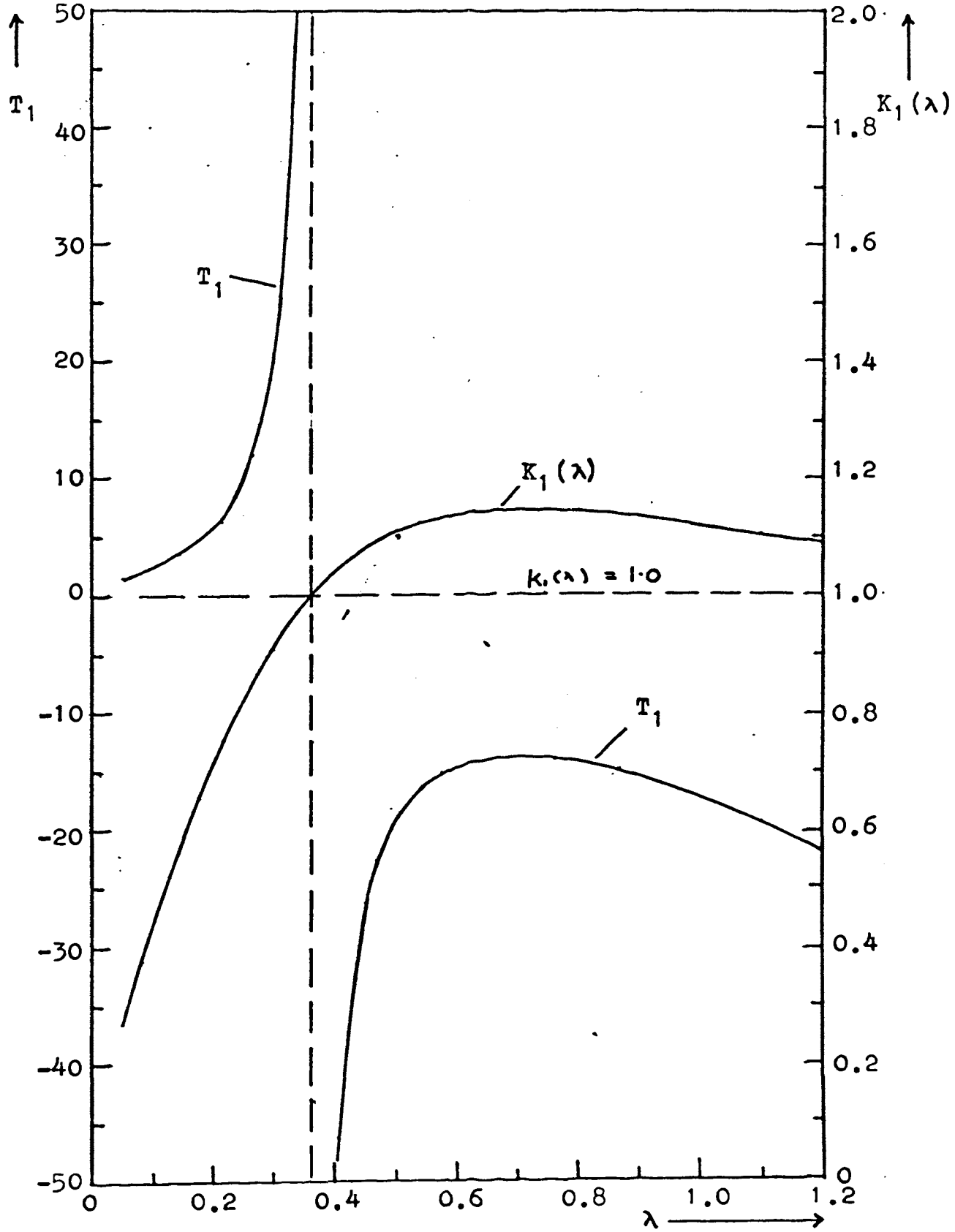

Fig. 4.15. The function T_1 and its related three-layer kernel. Case $\rho_1 : \rho_2 : \rho_3 = 1 : 10 : 1/10$, $d_1 : d_2 = 1 : 1/4$.

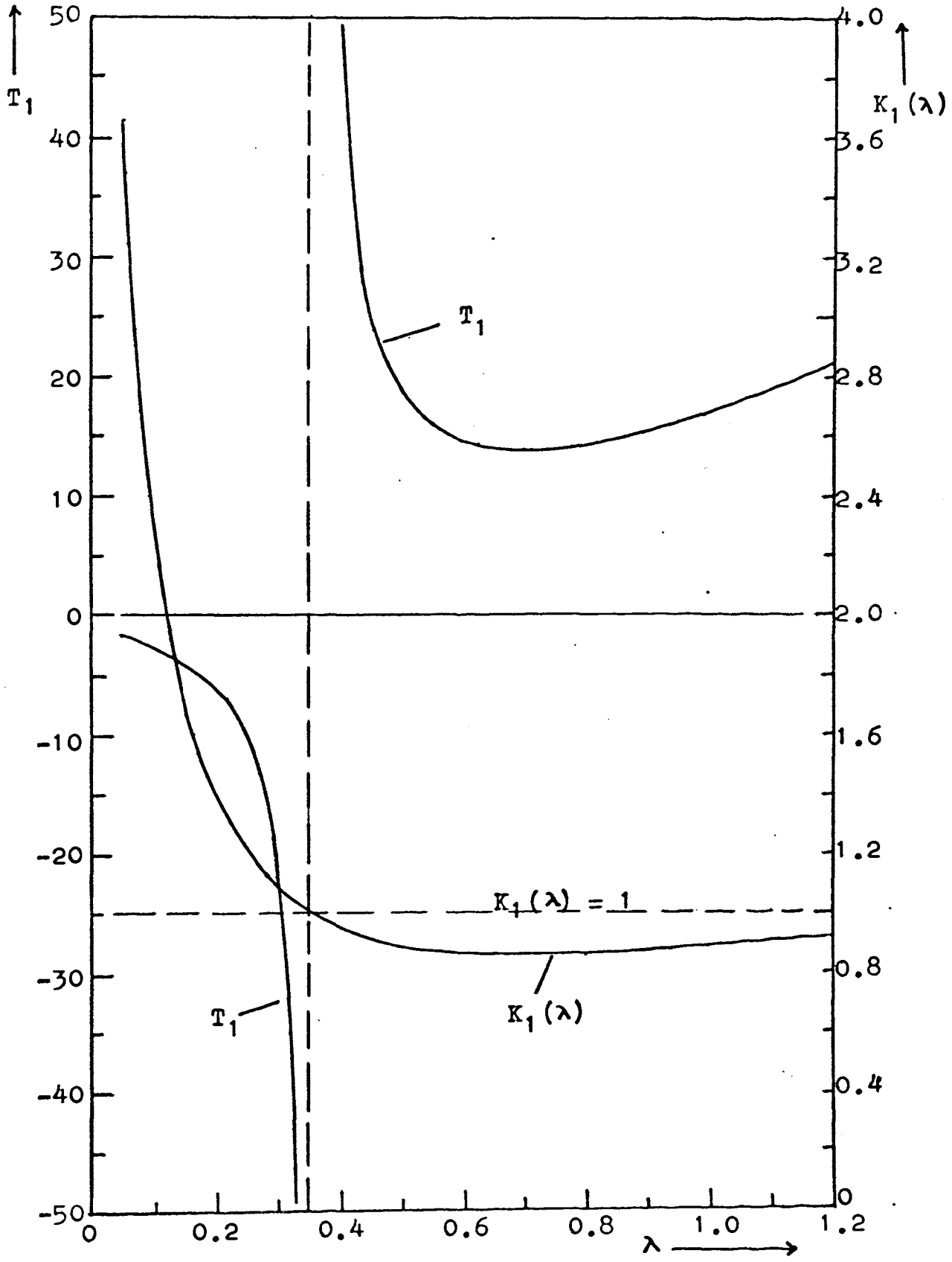

Fig. 4.16. The function T_1 and its related three-layer kernel. Case $\rho_1 : \rho_2 : \rho_3 = 1 : 1/10 : 10$, $d_1 : d_2 = 1 : 1/4$.

Analysis of the Associated Kernel: Numerical-Graphical Method

The associated kernel has been shown to be related to the kernel by the equation

$$B_1(\lambda) = K_1(\lambda) - \tfrac{1}{2} K_1(\lambda/2).$$

$K_1(\lambda)$ is expressed explicitly by (4.1) while $K_1(\lambda/2)$ may be obtained from (4.1) by replacing λ with $\lambda/2$. Thus after substituting $\lambda = \lambda/2$ into (4.1) we get

$$K_1(\lambda/2) = (1 - U_1' e^{-\lambda d_1})/(1 + U_1' e^{-\lambda d_1}). \qquad (4.25)$$

where

$$U_1' = (\rho_1 - \rho_2 K_2')/(\rho_1 + \rho_2 K_2')$$

$$K_2' = (1 - U_2' e^{-\lambda d_2})/(1 + U_2' e^{-\lambda d_2})$$

$$U_2' = (\rho_2 - \rho_3 K_3')/(\rho_2 + \rho_3 K_3')$$

.....

.....

$$K_i' = (1 - U_i' e^{-\lambda d_i})/(1 + U_i' e^{-\lambda d_i})$$

$$U_i' = (\rho_i - \rho_{i+1} K_{i+1}')/(\rho_i + \rho_{i+1} K_{i+1}')$$

.....

.....

$$K_{n-1}' = (1 - k_{n-1,n} e^{-\lambda d_{n-1}})/(1 + k_{n-1,n} e^{-\lambda d_{n-1}})$$

$$k_{n-1,n} = (\rho_{n-1} - \rho_n)/(\rho_{n-1} + \rho_n).$$

Although the associated kernel appears to be a more complicated function than the kernel similar technique of decomposition can be used to determine the layer resistivities and thicknesses.

Two-layer case. From (4.1) and (4.25) the associated kernel for the two-layer case is found to be given by the equation

$$B_1(\lambda) = \frac{1 - k_{12}e^{-2\lambda d_1}}{1 + k_{12}e^{-2\lambda d_1}} - \tfrac{1}{2}\,\frac{1 - k_{12}e^{-\lambda d_1}}{1 + k_{12}e^{-\lambda d_1}} \cdot \tag{4.26}$$

from which it can be shown that

$$\frac{2B_1(\lambda) + 1}{2B_1(\lambda) - 1} = \frac{1 + 2k_{12}e^{-\lambda d_1} - k_{12}e^{-2\lambda d_1}}{k_{12}e^{-\lambda d_1}(1 - e^{-\lambda d_1} - k_{12}e^{-2\lambda d_1})}$$

When λ is large, since $k_{12}^2 e^{-3\lambda d_1} \ll k_{12}e^{-2\lambda d_1} \ll 1$ we have the following approximation:

$$\frac{2B_1(\lambda) + 1}{2B_1(\lambda) - 1} \approx \frac{1 + 2k_{12}e^{-\lambda d_1}}{k_{12}e^{-\lambda d_1}} = \frac{e^{-\lambda d_1}}{k_{12}} + 2$$

By letting

$$Q_1 = \frac{2B_1(\lambda) + 1}{2B_1(\lambda) - 1} - 2 \tag{4.27}$$

we have

$$Q_1 \simeq e^{\lambda d_1}/k_{12}$$

for large values of λ. It follows that

$$\log |Q_1| \simeq \lambda d_1 \log e + \log|(1/k_{12})| \tag{4.28}$$

which is the equation of a straight line with slope $s_1 = (d_1 \log e)$ and intercept $c_1 = \log|(1/k_{12})|$. Thus d_1 and k_{12} are derivable from c_1 and s_1 which are associated with the asymptote of the function $\log|Q_1|$.

Three-layer case. The associated kernel for the three-layer case is given by

$$B_1(\lambda) = \frac{1 - U_1 e^{-2\lambda d_1}}{1 + U_1 e^{-2\lambda d_2}} - \tfrac{1}{2} \frac{1 - U_1' e^{-\lambda d_1}}{1 + U_1' e^{-\lambda d_1}} \tag{4.29}$$

where U_1 is given by (4.9a) and

$$U_1' = (\rho_1 - \rho_2 K_2')/(\rho_1 + \rho_2 K_2') \tag{4.30a}$$

$$K_2' = (1 - k_{23} e^{-\lambda d_2})/(1 + k_{23} e^{-\lambda d_2}) \cdot \tag{4.30b}$$

To analyze the associated kernel we may proceed as follows:

(i) Determination k_{12} and d_1 — From (2.29) it can be shown that

$$\frac{2B_1(\lambda) + 1}{2B_1(\lambda) - 1} = \frac{1 + 2U_1'e^{-\lambda d_1} - U_1e^{-2\lambda d_1}}{U_1'e^{-\lambda d} - U_1e^{-2\lambda d_1} - U_1U_1'e^{-3\lambda d_1}} .$$

When λ takes on such values that $U_1'e^{-\lambda d_1} >> U_1e^{-2\lambda d_1} >> U_1U_1'e^{-3\lambda d_1}$, we get the approximation

$$\frac{2B_1(\lambda) + 1}{2B_1(\lambda) - 1} \simeq \frac{1 + 2U_1'e^{-\lambda d_1}}{U_1'e^{-\lambda d_1}} .$$

from which we get

$$Q_1 = e^{\lambda d_1}/U_1' \tag{4.31}$$

where Q_1 has the same definition as before. It follows that

$$\log |Q_1| = \lambda d_1 \log e + \log|(1/U_1')| \tag{4.32}$$

When λ is very large $k_{23}e^{-\lambda d_2} << 1 \Rightarrow K_2' \to 1 \Rightarrow U_1' \to k_{12}$. Thus at very large values of λ the function $\log |Q_1|$ should approach asymptotically to the straight line

$$Y_1 = \lambda s_1 + c_1$$

where $s_1 = d_1 \log e$ and $c_1 = \log|(1/k_{12})|$. It follows that d_1 and k_{12} are derivable from s_1 and c_1 respectively.

(ii) Determination of k_{23} and d_2 — Since d_1 is now known U_1' can easily calculated from (4.31) or

$$U_1' = e^{\lambda d_1}/Q_1 \tag{4.33a}$$

From (4.30a) it can easily be shown that

$$K_2' = \rho_1 (1 - U_1')/\rho_2(1 + U_1') \qquad (4.33b)$$

By letting

$$Q_2 = (1 + K_2')/(1 - K_2') \qquad (4.34)$$

it follows from (4.30b) that

$$Q_2 = e^{\lambda d_2/k_{23}}$$

from which

$$\log |Q_2| = \lambda d_2 \log e + \log (1/k_{23}) \; . \qquad (4.35)$$

Thus it is obvious that the graph of $\log |Q_2|$ plotted against λ is a straight line with slope $s_2 = d_2 \log e$ and intercept $c_2 = \log|(1/k_{23})|$ from which one can determine d_2 and c_2.

Generalization to n-layer case. The method of analysis used for the three-layer associated kernel can easily be extended to deal with the n-layer associated kernel. The procedure may be outlined as follows:

(i) Determination of d_1 and k_{12} — This step is identical to step (i) of the three-layer case.

(ii) Determination of k_{23} and d_2 — All the equations involved in this step are identical with those of step (ii) of the

three-layer case, excepting that k_{23} is replaced by U_2' in each equation. Thus from (4.35) we have

$$\log|Q_2| = \lambda d_2 \log e + \log|(1/U_2')| \tag{4.36}$$

Here the function $\log|Q_2|$ is no longer a linear function of λ as in the three-layer case because U_2' is also a function of λ. But when λ is large, since U_2' approaches k_{23} the function $\log|Q_2|$ will approach an asymptote

$$Y_2 = \lambda s_2 + c_2$$

where $s_2 = d_2 \log e$ and $c_2 = \log|(1/k_{23})|$. It follows that d_2 and k_{23} are derivable from the slope and intercept of the asymptotic straight line respectively.

(iii) Determination of $k_{i,i+1}$ and d_i — By repeating the process described in step (ii) the parameters for each successive lower layer can be obtained. Now we can write down the equations for determining $k_{i,i+1}$ and d_i. These equations are

$$U_{i-1}' = e^{\lambda d_{i-1}/Q_{i-1}} \tag{4.37a}$$

$$K_i' = \rho_{i-1}(1 - U_{i-1}')/(1 + U_{i-1}')\rho_i \tag{4.37b}$$

$$\log|Q_i| = d_1 \log e + \log|(1/U_i')| \tag{4.37c}$$

where $Q_i = (1 + K_i')/(1 - K_i')$, $i = 2, 3, 4, \ldots, n-2$. Since

U_i' approaches $k_{i,i+1}$ at large λ, we have the asymptote of the function $\log|Q_i|$ given by

$$Y_i = \lambda s_i + c_i \tag{4.38}$$

where $s_i = d_i \log e$ and $c_i = \log|(1/k_{i,i+1})|$. It follows that

$$d_i = s_i / \log e \tag{4.39a}$$

$$|k_{i,i+1}| = 10^{-c} \tag{4.39b}$$

$$\rho_{i+1} = \rho_i(1 - k_{i,i+1})/(1 + k_{i,i+1}) \tag{4.39c}$$

(iv) Determination of $k_{n-1,n}$ and d_{n-1} — U'_{n-2} and K'_{n-1} can be obtained from (4.37a) and (4.37b) respectively. Since $U'_{n-1} = k_{n-1,n}$ it follows from (4.37c) that

$$\log|Q_{n-1}| = \lambda d_{n-1} \log e + \log|(1/k_{n-1,n})| \tag{4.40}$$

Equation (4.40) represents a straight line with slope $s_{n-1} = d_{n-1} \log e$ and intercept $c_{n-1} = \log|(1/k_{n-1,n})|$. It follows that d_{n-1} and $k_{n-1,n}$ can be determined from s_{n-1} and c_{n-1} respectively. Hence the n-layer case is completely solved.

Discussion of examples. Figs. 4.17 and 4.18 show some typical examples of the associated kernels for the two-layer case. The results of the analysis of these associated kernels are shown in Figs. 4.19 and 4.20. Examination of these results shows that unlike the function $\log|T_1|$ associated

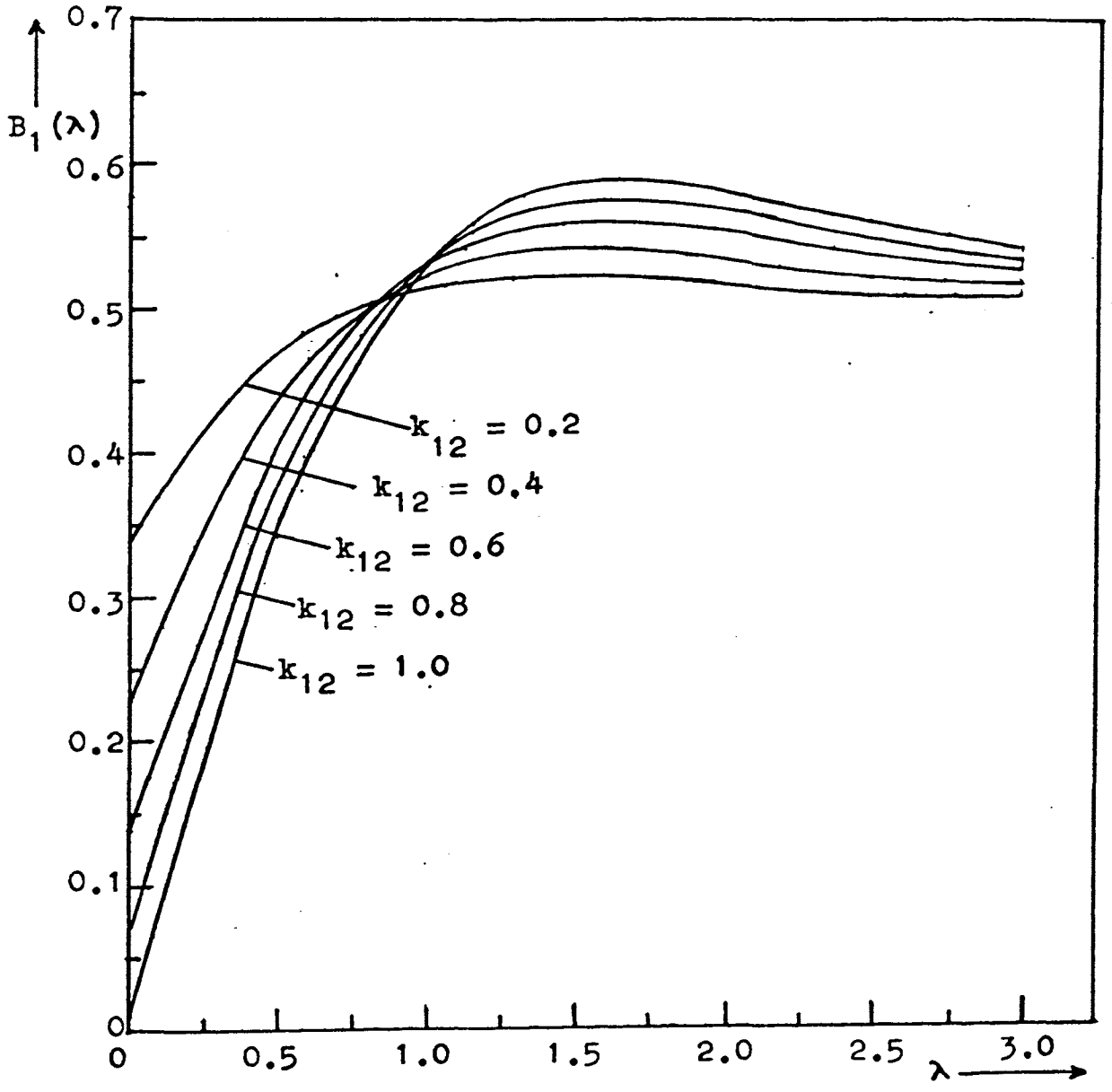

Fig. 4.17. Curves of two-layer associated kernels with positive reflection factors.

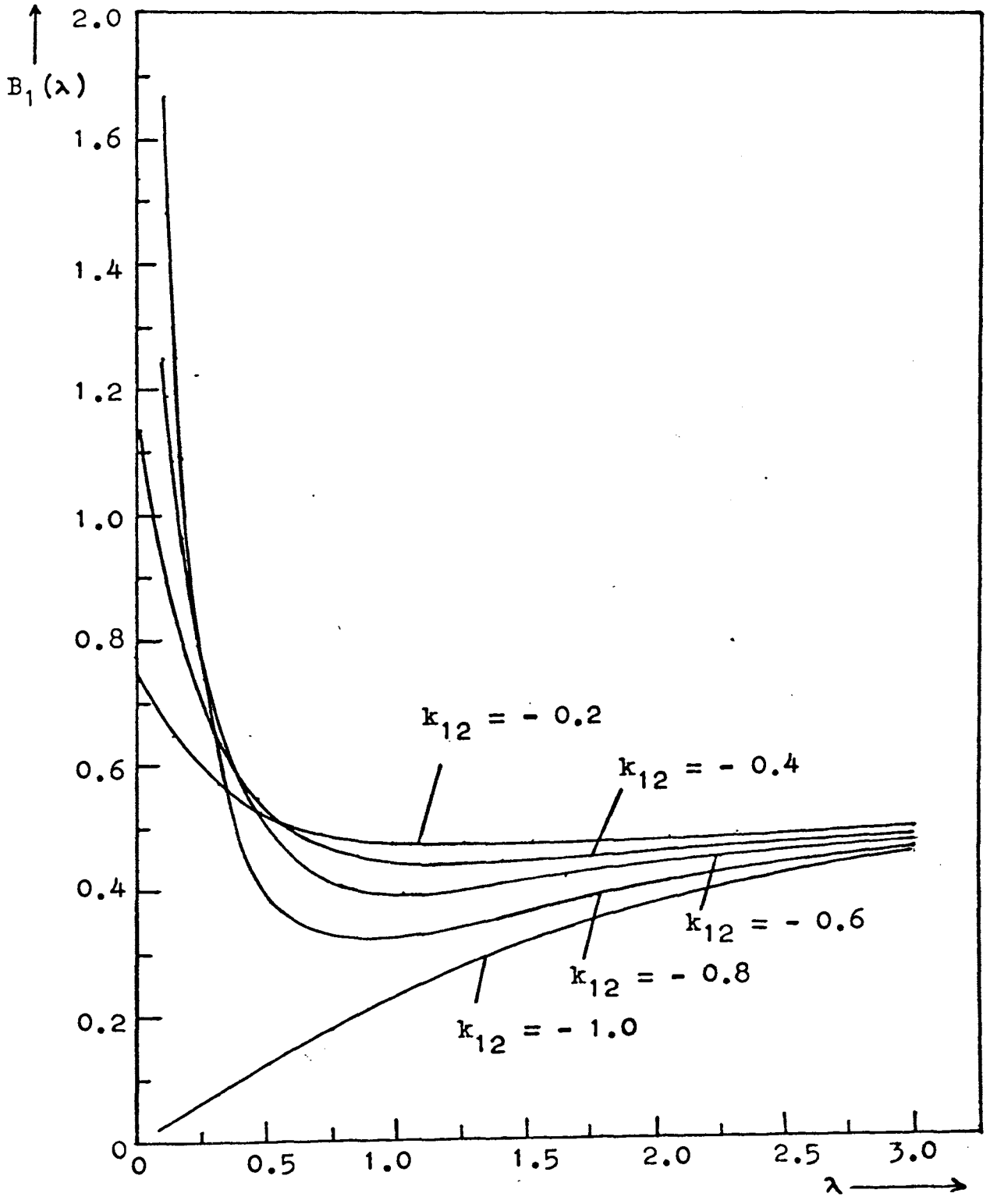

Fig. 4.18. Curves of two-layer associated kernels with negative reflection factors.

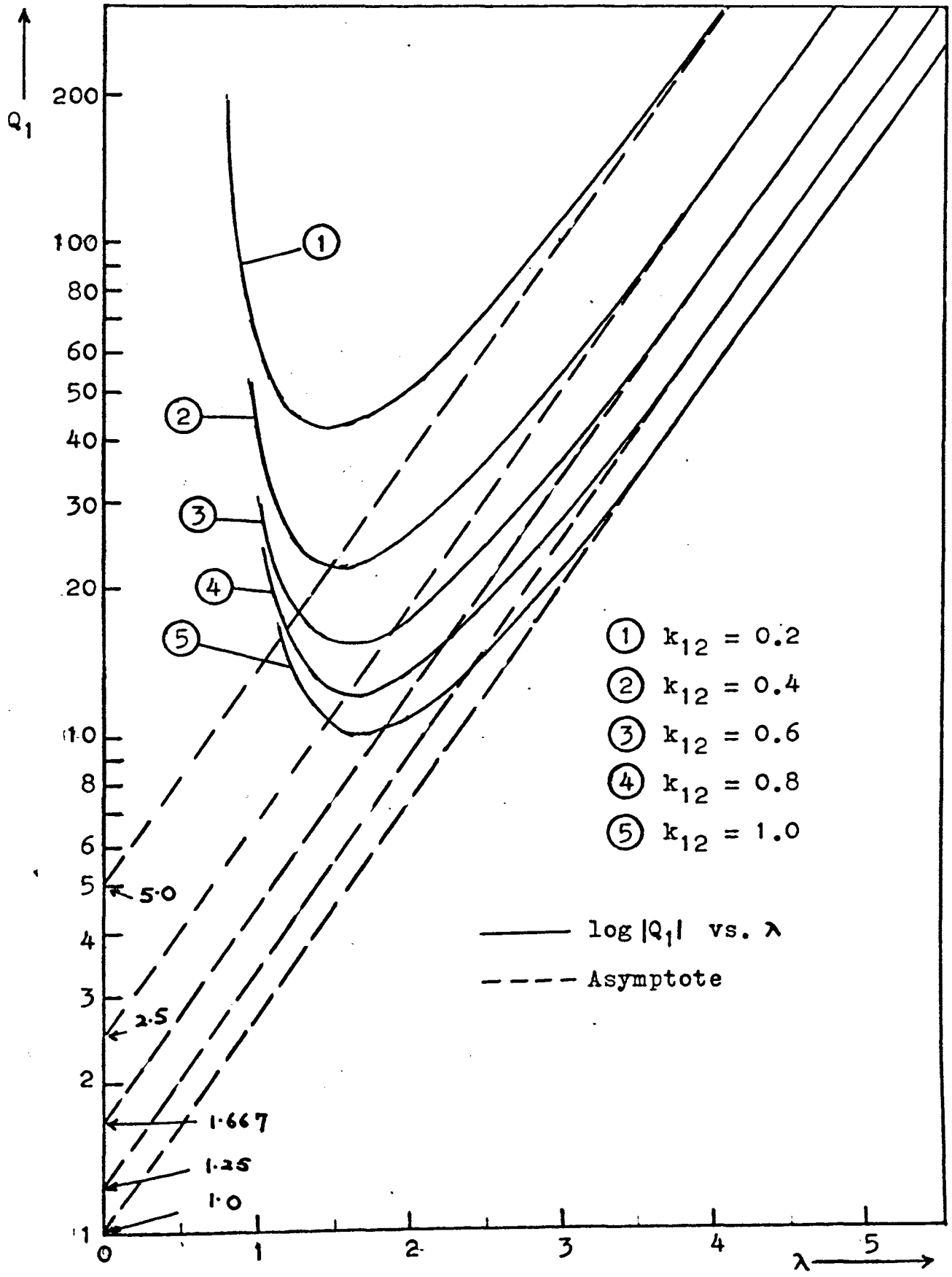

Fig. 4.19. Analysis of two-layer associated kernels with positive reflection factors.

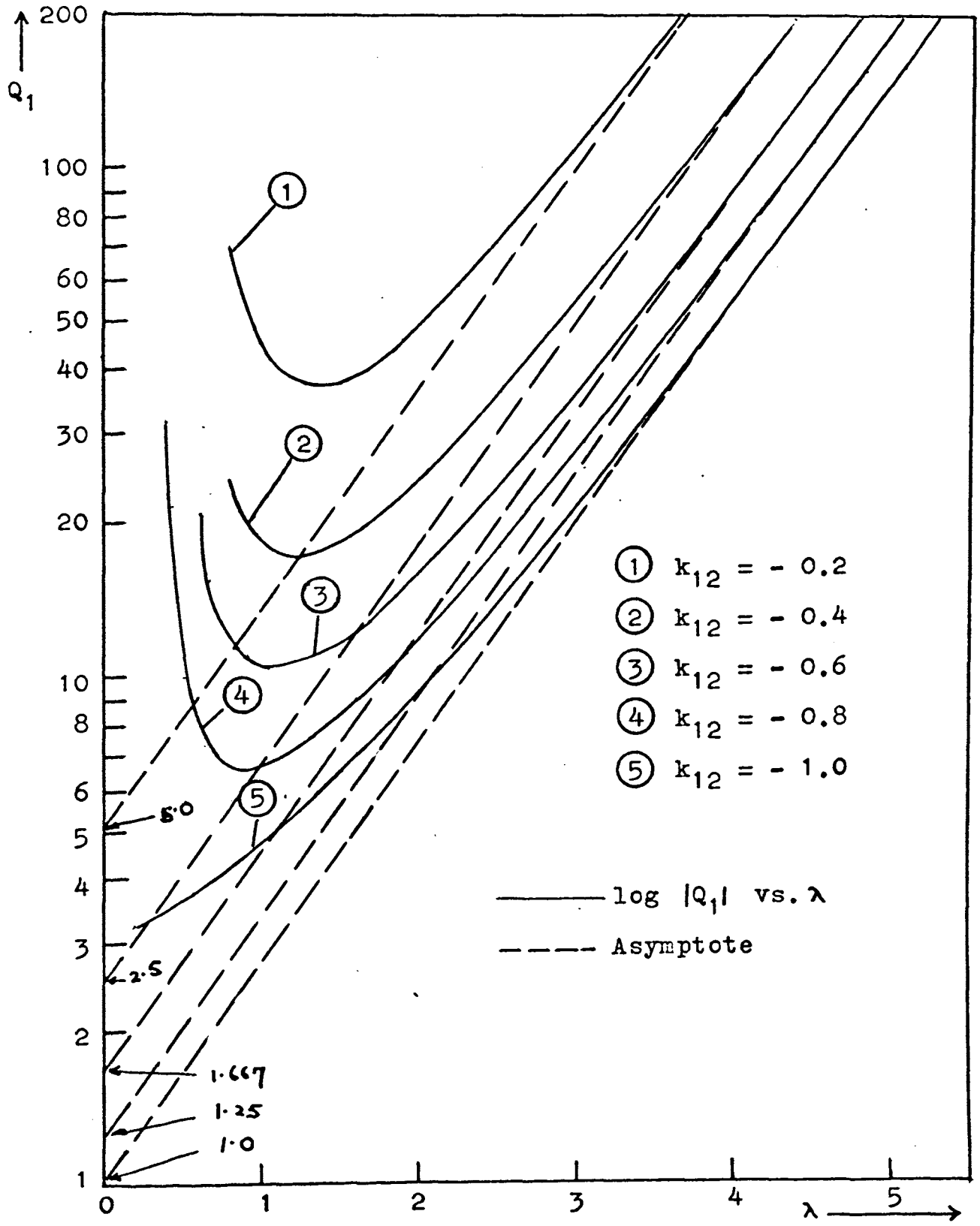

Fig. 4.20. Analysis of two-layer associated kernels with negative reflection factors.

with the two-layer kernel the function $\log|Q_1|$ is not a linear function of λ. Furthermore one notices that two different two-layer structures with identical thickness, but the reflection factors being of opposite signs, are associated two different $\log|Q_1|$ which approach to the same asymptote at large λ. This common asymptote is represented by (4.28) and its intersection with the vertical axis depends only on the absolute value of the reflection factor k_{12}.

The layer thickness d_1 and the absolute value of the reflection factor k_{12} for each two-layer structure are determined from the slope and the intercept of the asymptote respectively. These determinations can be carried out graphically by means of a master diagram of the asymptote similar to the one shown in Fig. 4.5. The correct sign of k_{12} cannot be determined from the graph of $\log|Q_1|$ itself. However, a study of the behavior of Q_1 as a function $B_1(\lambda)$ will provide the clue to the correct sign of k_{12}. From the definition of Q_1 given by (4.27) one observes that $Q_1 < 0$, $B_1(\lambda) < 0.5$; $Q_1 > 0$, $0.5 < B_1(\lambda) < 1.5$; $Q_1 < 0$, $B_1(\lambda) > 1.5$; $Q_1 \to -\infty$ as $B_1(\lambda) \to 0.5 -$; and $Q_1 \to +\infty$ as $B_1(\lambda) \to 0.5 +$. These properties of Q_1 are illustrated in Fig. 4.21. Fig. 4.22 shows the curve of an associated kernel for the case $k_{12} = 1.0$ and also the curve of the related function Q_1. Similar curves for the case $k_{12} = -0.8$ are shown in Fig. 4.23. We note that in the case with $k_{12} = 1.0$ Q_1 is positive beyond the point of discontinuity and its sign is reversed in the

case with $k_{12} = -0.8$. In general it is true that within the range in which the curve of $\log|Q_1|$ approaches its asymptote, k_{12} will be positive if Q_1 is positive and negative if Q_1 is negative.

Next, let us consider the analysis of the associated kernels of the three-layer case. Figs. 4.24, 4.25, 4.26, and 4.27 are typical examples of the curves of the associated kernels corresponding to the four groups of resistivity situations in the three-layer case, namely (i) $\rho_1 < \rho_2 > \rho_2$, (ii) $\rho_1 > \rho_2 < \rho_3$, (iii) $\rho_1 > \rho_2 > \rho_3$, and (iv) $\rho_1 < \rho_2 < \rho_3$. It may be noted that curves belonging to each group have a characteristic shape of their own.

Since the procedure of analysis is identical for all cases it is suffice for us to consider only the case $\rho_1 : \rho_2 : \rho_3 = 1 : 10 : 1/10$ for illustrative purpose. The results of the analysis is shown in Figs. 4.28, 4.29, 4.30, and 4.31. The first thing to be noted from these results is that the curve of $\log|Q_1|$ in each case looks almost like that of the function $\log|Q_1|$ obtained from the decomposition of two-layer associated kernel. Therefore, unlike the analysis of the kernel, it is not possible to tell from the graph of $\log|Q_1|$ whether one is dealing with a two-layer problem or with a more complicated multilayer problem. In order to make a decision a further step of calculation is needed to be carried out. This involves the calculation of U_1' from (4.33a). We note that $U_1' = k_{12}$ in the two-layer problem. Thus if the

result of computation indicates that U_1' is a constant equal to k_{12} then the structure under consideration is a two-layer one. The graph of $\log|Q_2|$ obtained from the second stage of decomposition is a straight line for each case. This result is in accordance with that predicted by (4.35). The fact that the graph of $\log|Q_2|$ is a straight line in the three-layer case can be used as an indication that no further inhomogeneity exists beneath the second boundary plane.

Next, let us study the behaviors of the functions Q_1 and Q_2. The behavior of the function Q_1 can readily be examined from each set of associated kernel curves together with Fig. 4.21 which shows the relation between Q_1 and $B_1(\lambda)$. Let us consider, for instance, the curves of Fig. 4.24. In each case the function Q_1 has two discontinuities because each curve of the associated kernel intersects the line $B_1(\lambda) = 0.5$ at two different points. Beyond the second point of intersection $B_1(\lambda)$ is less than 0.5 in all the four cases, thus implying that Q_1 will be negative beyond the second point of discontinuity along the λ-axis. We note that in this particular example the reflection factor k_{12} is negative because $\rho_1 < \rho_2$. Thus the sign of k_{12} is identical with that of Q_1 beyond the second point of discontinuity. Analysis of the other sets of curves of the associated kernel indicates the same conclusion.

According to (4.34) the behavior of Q_2 is dependent on K_2' which is defined by (4.30b). One may note that (4.30b)

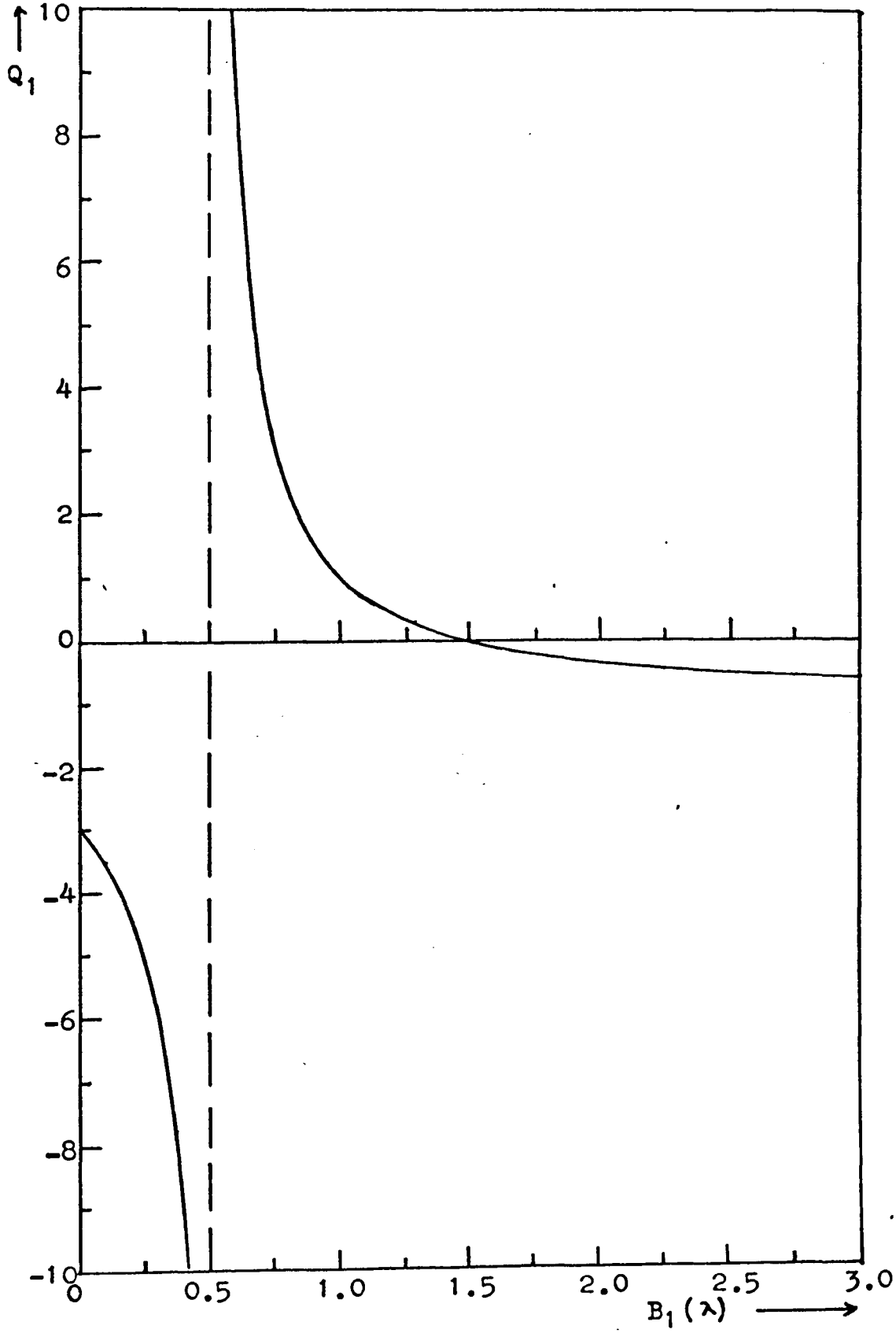

Fig. 4.21. General relation between the associated kernel and the function Q_1.

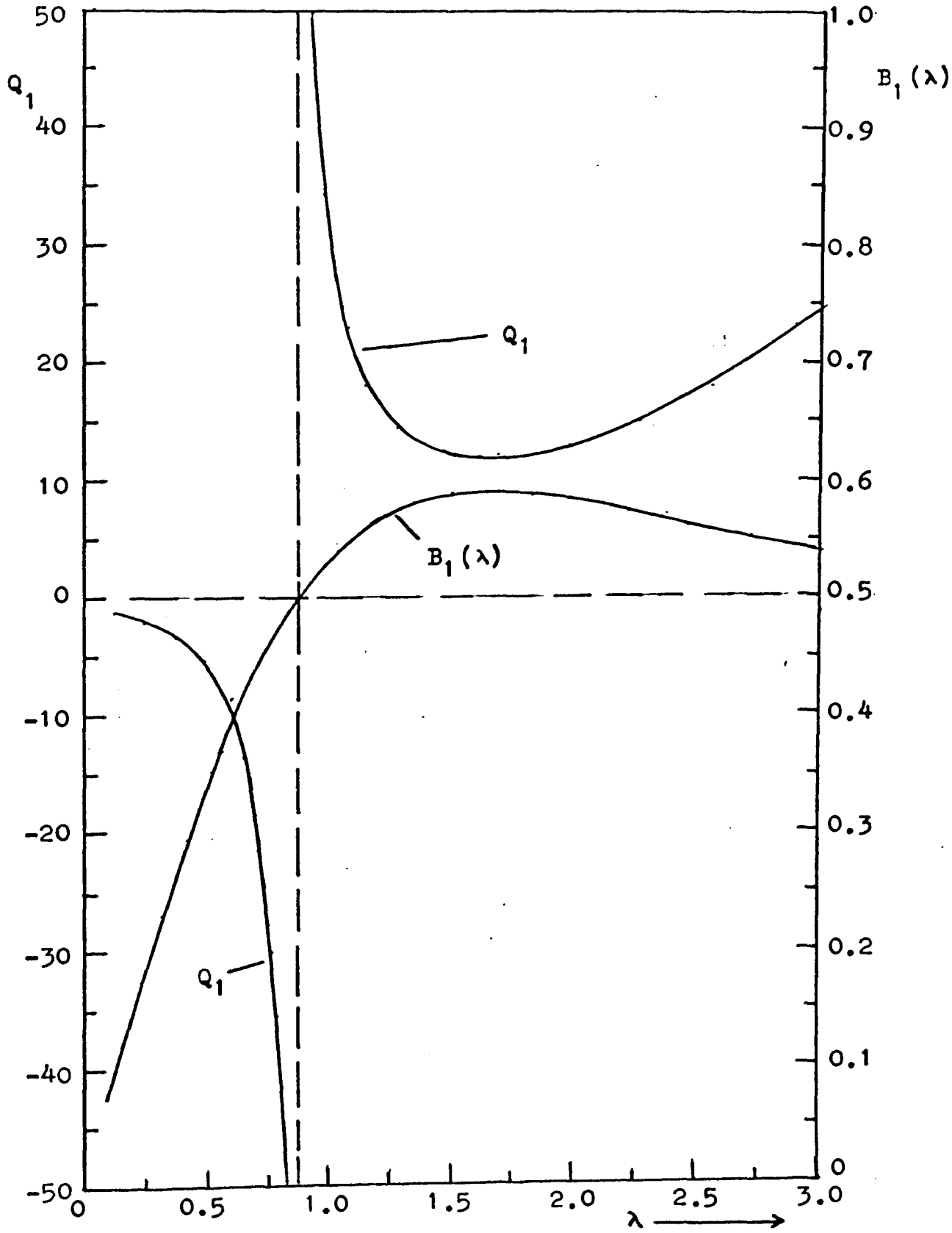

Fig. 4.22. The function Q_1 and its related two-layer associated kernel. Case $k_{12} = 1.0$.

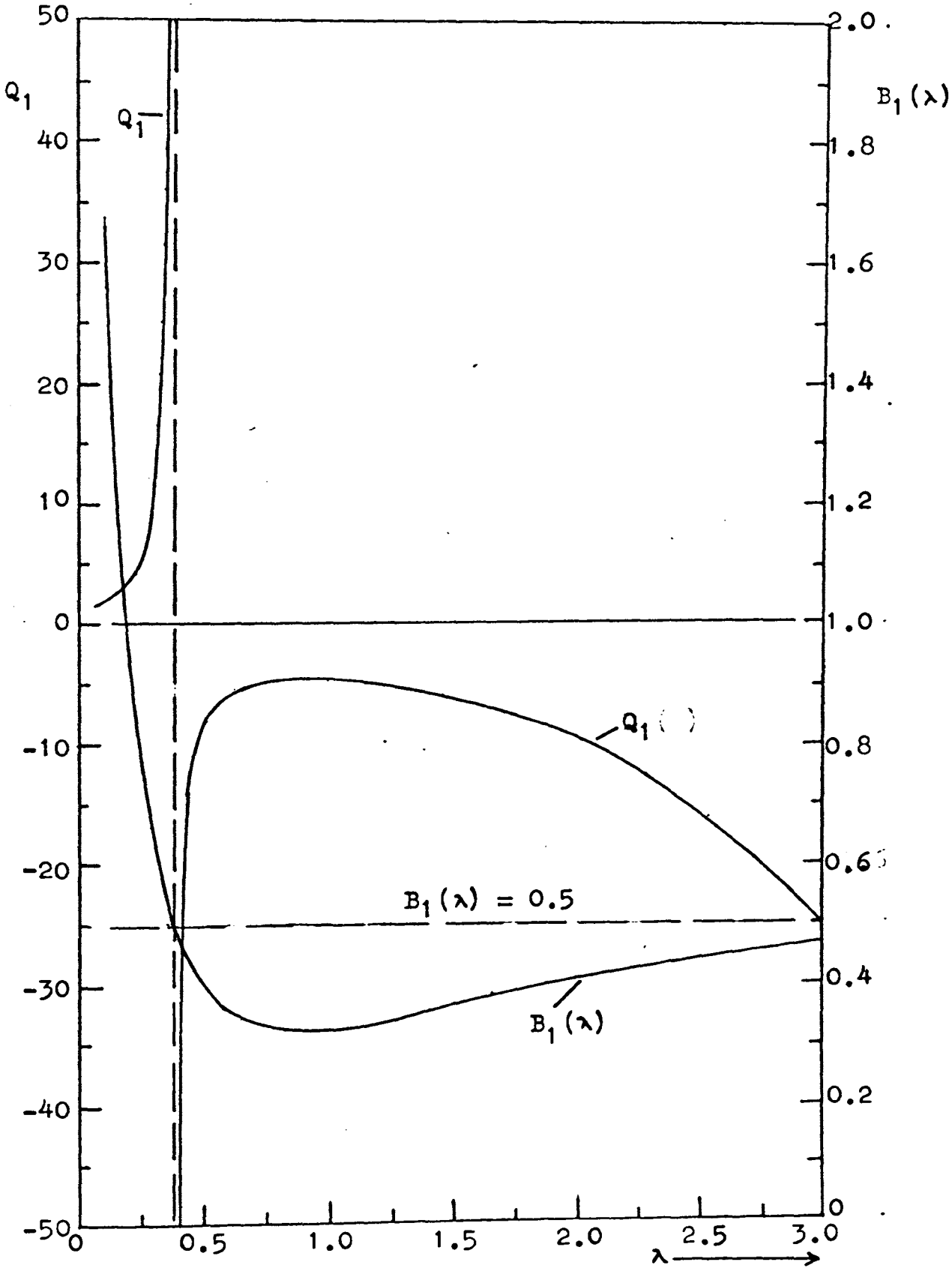

Fig. 4.23. The function Q_1 and its related two-layer associated kernel. Case $k_{12} = -0.8$.

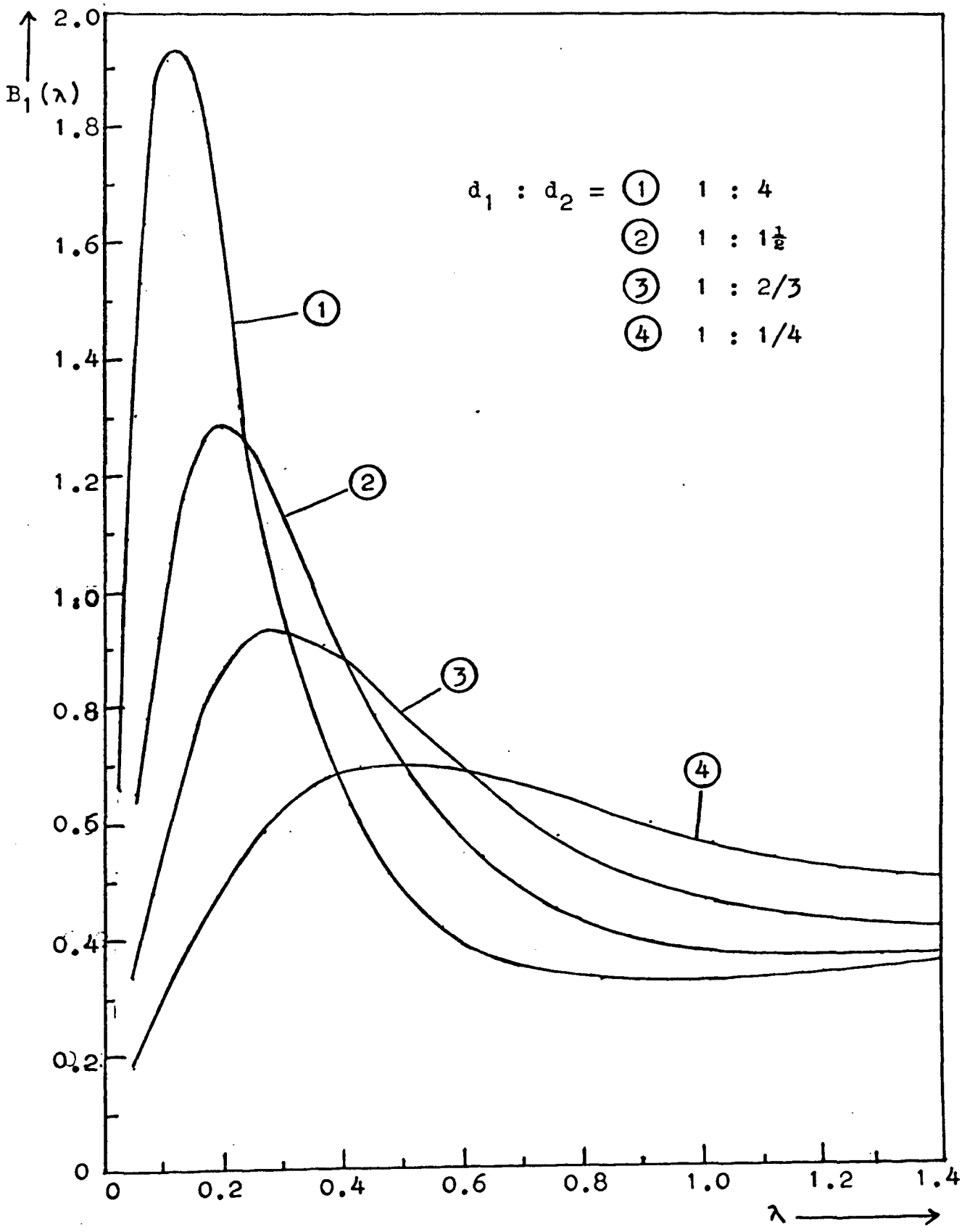

Fig. 4.24. Curves of three-layer associated kernels for the case $\rho_1 : \rho_2 : \rho_3 = 1 : 10 : 1/10$,

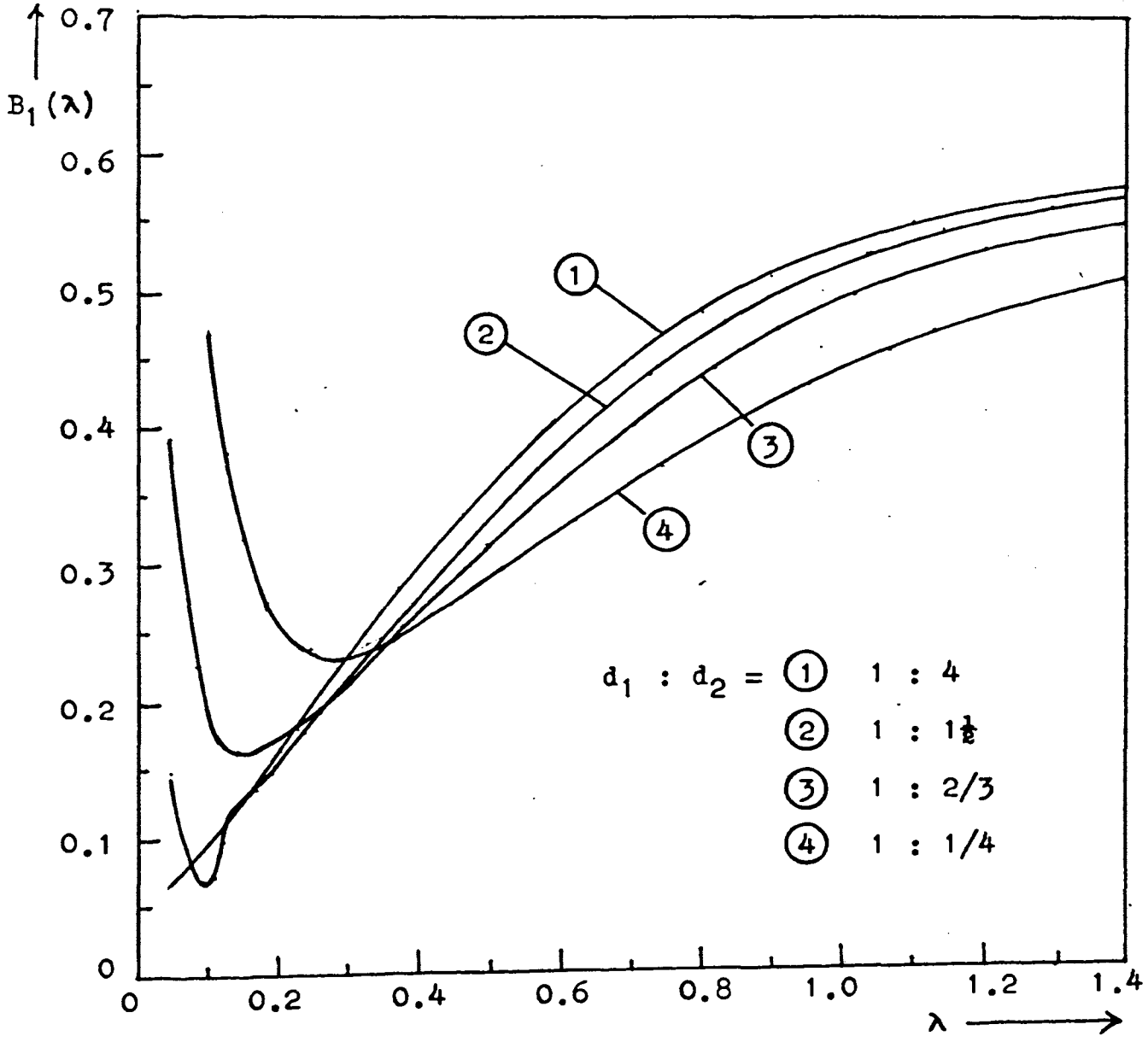

Fig. 4.25. Curves of three-layer associated kernels for the case $\rho_1 : \rho_2 : \rho_3 = 1 : 1/10 : 10$.

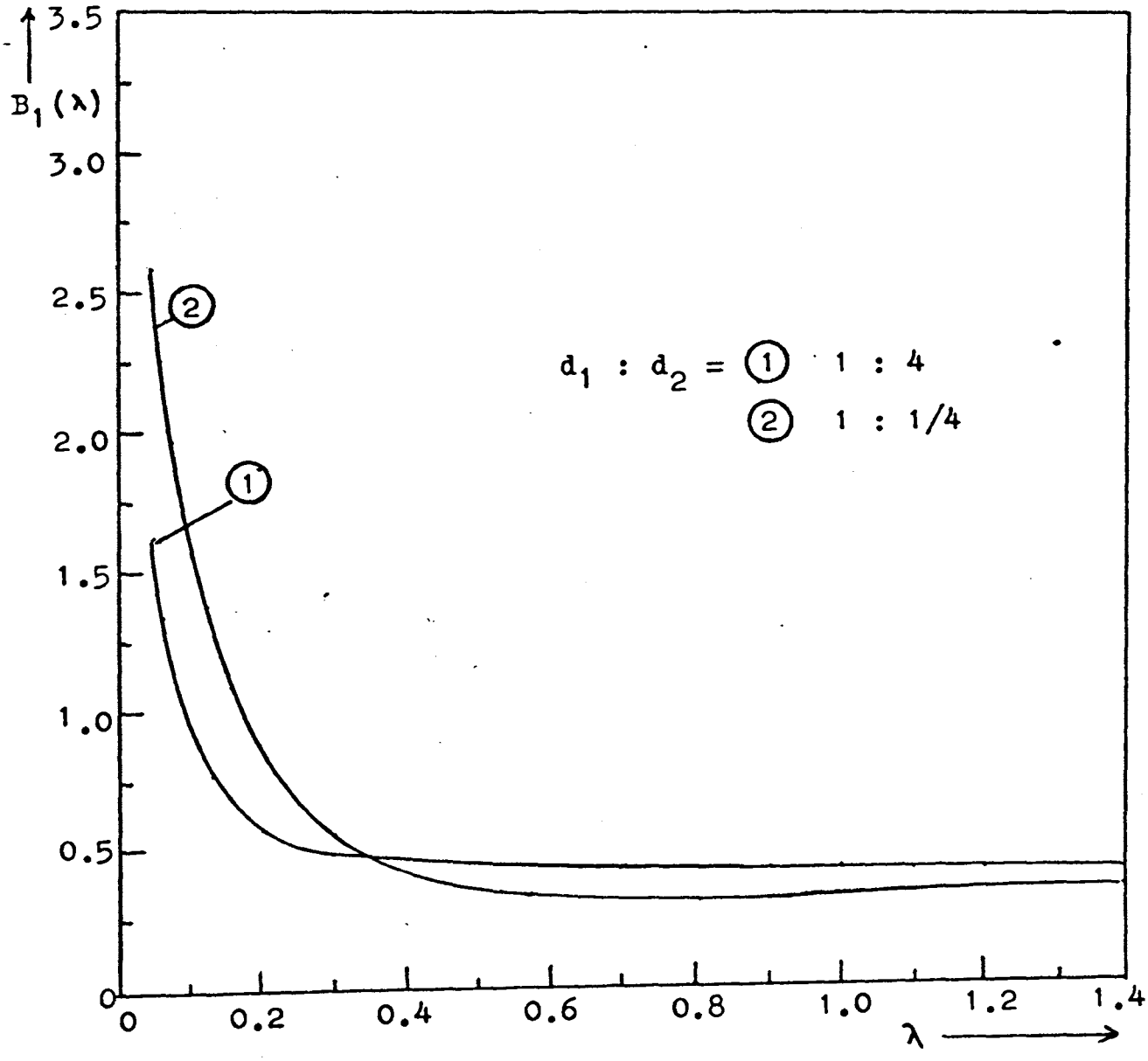

Fig. 4.26. Curves of three-layer associated kernels for the case $\rho_1 : \rho_2 : \rho_3 = 1 : 3 : 10$.

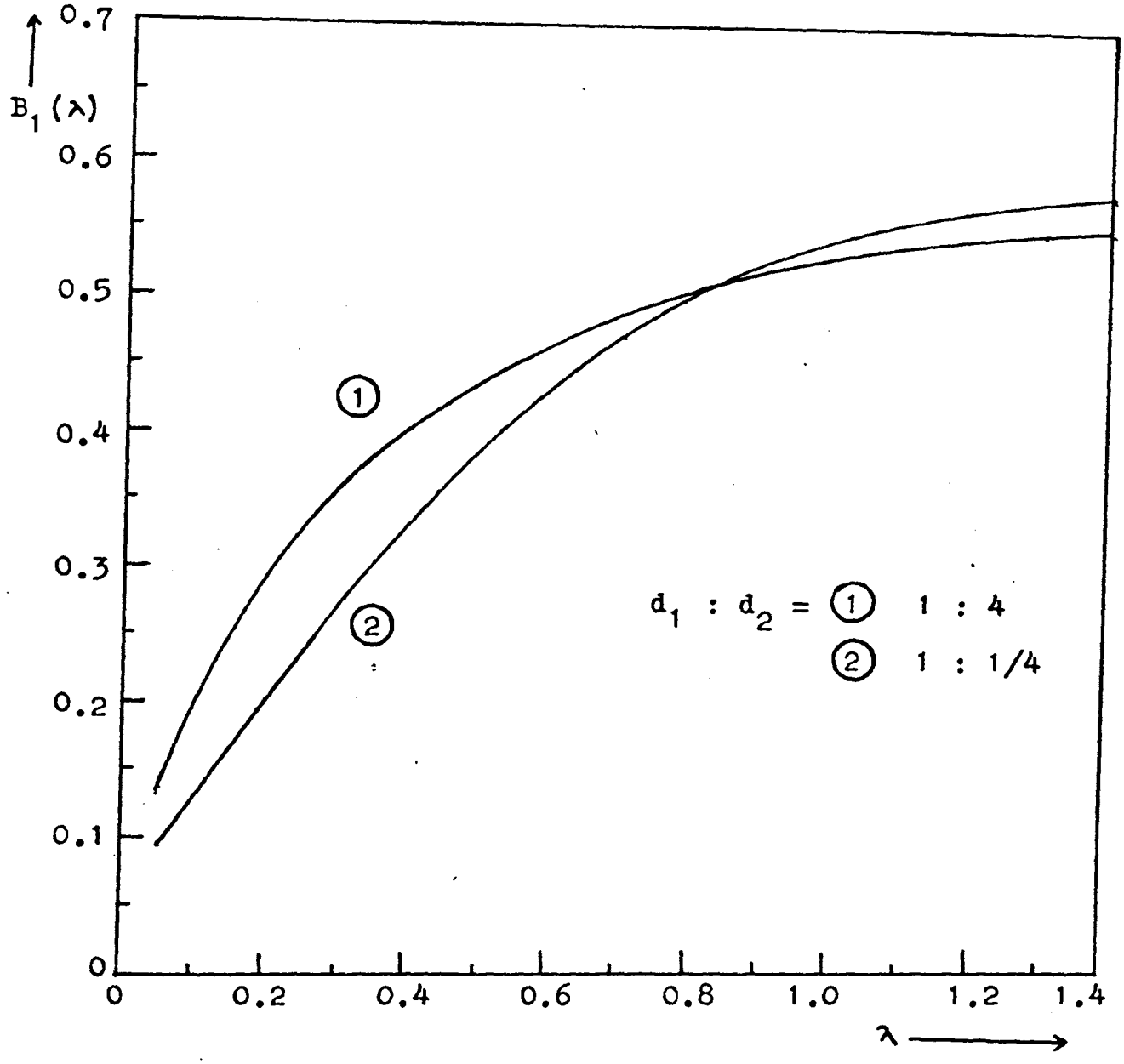

Fig. 4.27. Curves of three-layer associated kernels for the case $\rho_1 : \rho_2 : \rho_3 = 1 : 1/3 : 1/10$.

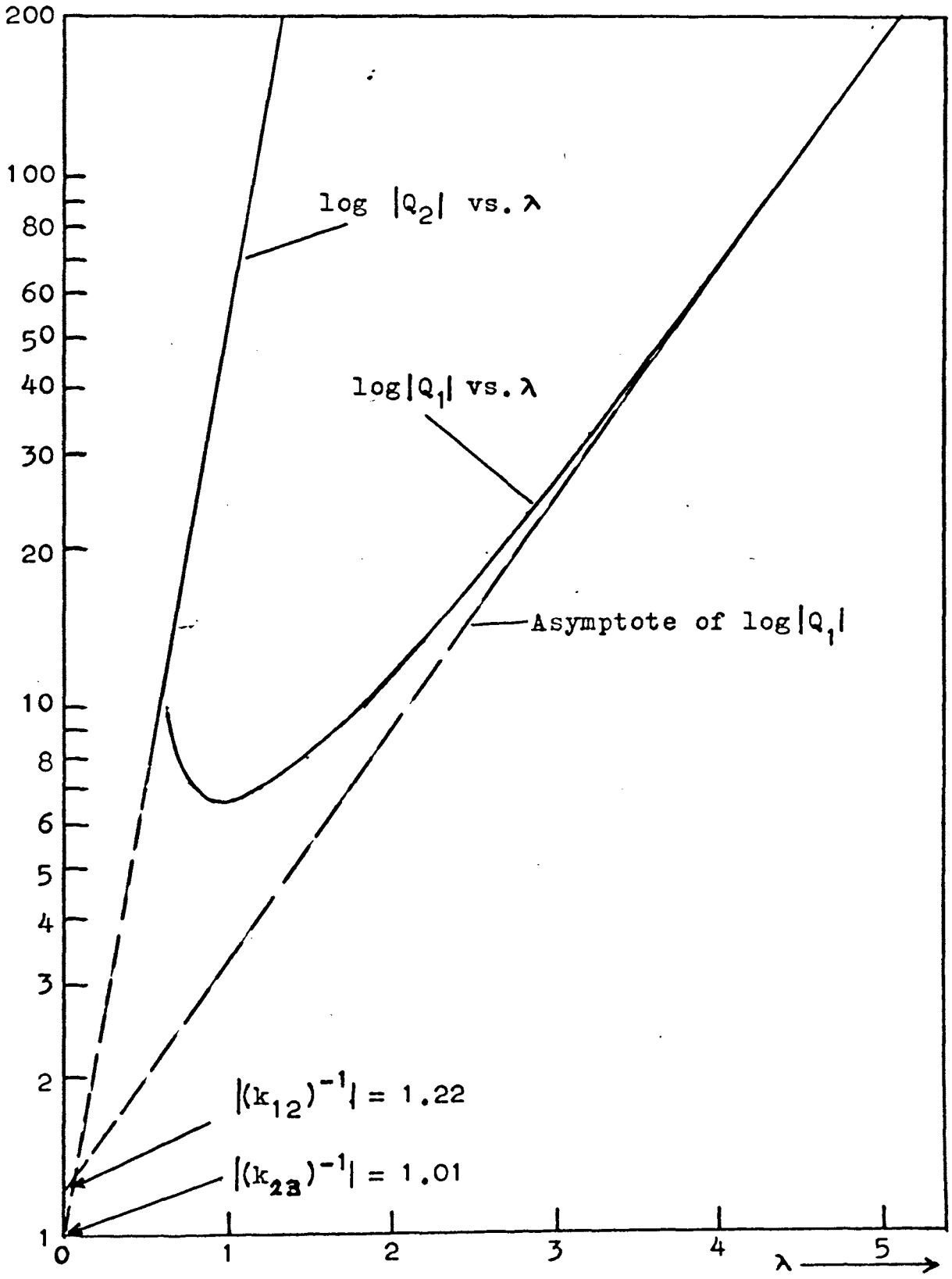

Fig. 4.28. Analysis of three-layer associated kernel of the case $\rho_1 : \rho_2 : \rho_3 = 1 : 10 : 1/10$, $d_1 : d_2 = 1 : 4$.

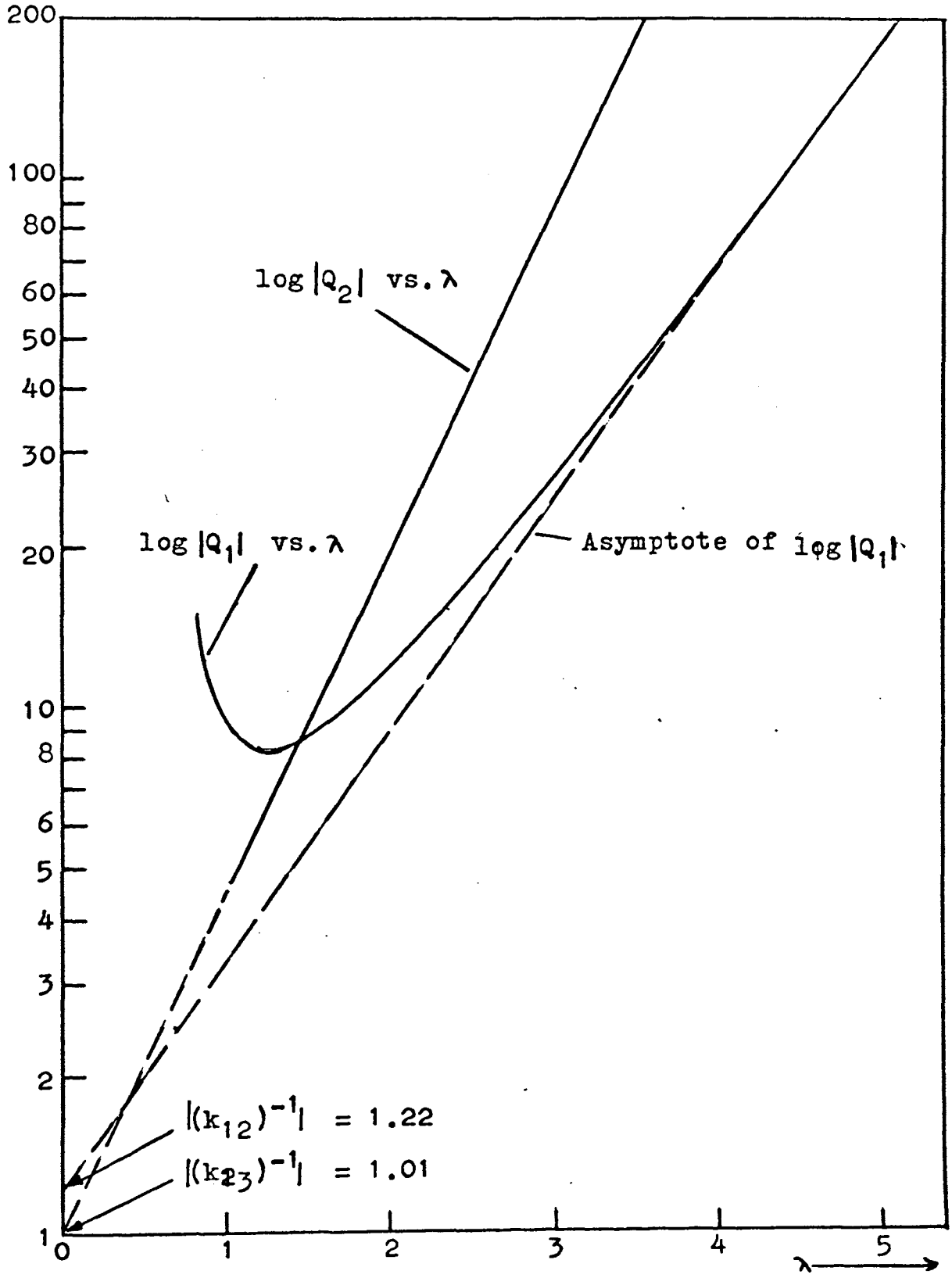

Fig. 4.29. Analysis of three-layer associated kernel of the case $\rho_1 : \rho_2 : \rho_3 = 1 : 10 : 1/10$, $d_1 : d_2 = 1 : 1\frac{1}{2}$.

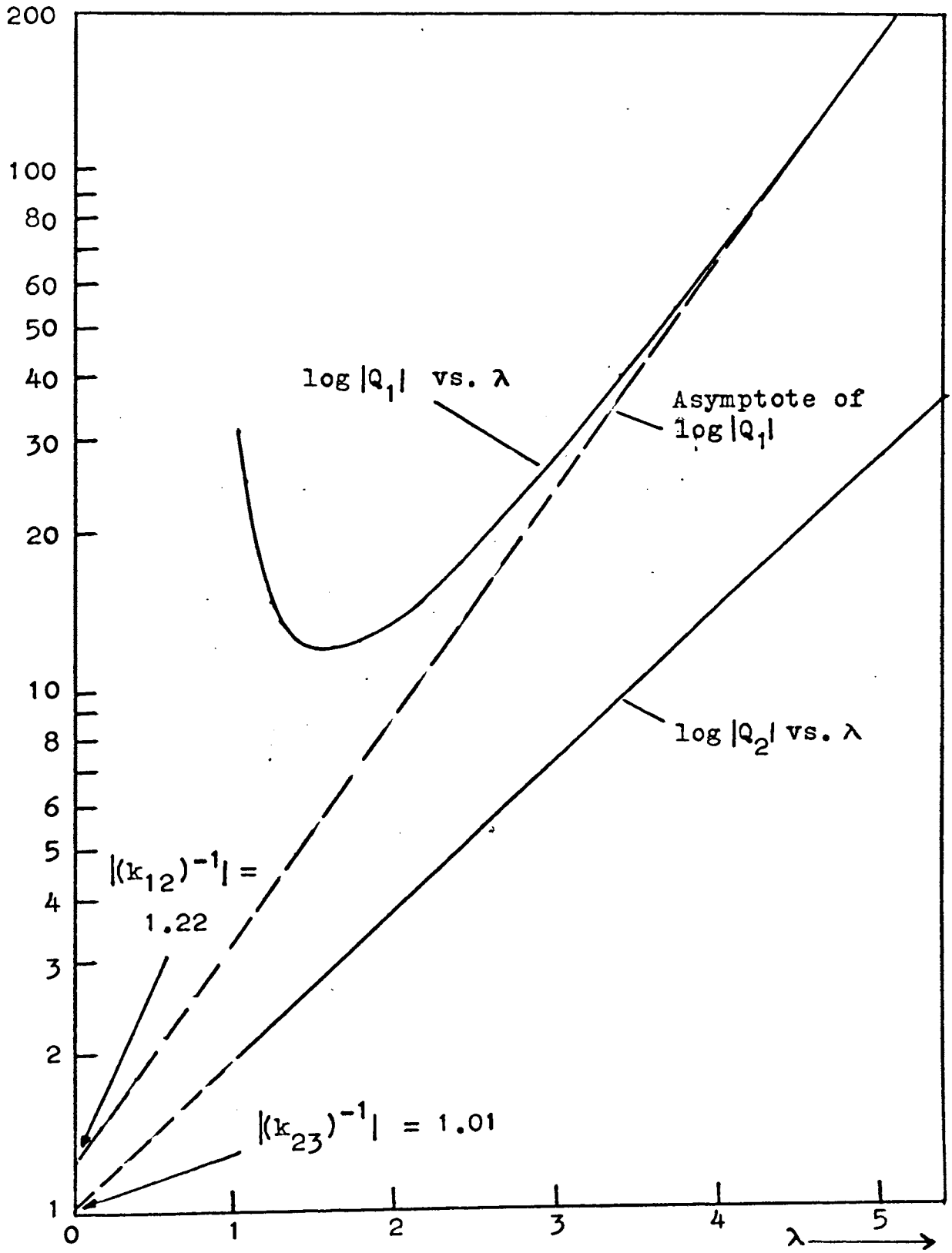

Fig. 4.30. Analysis of three-layer associated kernel of the case $\rho_1 : \rho_2 : \rho_3 = 1 : 10 : 1/10$, $d_1 : d_2 = 1 : 2/3$.

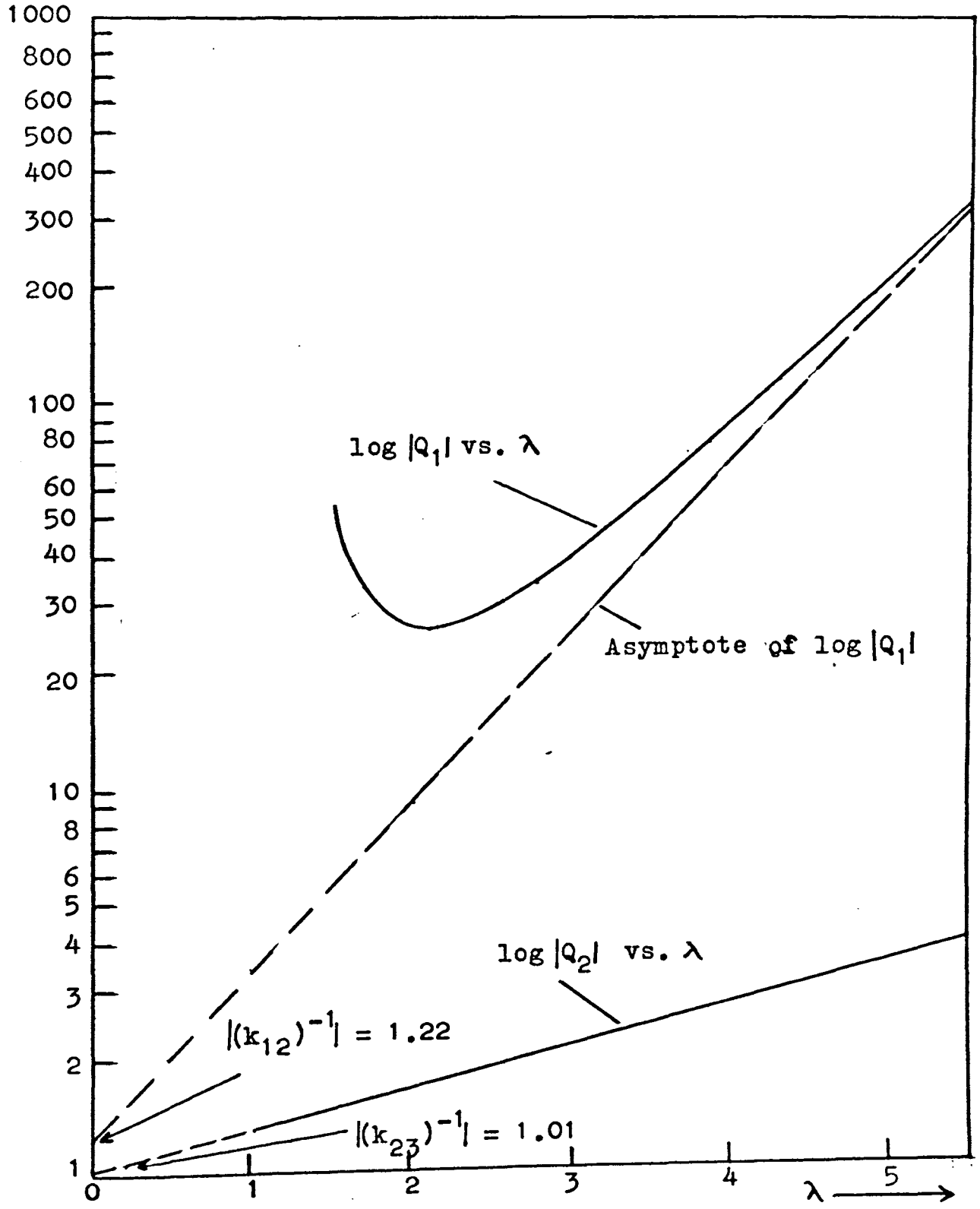

Fig. 4.31. Analysis of three-layer associated kernel of the case $\rho_1 : \rho_2 : \rho_3 = 1 : 10 : 1/10$, $d_1 : d_2 = 1 : 1/4$.

is almost identical with the equation for the two-layer kernel (i.e., equation (4.2)) excepting that 2λ has been replaced by λ. From (4.30b) it is evident that K_2' is less than unity if k_{23} is positive and is greater than unity if k_{23} is negative. Thus from (4.34), which is the definition of Q_2, one can conclude that positive values of Q_2 are related to positive reflection factor while negative values are related to negative reflection factor.

It may be noted that the thickness d_2 and the absolute value of k_{23} can be determined with the aid of a suitable master diagram of the asymptote of Q_1.

Since the analysis of other multilayer problems is exactly identical to that of the three-layer case we shall not consider further examples. An example of the analysis of a four-layer case is given in Appendix F.

Alternative Approach to the Analysis of the Kernel: Method of Logarithmic Curve-Matching

The technique of logarithmic curve-matching is well known to anyone who is concerned with the direct current resistivity method of prospecting. This technique was first developed for the analysis of apparent resistivity curves by Roman (1940) and is now widely used. The writer finds that with the aid of the formulas derived for the kernel it is possible to adopt the logarithmic curve-matching technique for the analysis of the kernel.

The principle of logarithmic curve-matching may be outlined as follows: Let us consider the two-layer kernel which is given by (4.2). The kernel may be written implicitly as

$$K_1 = f(\lambda d_1).$$

The coordinates of a point on the curve of K_1 plotted against λd_1 are $(K_1, \lambda d_1)$. In the logarithmic coordinate system the coordinates of the same point would be $(\log K_1, \log\lambda + \log d_1)$. Since d_1 is a constant the quantity $\log d_1$ is identical for all points on the curve. If an arbitrary value not equal to unity is assigned to d_1, then each point on the curve will be shifted a horizontal distance equal to $\log d_1$ with respect to the corresponding point on the curve for the case $d_1 = 1$. The shape of a curve plotted in logarithmic coordinates is preserved even when the abscissa of each point along the curve is multiplied by a constant factor. This preservation of curve shape in logarithmic coordinates is the basis for the curve-matching method of interpretation. We note that in this particular case of the two-layer kernel the shape of the curve of the kernel plotted in logarithmic coordinates is dependent only on the reflection factor k_{12}; two kernel curves having identical shape will correspond to two different two-layer structures which have the same reflection factor but their thicknesses for the first layer may be different.

Before we proceed to discuss the procedure for analyzing the kernel by means of the curve-matching method let us

recall some important properties of the kernel function. In our earlier analysis it has been shown that the function U_1 approaches k_{12} at large values of λ. This implies that the kernel $K_1(\lambda)$ of an n-layered structure is reduced essentially to one of a two-layer case when λ becomes very large. Next we note that the function K_i of Equation (4.1) is independent of the parameters d_j and ρ_j where j = i-1, i-2, i-3,.....3, 2, 1. Considering the three-layer case, for instance, the function K_2 is independent of d_1 and ρ_1, and it is identical to the kernel for a two-layer structure in which the top layer has a resistivity ρ_2 and thickness d_2, the bottom layer having a resistivity ρ_3 and an infinite thickness. From (4.1) one can see that the sequence of functions $\{K_i\}$, i = 1,2,... .., n-1, represents a sequence of n-1 layered structures, the number of layers in each structure being reduced by one as we go from one member of the sequence to the next member higher up in the sequence. Furthermore, each member of the sequence $\{K_i\}$ approaches the kernel of a two-layer structure having layer parameters $k_{i,i+1}$ and d_i, when λ becomes very large. The last function K_{n-1} is obviously the kernel of a two-layer structure.

The curve-matching method involves essentially the comparison of the curve of an unknown kernel with a master set of theoretical two-layer kernel curves computed for a series of different reflection factors, with the thickness d_1 being assumed to be unity. Figs. 4.32 and 4.33 are

examples of such curves. With the aid of the properties of the kernel function outlined above we can apply the curve-matching method to the decomposition of any multilayer kernel. The procedure of making analysis may be outlined as follows:

(i) The unknown kernel function is plotted on a tracing using bilogarithmic scales which are identical to those used for the master curves.

(ii) The tracing paper is then superimposed on the master diagram. With the abscissa on the tracing paper coinciding with that of the master curves the overlay is moved horizontally until a close fit is obtained between the unknown kernel and one of the theoretical curves.

It is important to note that if fitting is not possible for the entire range of λ then an attempt should be made to fit only that portion of the unknown kernel lying in the upper range of λ. In our discussion of the properties of the kernel we have noted that in multilayer problems the kernel function will approach asymptotically to the kernel for a two-layer structure when λ becomes large. Thus the fact that a complete matching between the unknown kernel and one of the theoretical curves is not possible means that the unknown kernel represents a structure that has more than two layers. This accounts for the reason why we should match only the upper portion of the unknown kernel when a complete matching is not possible.

In the case of complete matching the unknown kernel represents a two-layer structure which has a reflection factor identical to that of the theoretical curve that fits the unknown kernel. The thickness d_1 is given by the distance between the origin of the master diagram and the point at which the vertical axis of the tracing intersects the abscissa of the master diagram. If the unknown structure and the theoretical structure have the same thickness, then the two origins should coincide with each other.

In the case when only partial matching is obtained in the upper range of λ we have a multilayer problem. k_{12} and d_1 are still determined in the same way as in the two-layer case. In order to determine the next set of layer parameters, namely k_{23} and d_2, we proceed to the next step of our analysis.

(ii) Since d_1 is now a known quantity it is possible to calculate U_1 and subsequently K_2 from (4.18) and (4.19) respectively by putting i = 2. The resulting values of K_2 are then plotted on a tracing paper using bilogarithmic scales. The matching process is then repeated. If the unknown kernel represents a three-layer structure then the curve of K_2 should match one of the theoretical curves. Fig. 4.34 illustrates the analysis of a three-layer kernel for the case $\rho_1 : \rho_2 : \rho_3 = 1 : 10 : 1/10$, $d_1 = 1$ and $d_2 = 4$. We note that the curve of $K_1(\lambda)$ fits the theoretical curve with $k_{12} = -0.8$ at its upper range while the curve of K_2 matches the theoretical

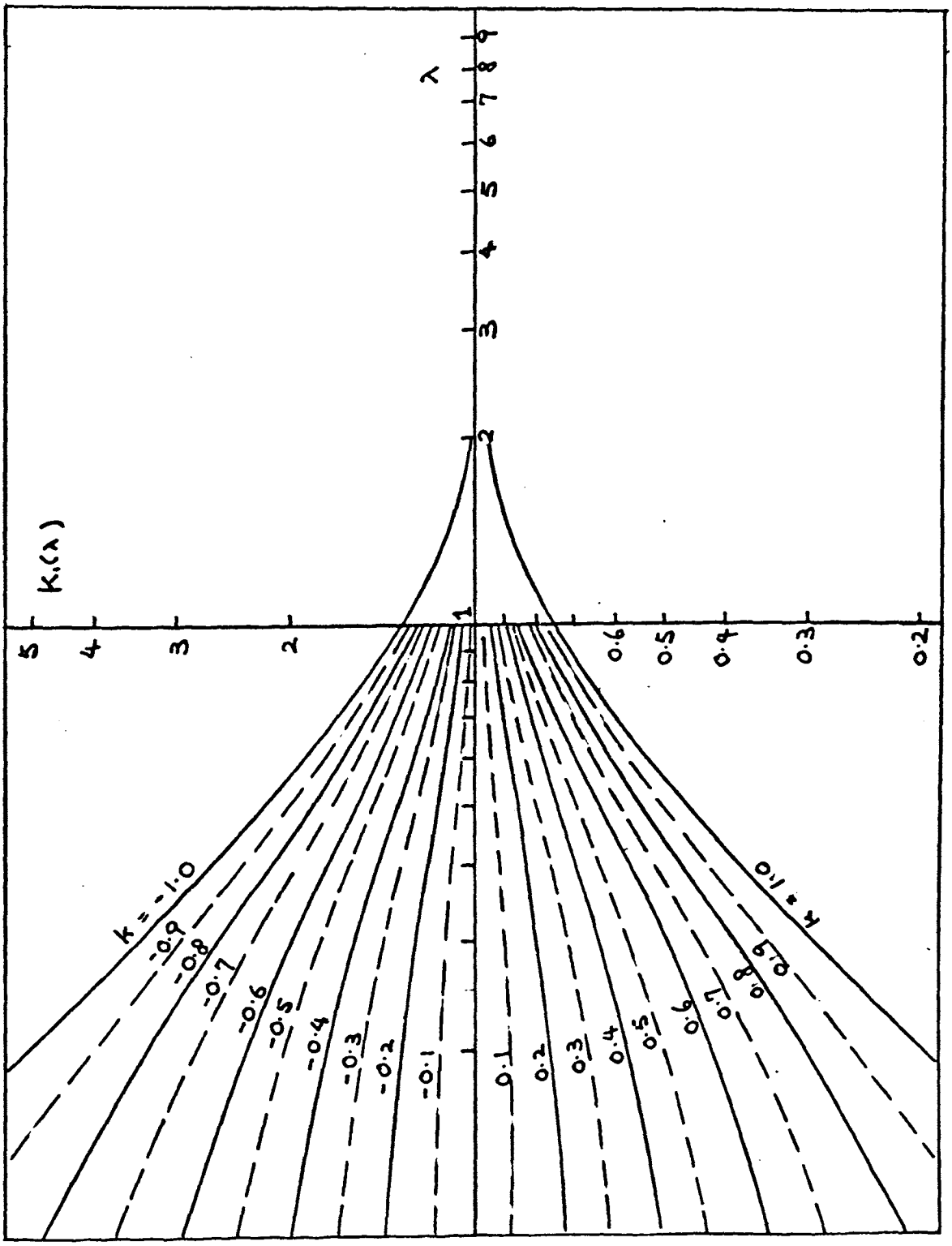

Fig. 4.32. Master set of two-layer kernel curves for cases with different reflection factors, logarithmic plotting.

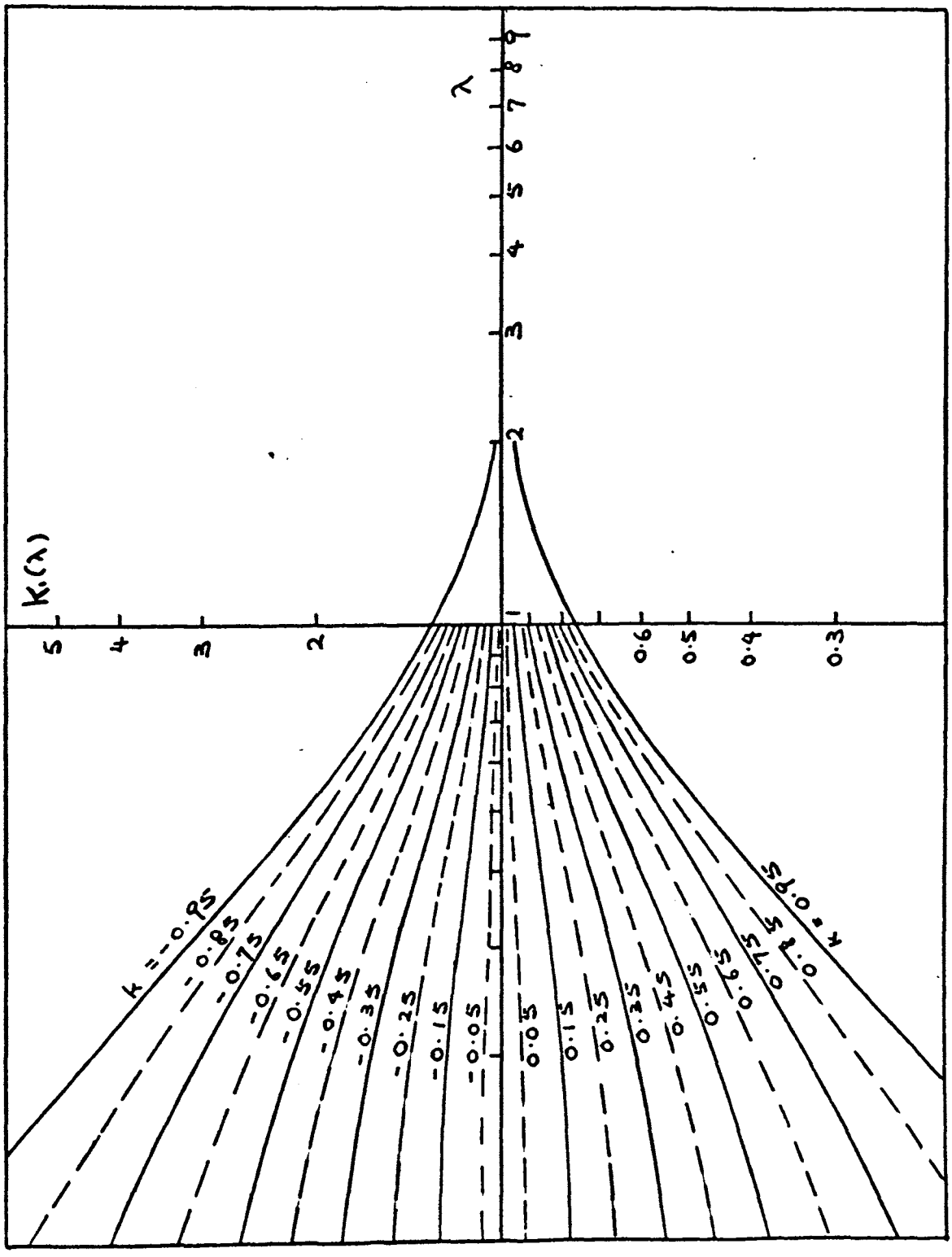

Fig. 4.33. Master set of two-layer kernel curves for cases with different reflection factors, logarithmic plotting.

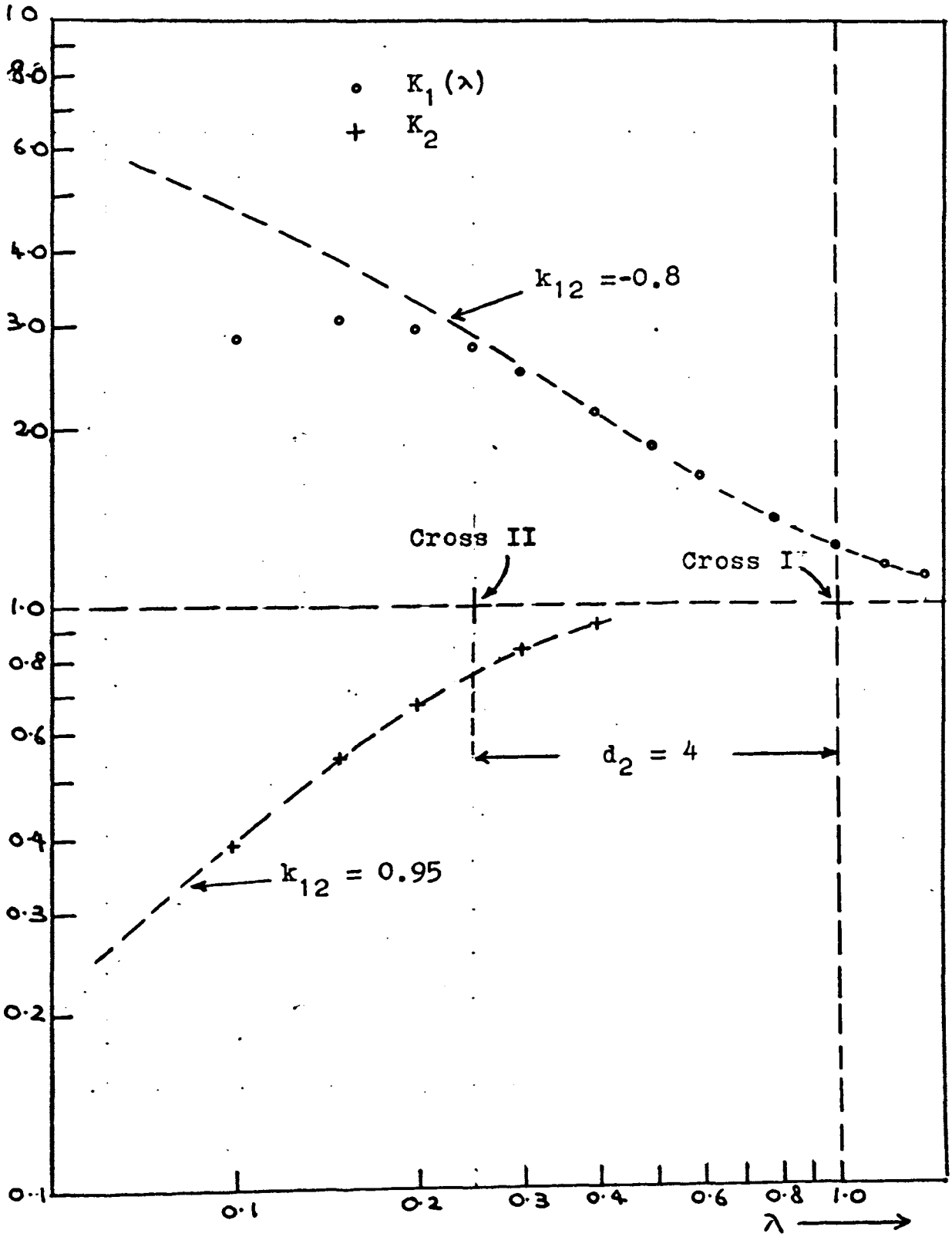

Fig. 4.34. Decomposition of a three-layer kernel by the method of logarithmic curve matching. Case $\rho_1 : \rho_2 : \rho_3 = 1 : 10 : 1/10$, $d_1 : d_2 = 1 : 4$.

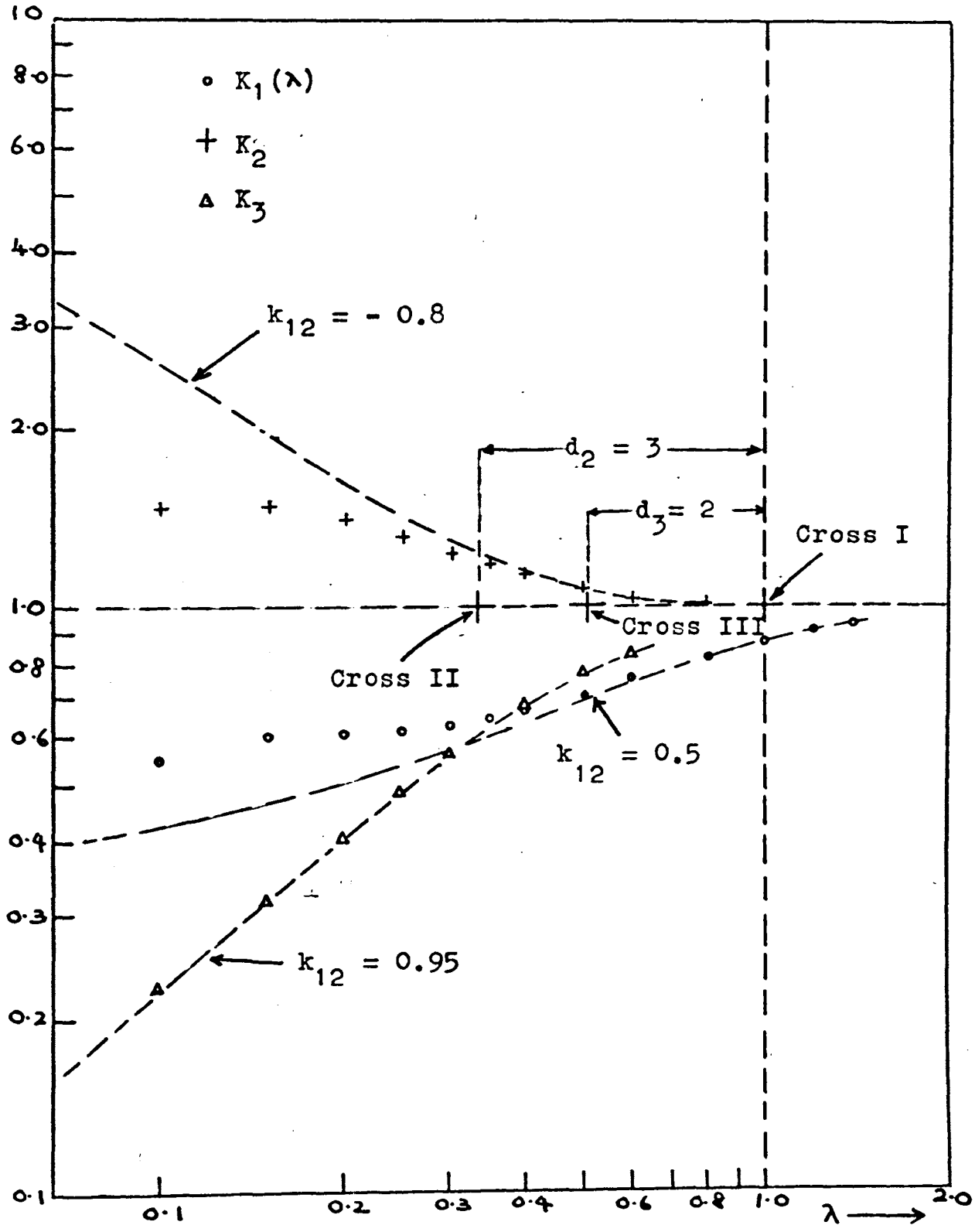

Fig. 4.35. Decomposition of a four-layer kernel by the method of logarithmic curve matching. Case $\rho_1 : \rho_2 : \rho_3 : \rho_4 = 1 : 1/3 : 3 : 1/10$, $d_1 : d_2 : d_3 = 1 : 3 : 2$.

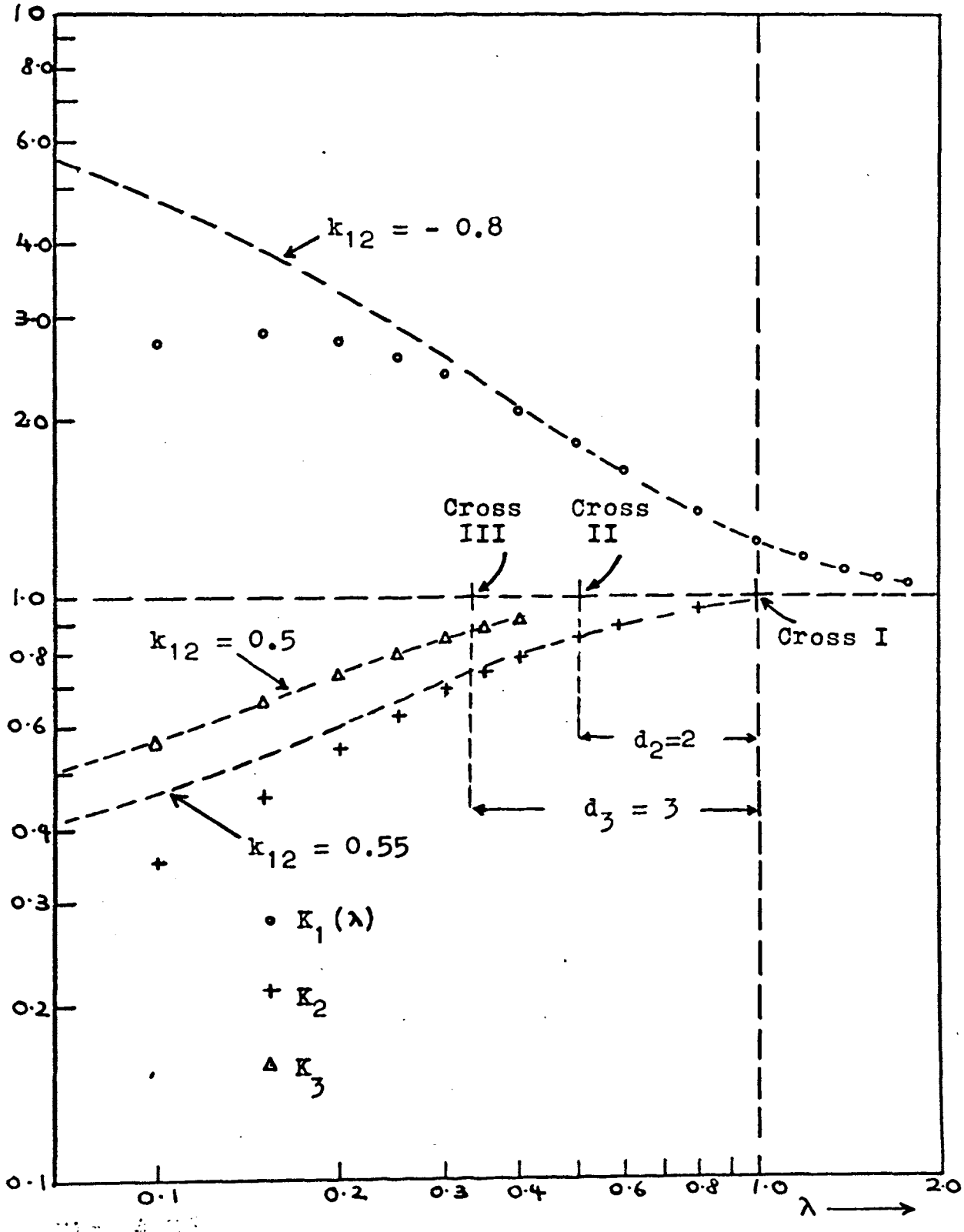

Fig. 4.36. Decomposition of a four-layer kernel by the method of logarithmic curve matching. Case $\rho_1 : \rho_2 : \rho_3 : \rho_4 = 1 : 10 : 3 : 1$, $d_1 : d_2 : d_3 = 1 : 2 : 3$.

curve with $k_{12} = 0.95$ completely. The crosses I and II are the positions of the origin of the master diagram for the first and second matchings respectively. From the positions of these crosses one finds that $d_1 = 1$ and $d_2 = 4$.

If only partial matching of the curve of K_2 is obtained this indicates the existence of a deeper layer (or layers). It is necessary to carry out the matching one step further by computing the functions U_2 and K_2 respectively from (4.18) and (4.19) with $i = 3$. Figs. 4.35 and 4.36 illustrate the analysis of two typical four-layer kernels.

(iv) In general the process of decomposing the kernel is considered to be completed if a complete match is obtained for the curve of K_i.

Limits of Solubility

In the study of apparent resistivity curves one may encounter the fact that certain three-layer resistivity situations, nominally quite different, have apparent resistivity curves which are identical to a first approximation. This problem is found to be associated with the cases of thin intermediate layers of resistivity either much higher or lower than that of the top and bottom layers. Explanation for this phenomenon may be obtained by examining the kernel function.

The three-layer kernel is expressed analytically by (4.9a). The function U_1 appearing in (4.9a) may be written

out explicitly in the form

$$U_1 = \frac{(\rho_1 - \rho_2)(\rho_2 + \rho_3) + (\rho_1 + \rho_2)(\rho_2 - \rho_3)e^{-2\lambda d_2}}{(\rho_1 + \rho_2)(\rho_2 + \rho_3) + (\rho_1 - \rho_2)(\rho_2 - \rho_3)e^{-2\lambda d_2}}$$

When the thickness of the intermediate layer is assumed to be so thin that $e^{-2\lambda d_2} \simeq (1 - 2\lambda d_2)$ the above expression for U_1 may be written as

$$U_1 = \frac{(\rho_1 - \rho_2)(\rho_2 + \rho_3) + (\rho_1 + \rho_2)(\rho_2 - \rho_3)(1 - 2\lambda d_2)}{(\rho_1 + \rho_2)(\rho_2 + \rho_3) + (\rho_1 - \rho_2)(\rho_2 - \rho_3)(1 - 2\lambda d_2)}$$

$$= \frac{1 - 3 - \dfrac{(\rho_1 + \rho_2)}{\rho_2} \cdot \dfrac{(\rho_2 - \rho_3)}{\rho_2} \lambda\rho_2 d_2}{1 + 3 - \dfrac{(\rho_1 - \rho_2)}{\rho_2} \cdot \dfrac{(\rho_2 - \rho_3)}{\rho_2} \lambda\rho_2 d_2} \qquad (4.41)$$

When the resistivity of the intermediate layer is very high, compared to ρ_1 and ρ_3, we have a further approximation as follows:

$$U_1 = \frac{\rho_1 - \rho_3 - \lambda\rho_2 d_2}{\rho_1 + \rho_3 + \lambda\rho_2 d_2} \qquad (4.42)$$

On the other hand, when the resistivity of the second layer is very low, compared to ρ_1 and ρ_3, (4.41) is reduced to

$$U_1 = \frac{\rho_1 - \rho_3 + \lambda\rho_1\rho_3 (d_2/\rho_2)}{\rho_1 + \rho_3 - \lambda\rho_1\rho_3 (d_2/\rho_2)} \quad . \qquad (4.43)$$

Let $C_1 = \rho_2 d_2$ and $C_2 = d_2/\rho_2$. When the values of d_2 and ρ_2 are such that C_1 or C_2 is a constant in all cases, this leads to the phenomenon that different three-layer resistivity situations have identical kernel to a first approximation, and thus identical apparent resistivity function also. Under such condition it is extremely difficult to distinguish any two cases that have identical C_1 or C_2. Fortunately the problem seldom arises as such in practice.

The problem of detecting a thin second layer still exists even though the resistivity of this layer does not belong to either one of the two extreme cases mentioned above. Let us consider two cases, the first of two layers

$$\rho_1 = 1 \qquad d_1 = 1$$

$$\rho_2 = 3 \qquad d_2 = \infty$$

and the second of three layers

$$\rho_1 = 1 \qquad d_1 = 1$$

$$\rho_2 = 10 \qquad d_2 = 1/10$$

$$\rho_3 = 3 \qquad d_3 = \infty$$

The values of the kernels corresponding to these cases are given in Table 4.1. Examination of these values shows that only a small difference exists between the value of the three-layer kernel and that of the two-layer kernel. In

TABLE 4.1 Comparison of a two-layer kernel with two three-layer kernels associated with the case of thin intermediate layer

λ	I	II	III
0.02	2.8491	2.8652	3.0261
0.04	2.7144	2.7433	3.0280
0.06	2.5936	2.6325	3.0100
0.08	2.4848	2.5315	2.9763
0.10	2.3862	2.4391	2.9305
0.20	2.0082	2.0753	2.6157
0.40	1.5795	1.6427	2.0159
0.60	1.3546	1.4050	1.6344
0.80	1.2246	1.2628	1.4042
1.00	1.1452	1.1736	1.2622

I. two-layer kernel with reflection factor $k_{12} = -0.5$

II. three-layer kernel for the case $\rho_1 : \rho_2 : \rho_3 =$ $1 : 10 : 3$, $d_1 : d_2 = 1 : 1/10$

III. three-layer kernel for the case $\rho_1 : \rho_2 : \rho_3 =$ $1 : 100 : 3$, $d_1 : d_2 = 1 : 1/10$

the last chapter we have shown that the deviations of the values of the kernel integrated from apparent resistivity data from its theoretical values are almost of the same order of magnitude. Thus it will be very difficult to detect the presence of a thin second layer by analyzing the kernel function, even when the resistivity of the second layer is 10 times greater than that of the surface layer. The increase in resistivity contrast may improve the resolving power of the kernel function associated with a thin second layer. This is evident by examining the values of the kernel for the case $\rho_2 = 100$ as shown in Table 4.1.

Further examples which illustrate the difficulty involved in distinguishing a three-layer kernel associated with a thin second layer from that of a two-layer case are shown in Figs. 4.9 and 4.10. The dash curves shown on these figures are curves of two-layer kernels. In Fig. 4.10 we can see that when the thickness d_2 of the intermediate layer is only ¼ that of the surface layer the three-layer kernel deviates only slightly from the two-layer kernel. The distinction between the two kernels is even worse in the case shown in Fig. 4.9.

In general one may conclude that the resolving power of the kernel is dependent both on the resistivity contrast and the relative thickness of the intermediate layer. The ability to distinguish between two nearly identical cases is limited by the accuracy of the data.

CHAPTER V

SUMMARY AND CONCLUSION

This investigation was primarily concerned with the interpretation of resistivity sounding data measured by the Wenner electrode system. More specifically, there were two main objectives: (i) to derive from the apparent resistivity data directly some functions from which the resistivity and thickness of each member of the sequence of layers composing the earth might be determined, and (ii) to devise suitable methods for the analysis of the resulting functions.

In this study it was assumed that the earth might be approximated by an n-layer model. It was shown that the solution of the boundary value problem associated with the model of an n-layer earth led to an integral equation for the Wenner electrode system. This integral equation relates the apparent resistivity function to an unknown function, termed the kernel, which depends on the layer resistivities and thicknesses. A solution of this integral equation was obtained by the use of a Hankel transform. The solution did not give rise to the kernel directly, but rather to a related function, termed the associated kernel. A simple relation exists between the kernel and the associated kernel and this is given by (2.20). From the associated kernel it was possible to derive an explicit integral expression of the kernel in terms of the known apparent resistivity function.

Numerical integration formulas based on the Legendre-Gauss quadrature formula were developed for the calculation of the kernel and the associated kernel respectively from apparent resistivity data. Since the apparent resistivity function is generally known only at a certain number of electrode separations by direct field observation, a method for generating unknown values of the apparent resistivity function from the known data is necessary because the process of integration requires a knowledge of the apparent resistivity function at points other than those input data points. It was found that the unknown values could be generated quite satisfactorily by the method of least-squares approximation using orthogonal polynomials obtained by Forsythe's method. Results of numerical integration show that there was close agreement between the integrated values of both the kernel and the associated kernel and their respective theoretical values.

It is of importance to note that in order to take care of the oscillating nature of the integrands associated with the integrals of both the kernel and the associated kernel it was necessary to divide the interval of integration into a number of subintervals so that the integrand of each integral might be sampled accurately. The choice of the number of subintervals is dependent on the parameter λ; generally the larger the value of λ the greater the number of subintervals will be needed. When a very large number of subintervals is

used the roundoff errors in the quadrature formulas may become a serious problem. So this appears to be the limitation on the use of the numerical integration formulas developed in this investigation. Fortunately in the course of analyzing the kernel and the associated kernel it was found that the values of these functions which are of interest for the determination of layer resistivities and thicknesses were associated with those values of λ lying within a small range (0,5). Within this range of λ we had obtained satisfactory results with the integration formulas.

In practice, apart from the errors inherent in the integration formulas, several other factors may influence the results of integration. These factors are (i) inaccuracy in the measurement of the apparent resistivity data, (ii) error in the least-squares approximation, (iii) uncertainty associated with the determination of a and b, and (iv) error in the measurement of ρ_1 and ρ_n.

Two methods were developed for the determination of layer resistivities and thicknesses. The first one is the numerical-graphical method which can be used for the analysis of both the kernel and the associated kernel. The other method which was developed mainly for the decomposition of the kernel is the method of logarithmic curve-matching. In practice, the numerical-graphical method may suffer two disadvantages: (i) there is not much latitude in the choice of the slope of the asymptote, and (ii) for large values of

thickness the intersection of the asymptote with the ordinate axis may not be very sharply defined due to steep slopes. These disadvantages may be partially offset by varying the scale of either the abscissa or the ordinate. The logarithmic curve-matching method does not possess these disadvantages.

The problem of detecting a thin intermediate layer in the three-layer case was considered. It was shown that unless a great contrast in resistivity exists the ability to detect the presence of a thin second layer is limited by the accuracy of the data.

REFERENCES

Bowman, Frank, 1958, Introduction to Bessel Functions: New York, Dover Publications, Inc., 135p.

Forsythe, G. E., 1957, Generation and use of orthogonal polynomials for data fitting with a digital computer: Journ. Soc. Indust. Appl. Math., V. 5, No. 2, p. 74 - 87.

Grant, F. S., and West, G. F., 1965, Interpretation theory in applied geophysics: New York, McGraw-Hill, 583p.

Hildebrand, F. B., 1956, Introduction to numerical analysis: New York, McGraw-Hill, 511p.

Kaplan, Wilfred, 1952, Advanced calculus: Reading, Addison-Wesley, 679p.

Keller, G. V., and Frischknecht, F. C., 1966, Electrical methods in geophysical prospecting: New York, Pergamon Press, 517p.

Koefoed, O., 1965, Direct methods of interpreting resistivity observations: Geophysical Prospecting, V. 13, No. 4, p. 568 - 592.

_____, 1966, The direct interpretation of resistivity observations made with a Wenner electrode configuration: Geophysical Prospecting, V. 14, No. 1, p. 71 - 79.

Langer, R. E., 1933, An inverse problem in differential equations: Am. Math. Soc. Bull., V. 39, p. 814 - 820.

Oliver, F. W. J., 1965, Bessel function of integer order, in Handbook of Mathematical Functions: New York, Dover Publications, Inc., 1046p.

Mooney, H. M., and Wetzel, W. W., 1956, The potentials about a point electrode and apparent resistivity curves for a two-, three-, and four-layer earth: Minneapolis, University of Minnesota Press, 146p. and 243 loose sheets of reference curves.

Pekeris, C. L., 1940, Direct method of interpretation in resistivity prospecting: Geophysics, V. 5, No. 1, p. 31 - 42.

Paul, M. K., 1968, A note on the direct interpretation of resistivity profiles for Wenner electrode configuration: Geophysical Prospecting, V. 16, No. 1, p. 159 - 162.

Ralston, Anthony, 1965, A first course in numerical analysis: New York, McGraw-Hill, 578p.

Roman, Irwin, 1940, Superposition in the interpretation of two-layer earth resistivity curves: U. S. Geol. Survey Bull. 927-A, 18p.

_____, 1960, Apparent resistivity of a single uniform overburden: U. S. Geol. Survey Prof. Paper 356, 99p.

Scott, E. J., 1955, Transform calculus: New York, Harper and Row, 330p.

Slichter, L. B., 1933, The interpretation of the resistivity prospecting method for horizontal structure: Physics, V. 4, p. 307 - 322.

Sneddon, Ian N., 1951, Fouries transform: New York, McGraw-Hill, 542p.

_____, 1955, Functional analysis, in Encyclopedia of Physics, V. 2: Berlin, Springer-Verlag, p. 198 - 347.

Stroud, A. H., and Secrest, Don, 1966, Gaussian quadrature formulas: New Jersey, Prentice Hall, Inc., 374p.

Sunde, Earling D., 1949, Earth conduction effects in transmission systems: Princeton, D. Van Nostrand, 370p.

Van Nostrand, R. G., and Cook, K. L., 1966, Interpretation of resistivity data: U. S. Geol. Survey Prof. Paper 499, 310p.

Vozoff, Keeva, 1956, Numerical resistivity analysis: Geophysics, V. 23, No. 3, p. 536 - 556.

APPENDIX A

CONCEPT OF APPARENT RESISTIVITY

The potential about a point current electrode located on the surface of a homogeneous ground of resistivity ρ_1 (Fig. A.1) is given by the equation

$$V = I\rho_1/2\pi R \qquad (A.1)$$

where R is the distance from the current electrode and I is the current introduced into the ground by the electrode. Suppose that we have a general four-electrode configuration located on the surface of the ground as shown in Fig. A.2. A potential difference of ΔV volts exists between the potential electrodes P_1 and P_2 when a direct current of I amperes flows between the current electrodes C_1 and C_2. This potential difference ΔV can readily be calculated by using (A.1). We note that since the potential function V is a scalar, then by the principle of superposition the potential at any point due to a number of current sources is simply equal to the sum of the potential contributions from each individual current source considered independently. Thus

$$\Delta V = I\rho_1 f/2\pi \qquad (A.2)$$

where

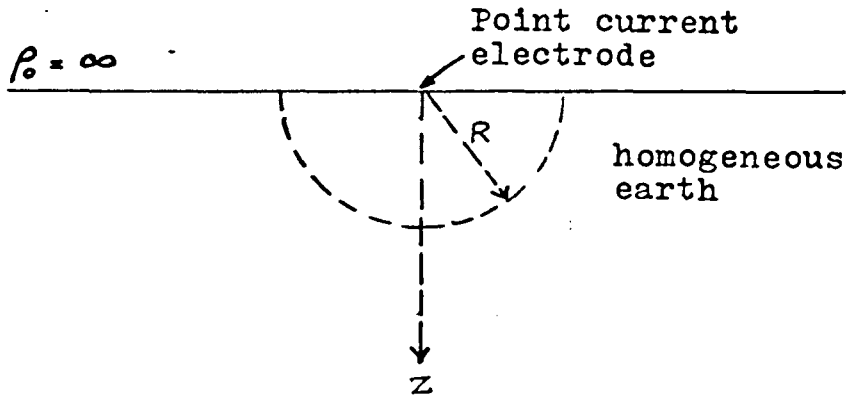

Fig. A.1. Point current electrode on surface of homogeneous earth.

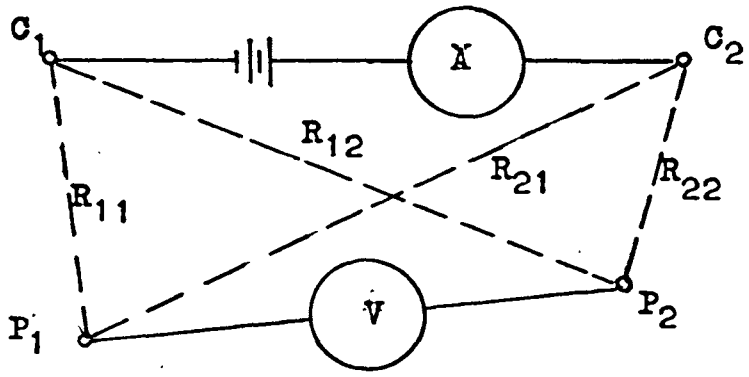

Fig. A.2. A general four-electrode configuration

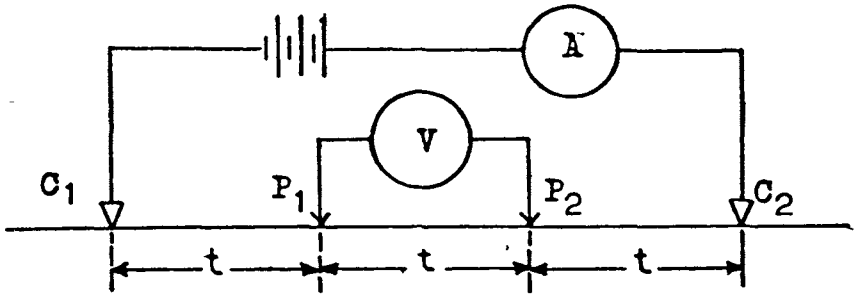

Fig. A.3. The Wenner configuration

$$f = \{\frac{1}{R_{11}} - \frac{1}{R_{21}} - \frac{1}{R_{12}} + \frac{1}{R_{22}}\} .$$

The function f which is generally known as the 'form factor' is clearly dependent only on the geometry of the electrode configuration. In practice the four electrodes are usually arranged along a straight line and there are many ways of positioning the potential electrodes with respect to the positions of the current electrodes. One of the most widely used configuration is the Wenner system as shown in Fig. A.3. In this configuration the electrodes are spaced at an equal distance t apart. The form factor f of this particular system takes a very simple form $f = 1/t$. It follows that the potential difference between P_1 and P_2 is given by

$$\Delta V = I\rho_1/2\pi t. \qquad (A.4)$$

Since only the Wenner configuration will be considered in this thesis we shall not describe the other electrode configurations here. The description of other electrode systems can be found in many references (e.g., Grant and West, 1965).

If the ground is completely homogeneous (A.4) can be used to calculate the true resistivity of the ground when measurements are made with the Wenner electrode configuration. If the ground is inhomogeneous then (A.4) is used as a definition for the 'apparent resistivity' of the ground -- the resistivity which the ground would have if it were homogeneous. By letting ρ_a to denote the apparent resistivity, it follows

from (A.4) that

$$\rho_a = 2\pi t \frac{\Delta V}{I} \qquad (A.5)$$

The apparent resistivity may bear no relation to any actual value of the resistivity in the inhomogeneous ground. It usually falls within the range of the true resistivities of the materials within the ground over which the measurements are made.

APPENDIX B

SOLUTION OF LAPLACE'S EQUATION IN THE N-LAYER CASE

The Laplace's equation

$$\frac{\partial^2 V}{\partial r^2} + \frac{1}{r}\frac{\partial V}{\partial r} + \frac{\partial^2 V}{\partial z^2} = 0 \qquad (B.1)$$

which was derived in Chapter II can be solved by the well known method of separation of variables. By assuming that $V(r,z) = F(r)G(z)$ in which $F(r)$ is a function of r only and $G(z)$ is a function of z only, (B.1) can be reduced to the following two ordinary differential equations:

$$\frac{d^2 G}{dz^2} - \lambda^2 G = 0 \qquad (B.2)$$

and

$$\frac{d^2 F}{dr^2} + \frac{1}{r}\frac{dF}{dr} + \lambda^2 F = 0 \qquad (B.3)$$

where λ is the separation constant. The two linearly independent solutions of (B.2) are $e^{\lambda z}$ and $e^{-\lambda z}$ while the two linearly independent solutions to (B.3) are the Bessel functions of zero order, namely $J_0(\lambda r)$ and $Y_0(\lambda r)$.

We note that $Y_0(\lambda r)$ has a logarithmic singularity at $r = 0$. Since the potential function $V(r,z)$ must be continuous along the positive z-axis except at the origin where the

current source is located, the solution which contains $Y_0(\lambda r)$ is not acceptable. The general solution to (B.1) which is obtained by linear superposition of terms of two types, namely $J_0(\lambda r)\ e^{\lambda z}$ and $J_0(\lambda t)\ e^{-\lambda z}$, is given by

$$V(r,z) = \int_0^\infty (A(\lambda)e^{-\lambda z} + B(\lambda)e^{\lambda z})J_0(\lambda t)\ d\lambda \qquad (B.4)$$

where $A(\lambda)$ and $B(\lambda)$ are arbitrary functions of λ.

Next, we note that the function,

$$V_p = I\rho_1/2\pi R$$

where $R = (r^2 + z^2)^{\frac{1}{2}}$, is also a solution of Laplace's equation. One immediately recognizes the fact that the function V_p is actually the potential about a point current source in a homogeneous medium. It is obvious that the sum of $V(r,z)$ and V_p is a solution of Laplace's equation. Thus we may write the solution to (2.11) as

$$V_i(r,z) = \frac{I\ \rho_1}{2\pi R} + \int_0^\infty (A_i(\lambda)e^{-\lambda z} + B_i(\lambda)e^{\lambda z})J_0(\lambda r)\ d\lambda \qquad (B.5)$$

where $i = 1,2,3,.....,n$. The inclusion of V_p into the solution makes the potential function V_1 satisfy the condition near the current source automatically.

The Laplace transform of $J_0(pr)$ is given by

$$\int_0^\infty J_0(pr)e^{-sp}\,dp = \frac{1}{(r^2 + s^2)^{\frac{1}{2}}}$$

(Scott, 1955). If we let s = z and p = λ then we get

$$\frac{1}{R} = \frac{1}{(r^2 + z^2)^{\frac{1}{2}}} = \int_0^\infty J_0(\ r)e^{-\lambda z}\ \ d\lambda\ .$$

Thus (B.5) can be written as

$$V_i(r,z) = \frac{I\rho_1}{2\pi}\int_0^\infty e^{-\lambda z}\ J_0(\lambda r)\ \ d\lambda$$

$$+ \int_0^\infty (A_i(\lambda)e^{-\lambda z} + B_i(\lambda)e^{\lambda z})J_0(\lambda r)\ \ d\lambda \qquad (B.6)$$

The functions $A_i(\lambda)$ and $B_i(\lambda)$ are to be determined from the boundary conditions. The potential function in the first layer is given by

$$V_1 = \frac{I\rho_1}{2\pi}\,\frac{1}{(r^2 + z^2)^{\frac{1}{2}}} + \int_0^\infty (A_1(\lambda)e^{-\lambda z} + B_1(\lambda)e^{\lambda z})J_0(\lambda r)\ \ d\lambda$$

At z = 0, V_1 has to satisfy the condition that

$$\frac{1}{\rho_1}\frac{\partial V_1}{\partial z}\bigg|_{z=0} = 0.$$

This condition can be satisfied if $A_1(\lambda) = B_1(\lambda)$. Thus the above expression for V_1 is reduced to

$$V_1 = \frac{I\rho_1}{2\pi}\int_0^\infty e^{-\lambda z} J_0(\lambda r)d\lambda + \int_0^\infty A_1(\lambda)(e^{-\lambda z} + e^{\lambda z})J_0(\lambda r)\ d\lambda \tag{B.7}$$

By considering the boundary condition that $V_n(r,z) \to 0$ as $z \to \infty$, one can see that the function $B_n(\lambda)$ which appears in the integral expression of V_n must vanish. Thus

$$V_n = \frac{I\rho_1}{2\pi}\int_0^\infty e^{-\lambda z} J_0(\lambda r)d\lambda + \int_0^\infty A_n(\lambda)e^{-\lambda z} J_0(\lambda r)\ d\lambda \tag{B.8}$$

Next, we will consider the conditions of continuity of the potential and of the normal component of current density at each boundary plane. The application of the condition of continuity of the potential to (B.7), (B.6), and (B.8), respectively leads to the following set of equations:

$$A_1(\lambda)(e^{-\lambda z_1} + e^{\lambda z_1}) = A_2(\lambda)e^{-\lambda z_1} + B_2(\lambda)e^{\lambda z_1}$$

$$A_i(\lambda)e^{-\lambda z_i} + B_i(\lambda)e^{\lambda z_i} = A_{i+1}(\lambda)e^{-\lambda z_i} + B_{i+1}(\lambda)e^{\lambda z_i} \tag{B.9}$$

where $i = 2, 3, \ldots, n-2$.

$$A_{n-1}(\lambda)e^{-\lambda z_{n-1}} + B_{n-1}(\lambda)e^{\lambda}{}_{n-1} = A_n(\lambda)e^{-\lambda z_{n-1}}$$

Another set of equations is obtained from the condition of continuity of normal component of current density:

$$\{-ce^{-\lambda z_1} + A_1(\lambda)(-e^{-\lambda z_1} + e^{\lambda z_1})\} = \frac{\rho_1}{\rho_2}\{-ce^{-\lambda z_1} - A_2(\lambda)e^{-\lambda z_1} + B_2(\lambda)e^{\lambda z_1}\}$$

$$\{-ce^{-\lambda z_i} - A_i(\lambda)e^{-\lambda z_i} + B_i(\lambda)e^{\lambda z_i}\} = \frac{\rho_i}{\rho_{i+1}}\{-ce^{-\lambda z_i} - A_{i+1}(\lambda)e^{-\lambda z_i} + B_{i+1}(\lambda)e^{\lambda z_i}\} \qquad (B.10)$$

$$\{-ce^{-\lambda z_{n-1}} - A_{n-1}(\lambda)e^{-\lambda z_{n-1}} + B_{n-1}(\lambda)e^{\lambda z_{n-1}}\} = \frac{\rho_{n-1}}{\rho_n}\{-ce^{-\lambda z_{n-1}} - A_n(\lambda)e^{-\lambda z_{n-1}}\}$$

where $c = I\rho_1/2\pi$.

By solving the above two sets of equations one can determine all the $A(\lambda)$ and $B(\lambda)$. Since only the potential V_1 is of interest to us it is not necessary to solve for all the unknown functions of λ except $A_1(\lambda)$.

For example, by solving the equations for the two- and three-layer cases respectively, we obtain the following results:

(i) Two-layer case

$$A_1(\lambda) = -\frac{I\rho_1}{2\pi}\frac{k_{12}e^{-2\lambda d_1}}{1+k_{12}e^{-2\lambda d_1}} \qquad \text{(B.11)}$$

(ii) Three-layer case

$$A_1(\lambda) = D_1/D \qquad \text{(B.12)}$$

where

$$D_1 = \frac{I\rho_1}{2\pi} e^{-2\lambda d_1} \{\rho_1 - \rho_2 \frac{(1 - k_{23}e^{-2\lambda d_2})}{(1 + k_{23}e^{-2\lambda d_2})} \} /$$

$$\{\rho_1 + \rho_2 \frac{(1 - k_{23}e^{-2\lambda d_2})}{(1 + k_{23}e^{-2\lambda d_2})}\}$$

and

$$D = 1 + e^{-2\lambda d_1} \{\rho_1 - \rho_2 \frac{(1 - k_{23}e^{-2\lambda d_2})}{(1 + k_{23}e^{-2\lambda d_2})}\} /$$

$$\{\rho_1 + \rho_2 \frac{(1 - k_{23}e^{-2\lambda d_2})}{(1 + k_{23}e^{-2\lambda d_2})}\}$$

The quantitits k_{12} and k_{23} are called the reflection factors which have the general form $k_{i,i+1} = (\rho_i - \rho_{i+1})/(\rho_i + \rho_{i+1})$. It may also be noted that $z_1 = d_1$ and $z_2 = d_1 + d_2$ (see Fig. 2.1).

By substituting (B.10) or (B.11) into (B.7) and then putting $z = 0$ we obtain the potential on the ground surface

for the two-layer or three-layer case. Thus in the two-layer case

$$V_1(r,0) = \frac{I\rho_1}{2\pi} \int_0^\infty \{\frac{1 - k_{12}e^{-2\lambda d_1}}{1 + k_{12}e^{-2\lambda d_1}}\} J_0(\lambda r) \quad d\lambda \qquad \text{(B.13)}$$

where

$$k_{12} = \frac{\rho_1 - \rho_2}{\rho_1 + \rho_2} \quad ,$$

and in the three-layer case

$$V_1(r,0) = \frac{I\rho_1}{2\pi} \int_0^\infty \{\frac{1 - U_1e^{-2\lambda d_1}}{1 + U_1e^{-2\lambda d_1}}\} J_0(\lambda r) \quad d\lambda \qquad \text{(B.14)}$$

where

$$U_1 = \frac{\rho_1 - \rho_2 K_2}{\rho_1 + \rho_2 K_2} \quad ,$$

$$K_2 = \frac{1 - k_{23}e^{-2\lambda d_2}}{1 + k_{23}e^{-2\lambda d_2}} \quad ,$$

$$k_{23} = (\rho_2 - \rho_3)/(\rho_2 + \rho_3).$$

By similar analysis one can show that the surface potential for the n-layer problem is given by

$$V_1(r,0) = \frac{I\rho_1}{2\pi} \int_0^{\infty} \{\frac{1 - U_1 e^{-2\lambda d_1}}{1 + U_1 e^{-2\eta d_1}}\} J_0(\lambda r) \quad d\lambda \qquad \text{(B.15)}$$

where

$$U_1 = (\rho_1 - \rho_2 K_2)/(\rho_1 + \rho_2 K_2),$$

$$K_2 = (1 - U_2 e^{-2\lambda d_2})/(1 + U_2 e^{-2\lambda d_2}),$$

$$U_2 = (\rho_2 - \rho_3 K_3)/(\rho_2 + \rho_3 K_3), \qquad \text{(B.15a)}$$

.....

.....

$$K_i = (1 - U_i e^{-2\lambda d_i})/(1 + U_i e^{-2\lambda d_i}),$$

$$U_i = (\rho_i - \rho_{i+1} K_{i+1})/(\rho_{i+} + \rho_{i+1} K_{i+1}),$$

.....

$$K_{n-1} = (1 - U_{n-1} e^{-2\lambda d_{n-1}})/(1 + U_{n-1} e^{-2\lambda d_{n-1}})$$

$$U_{n-1} = k_{n-1,n} = (\rho_{n-1} - \rho_n)/(\rho_{n-1} + \rho_n).$$

Let $K_1(\lambda)$ denote the bracketed quantity under the integral sign of (B.14). Then the general expression for the potential function takes the form

$$V_1(r,0) = \frac{I\rho_1}{2\pi} \int_0^\infty K_1(\lambda) J_0(\lambda r) \, d\lambda \qquad \text{(B.16)}$$

This form of the potential function was originally derived by Sunde (1949), but is seldom encountered in the literature. The writer finds that the function $K_1(\lambda)$ is a very convenient formula for the determination of the layer resistivities and thicknesses. The method for analyzing $K_1(\lambda)$ will be presented in Chapter IV.

It may be noted that the potential function is often written as

$$V_1(r,0) = \frac{I\rho_1}{2\pi} \frac{1}{r} + 2 \int_0^\infty A_1(\lambda) J_0(\lambda r) \, d\lambda \quad , \qquad \text{(B.17)}$$

particularly in the European literatures (e.g., Koefoed, 1965). The function $A_1(\lambda)$ is called the Slichter's kernel. In our discussions we reserve the term 'kernel' for the function $K_1(\lambda)$ only.

APPENDIX C

SOME PROPERTIES OF THE FUNCTION $F(\lambda t)$

The function $F(\lambda t)$ which is defined by the infinite series (2.18) may be written in the form

$$F(x) = J_0(x) + f(x) \tag{C.1}$$

where

$$f(x) = \sum_{k=1}^{\infty} \frac{1}{2^{2k}} J_0(x/2^k) \tag{C.2}$$

and

$$x = \lambda t.$$

To test the convergence of $f(x)$ let us compare it with an infinite series of constants

$$S = \sum_{k=1}^{\infty} 1/2^{2k} . \tag{C.3}$$

The infinite series S can easily be shown to converge absolutely. By comparing the n term of (C.2) with that of (C.3) it is obvious that

$$\left| \frac{1}{2^{2n}} J_0(x/2^n) \right| \leq \frac{1}{2^{2n}}$$

for all x where $0 < x < \infty$. Thus according to Weierstrass M test for uniform convergence, the series $f(x)$ converges

absolutely for each x and is uniformly convergent in the interval $(0,\infty)$. Since both $J_0(x)$ and $f(x)$ are convergent it follows that their sum $F(x)$ must also be convergent.

Next, we will consider the calculation of the series $f(x)$. Since $f(x)$ is a convergent series approximate values of $f(x)$ may be obtained by truncating the series after an appropriate number, say N, of terms. So the question now is to determine N such that the truncated series would give us the values of $f(x)$ to the desirable degree of accuracy.

$f(x)$ may be written as

$$f(x) = P_n + Q_n$$

where P_n is the partial sum of the first n terms of the series and Q_n is the remainder. We want to find an $N(\varepsilon)$ such that

$$|Q_n| < \varepsilon \qquad \text{for } n > N(\varepsilon)$$

where ε is some small positive number. Since $f(x)$ is a convergent series we can find a sequence T_n converging to zero for which

$$|Q_n| < T_n \qquad \text{for } n > n_1 .$$

If the sequence T_n is monotone decreasing then we can choose $N(\varepsilon)$ as the smallest integer after which $T_n < \varepsilon$. For if $N(\varepsilon)$ is so chosen and $n \geq N(\varepsilon)$, then

$$|Q_n| < T_n \leq T_{N(\varepsilon)} < \varepsilon .$$

Kaplan (1952) shows that if a series converges by the comparison test, then the remainder is in absolute value at most equal to that of the comparison series. Thus if we let T_n denote the remainder of (C.3) it can be shown that

$$T_n = 1/3\ (2)^{-2n}$$

It follows that

$$|Q_n| = \left| \sum_{k=n+1}^{\infty} \frac{1}{2^{2k}} J_0(x/2^k) \right| < \frac{1}{3\ (2)^{2n}}$$

Hence the upper bound of the error introduced by truncating the series f(x) after the first n terms is $\varepsilon = 1/3\ (2)^{-2n}$. If ε is given then $N(\varepsilon)$ can be found from

$$N(\varepsilon) = -(\log \varepsilon + \log 3)/\log 4. \qquad (C.4)$$

From (C.1) we can see that the approximate value of F(x) is given by

$$F(x) = J_0(x) + \sum_{k=1}^{N(\varepsilon)} \frac{1}{2^{2k}} J_0(x/2^k)$$

$$= \sum_{k=1}^{N(\varepsilon)} \frac{1}{2^{2k}} J_0(x/2^k) . \qquad (C.5)$$

It may be noted that the calculation of F(x) involves the evaluation of the Bessel function of first kind of zero

order which is defined by the infinite series

$$J_0(z) = \sum_{k=0}^{\infty} \frac{(-1)^k}{(k!)^2} \left\{\frac{z}{2}\right\}^{2k} .$$

This series representation of $J_0(z)$ is not suitable for numerical calculations when the values of z is large, say 10 or greater. The writer finds that the polynomial approximations of $J_0(z)$ presented by Oliver (1965) are more suitable for computational purposes than the original infinite series. An outline of these polynomial approximations is given below:

For $0 \leq z \leq 3$

$$\begin{aligned} J_0(z) = 1 &- 2.2499997(z/3)^2 + 1.2656208(z/3)^4 \\ &- 0.3163866(z/3)^6 + 0.0444479(z/3)^8 \\ &- 0.0039444(z/3)^{10} + 0.0002100(z/3)^{12} \\ &+ \varepsilon \end{aligned} \qquad (C.6)$$

$$|\varepsilon| < 5 \times 10^{-8}$$

For $3 \leq z < \infty$ (C.7)

$$J_0(z) = f \cos Y / (z)^{\frac{1}{2}}$$

where

$$f = 0.79788456 - 0.00000077(3/z) - 0.00552740(3/z)^2$$

$$- 0.00009512(3/z)^3 + 0.00137237(3/z)^4$$

$$- 0.00072805(3/z)^5 + 0.00014476(3/z)^6$$

$$+ \varepsilon$$

$$|\varepsilon| < 1.6 \times 10^{-8}$$

$$Y = z - 0.78539816 - 0.04166397(3/z) - 0.00003954(3/z)^3$$

$$+ 0.00262573(3/z)^3 - 0.00054125(3/z)^4$$

$$- 0.00029333(3/z)^5 + 0.00013558(3/z)^6$$

$$+ \varepsilon$$

$$|\varepsilon| < 7 \times 10^{-8}$$

Results of numerical calculations show that the function F(x) behaves almost like the Bessel functions, that is, it oscillates about zero and decreases in amplitude as x increases. Fig. C.1 shows the graph of F(x).

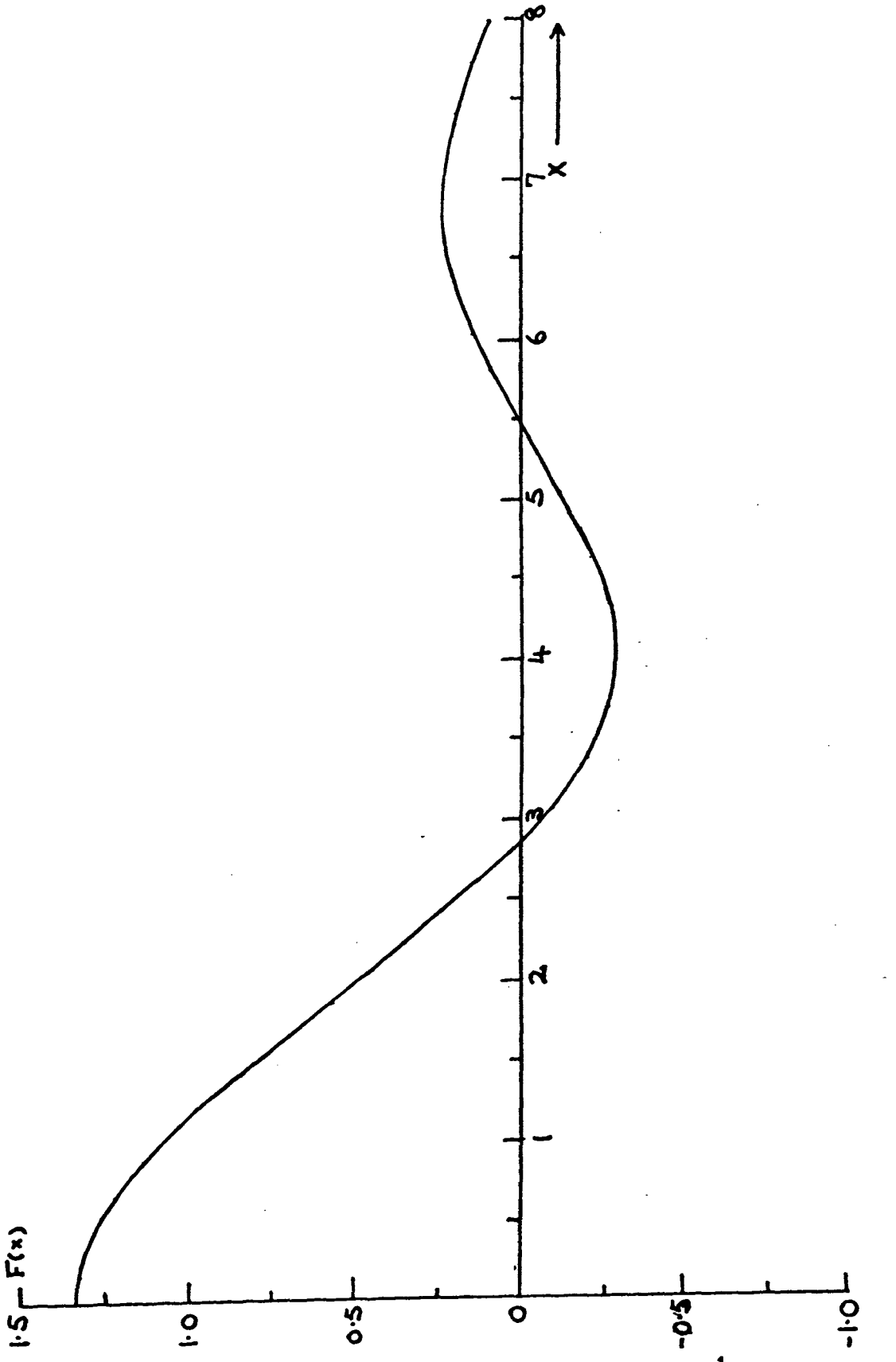

Fig. C.1. Graph of the function $F(x) = \sum_{k=0}^{\infty} \frac{1}{2^{2k}} J_0(x/2^k)$

APPENDIX D

LAGRANGIAN INTERPOLATING FORMULAS

Suppose that the apparent resistivity function $\rho_a(t)$ is known at n+1 points t_0, t_1, t_2,....., t_n, which may or may not be equally spaced. It can be shown that the Lagrangian approximation to $\rho_a(t)$ is given by

$$\rho_a(t) \simeq \sum_{k=0}^{n} l_k(t)\,\rho_a(t_k) \qquad (D.1)$$

where

$$l_k(t) = \frac{(t - t_0)\ldots(t - t_{k-1})(t - t_{k+1})\ldots(t - t_n)}{(t_k - t_0)\ldots(t_k - t_{k-1})(t_k - t_{k+1})\ldots(t_k - t_n)}\,.$$

(Hildebrand, 1956). When n = 2 we have the coefficients of the three-point interpolating formula given by

$$l_0(t) = (t-t_1)(t-t_2)/(t_0-t_1)(t_0-t_2);$$

$$l_1(t) = (t-t_0)(t-t_2)/(t_1-t_0)(t_1-t_2);$$

$$l_2(t) = (t-t_0)(t-t_1)/(t_2-t_1)(t_2-t_0).$$

When the three points are equally spaced the above coefficients can be reduced to a more convenient form for computation by a change of variable

$$t = t_0 + sh$$

where s is the new variable and h is the spacing between any two consecutive given points. After making the change of variable (D.1) can easily be shown to take the form

$$\begin{aligned} \rho_a(t_0+sh) = {} & \tfrac{1}{2}(s-1)(s-2)\,\rho_a(t_0) \\ & - s(s-2)\,\rho_a(t_1) \\ & + \tfrac{1}{2}s(s-1)\,\rho_a(t_2) \end{aligned} \qquad (D.2)$$

which is the three-point Lagrangian interpolating formula for use with equally spaced data points. Other Lagrangian formulas can, of course, be derived quite easily from (D.1).

APPENDIX E

COMPUTER FLOW DIAGRAMS FOR LEAST-SQUARES APPROXIMATION AND FOR CALCULATION OF THE KERNEL AND ASSOCIATED KERNEL

COMPUTER FLOW DIAGRAM FOR LEAST-SQUARES APPROXIMATION

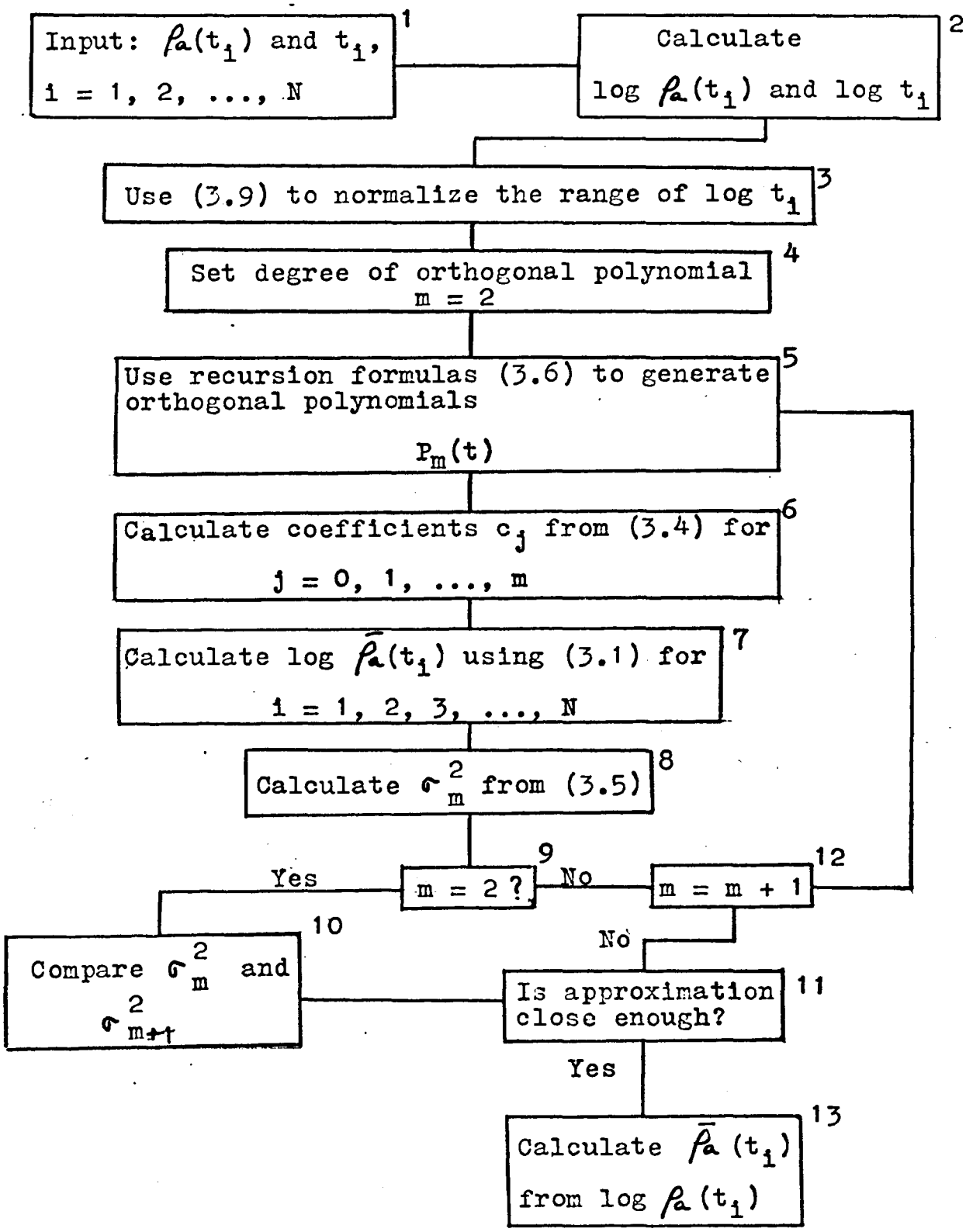

COMPUTER FLOW DIAGRAM FOR CALCULATING THE KERNEL — PROCEDURE I

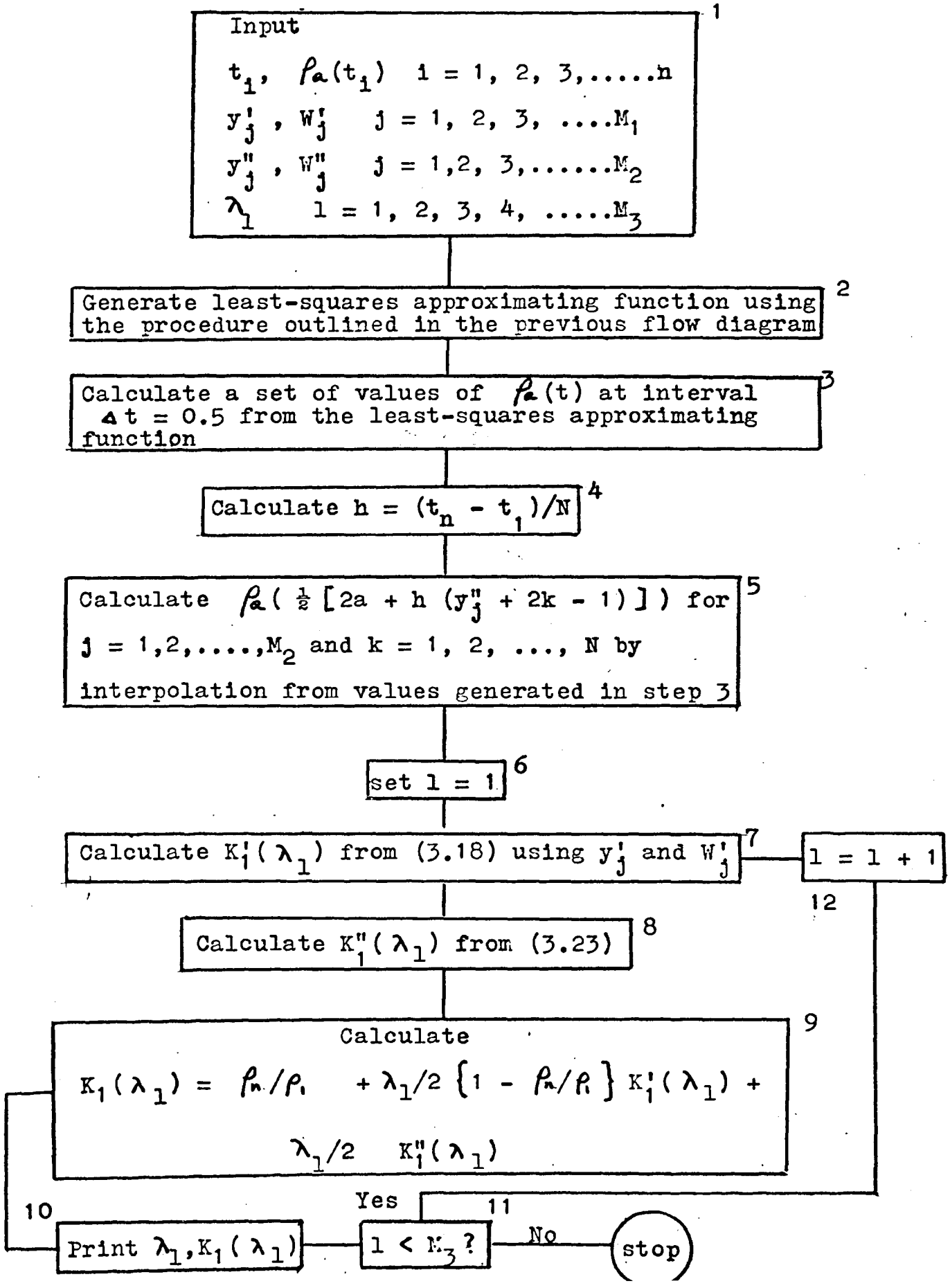

COMPUTER FLOW DIAGRAM FOR CALCULATING THE KERNEL — PROCDEURE II

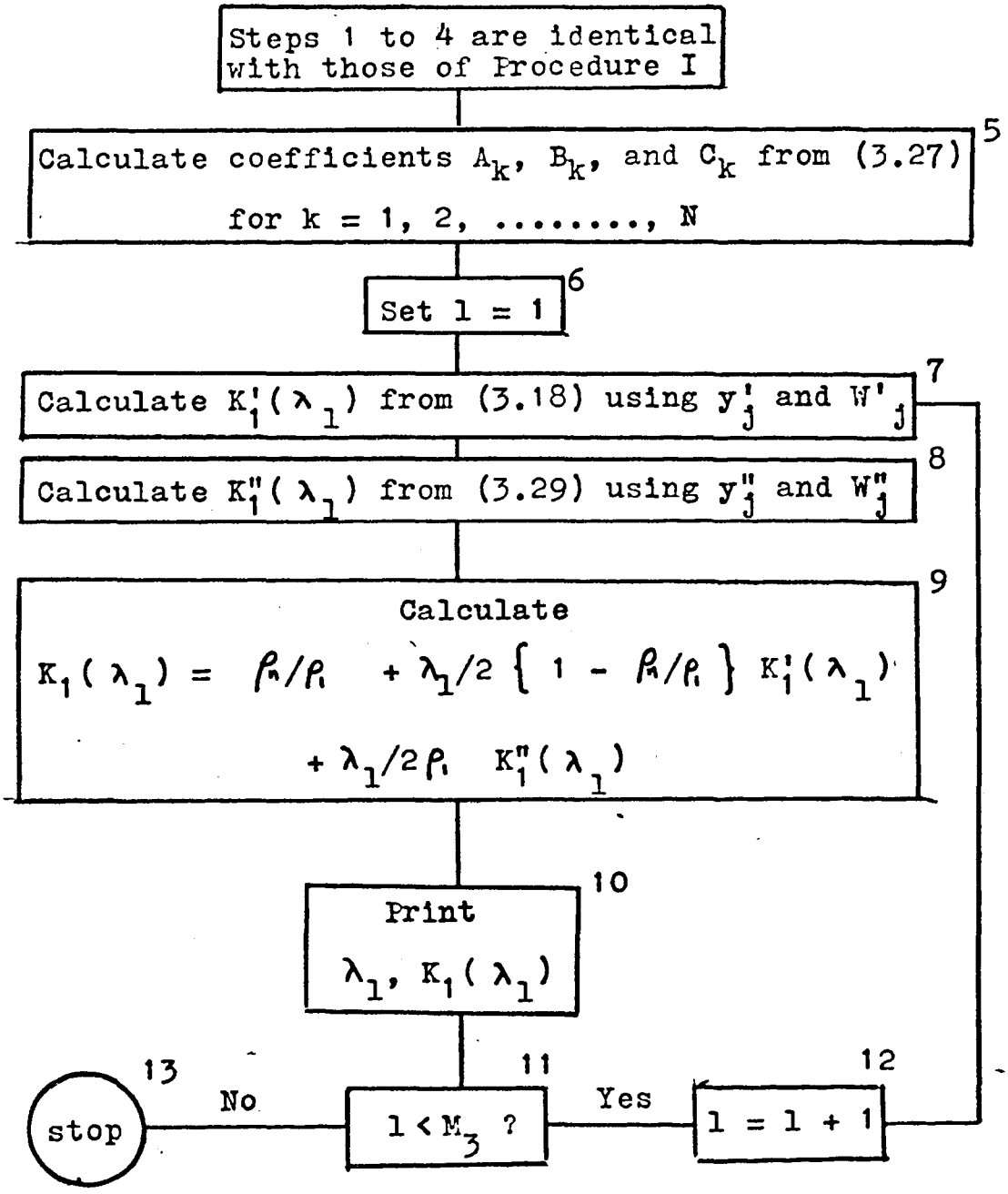

COMPUTER FLOW DIAGRAM FOR CALCULATING THE ASSOCIATED KERNEL — PROCEDURE I

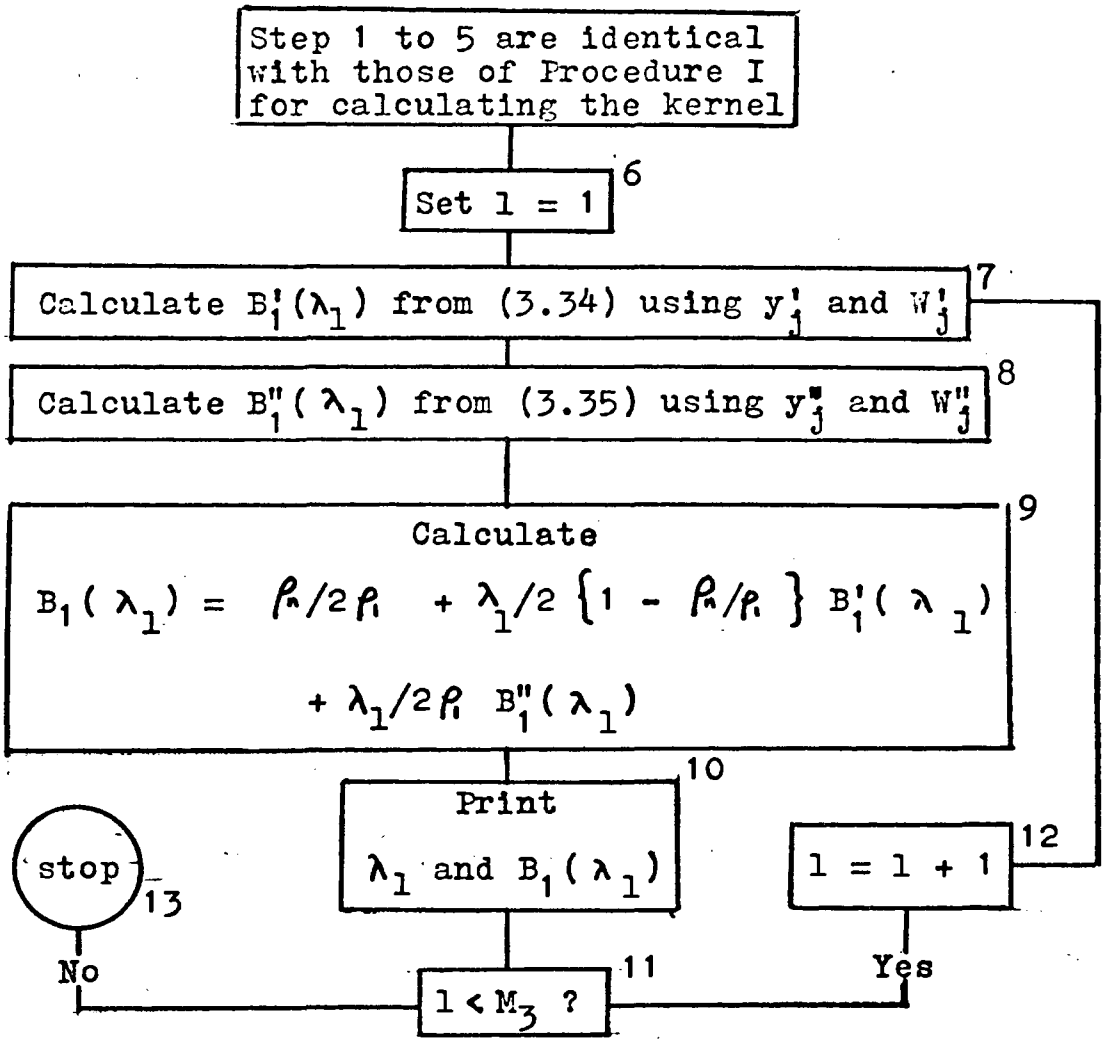

Note: The input values of y_j', W_j', y_j'', and W_j'' may not be the same as those used for the calculation of the kernel.

COMPUTER FLOW DIAGRAM FOR CALCULATING THE ASSOCIATED KERNEL — PROCEDURE II

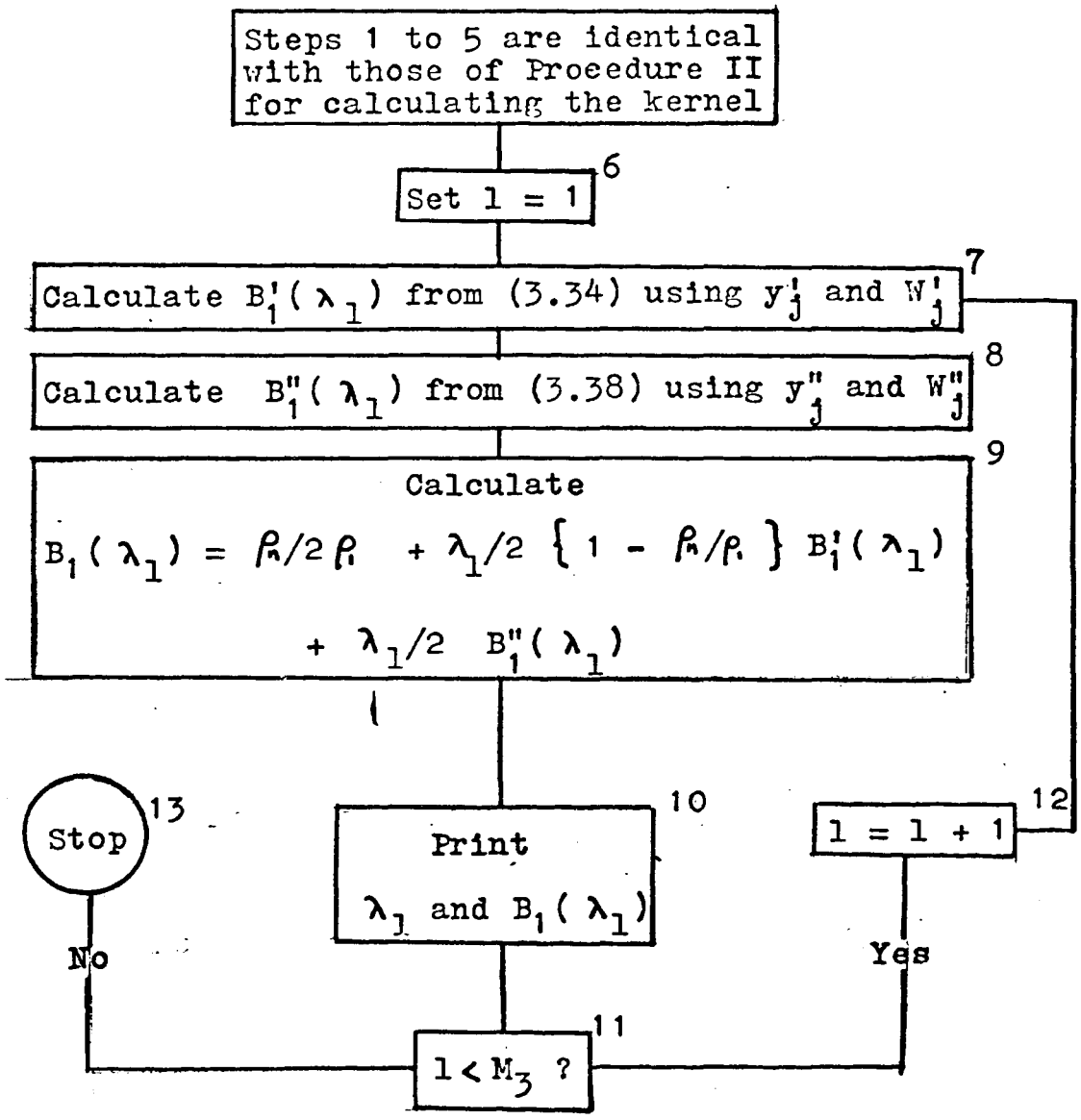

APPENDIX F

EXAMPLES OF THE ANALYSIS OF THE FOUR-LAYER KERNEL AND ASSOCIATED KERNEL

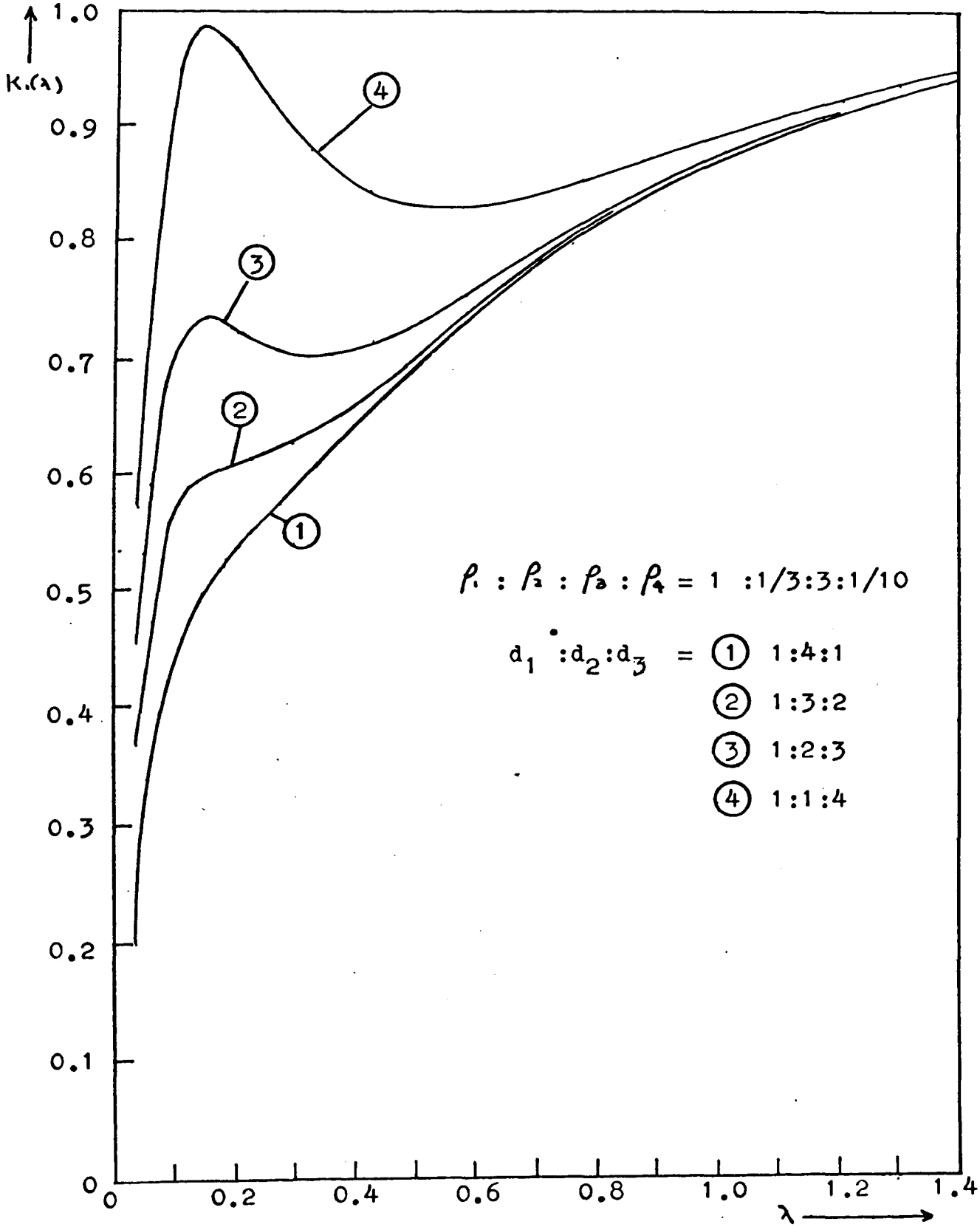

Fig. F.1. Examples of the curves of kernel of four-layer earth.

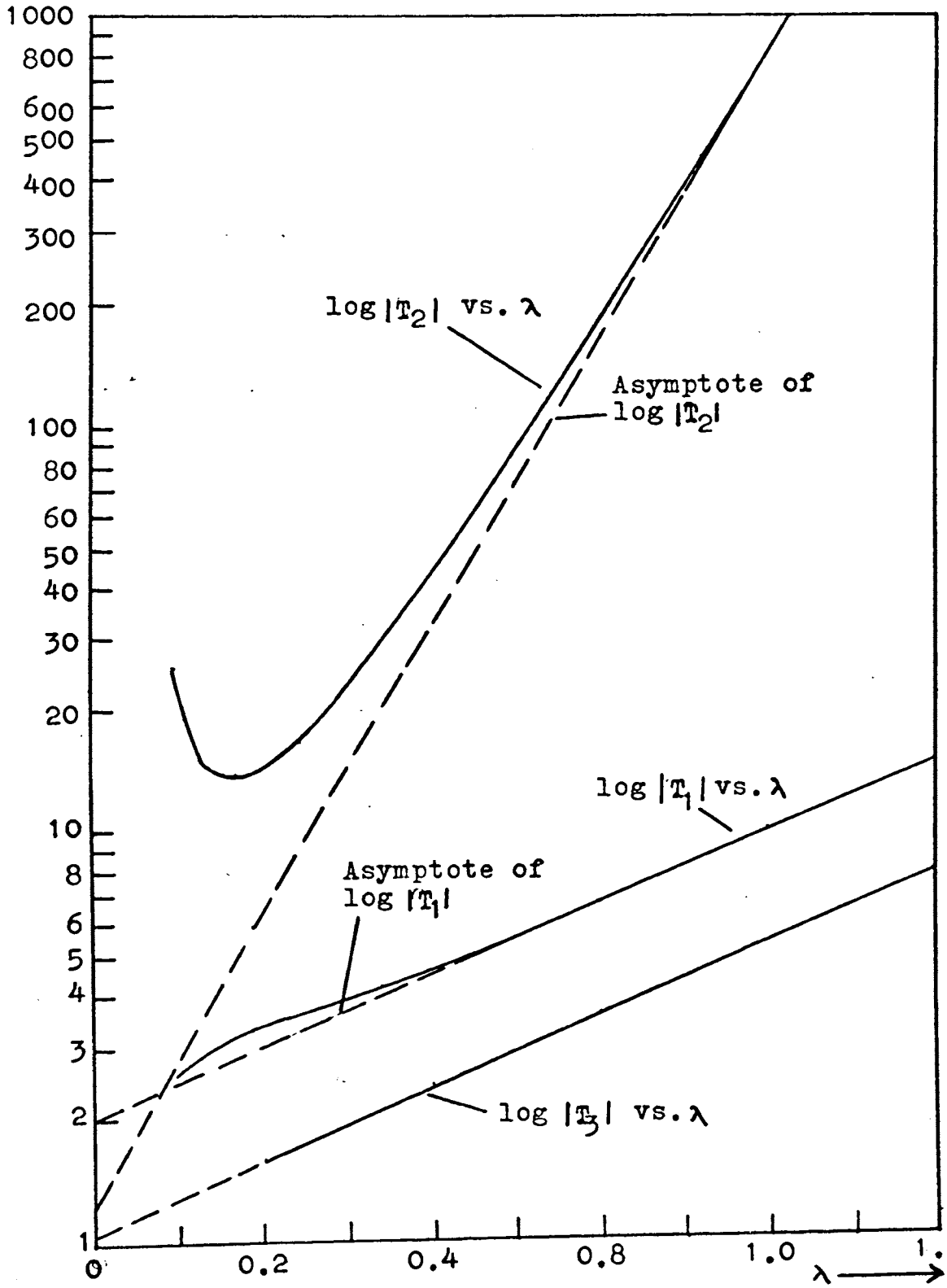

Fig. F.2. Analysis of a four-layer kernel by numerical graphical method. Case $\rho_1 : \rho_2 : \rho_3 : \rho_4 = 1 : 1/3 : 3 : 1/10$, $d_1 : d_2 : d_3 = 1 : 4 : 1$.

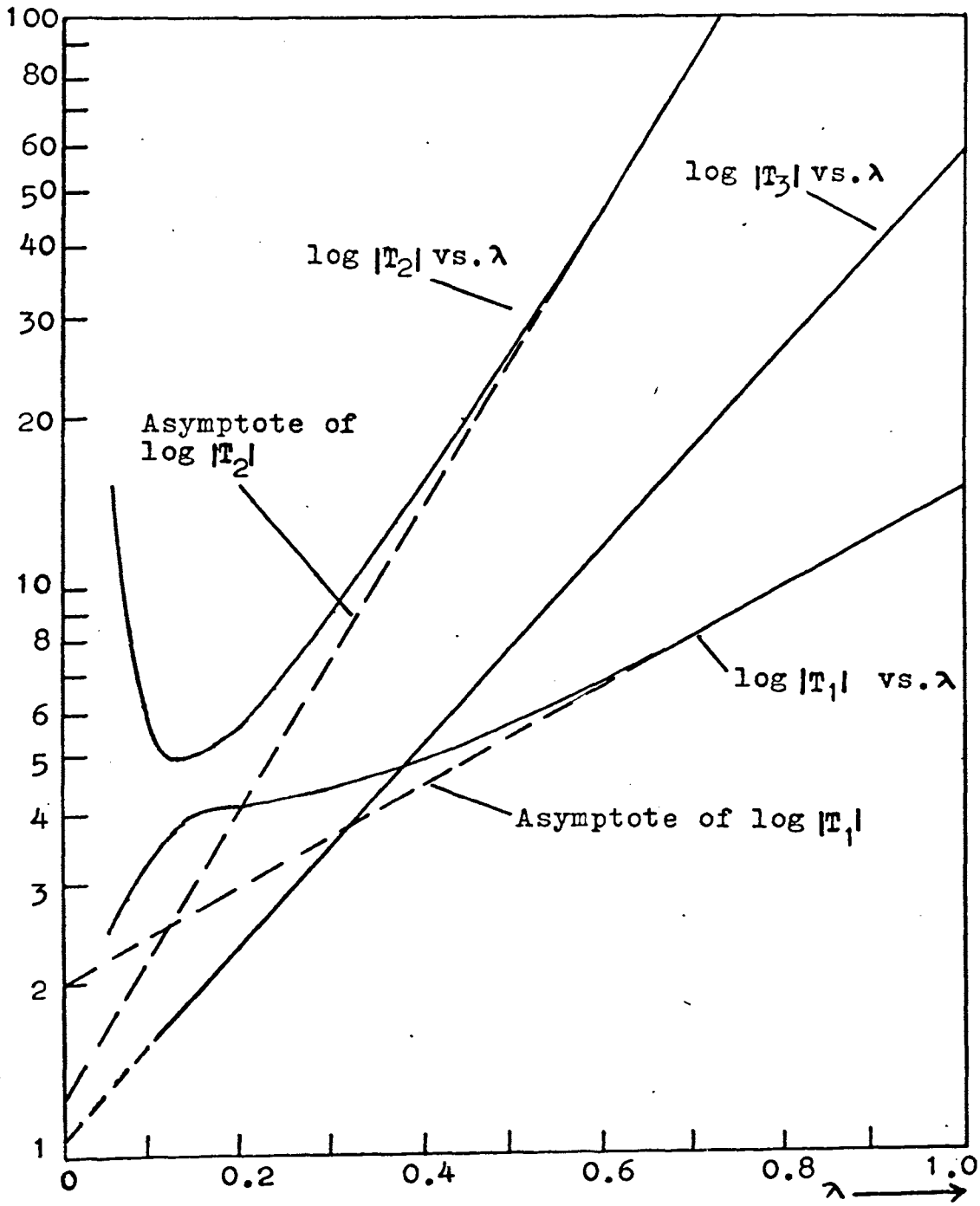

Fig. F.3. Analysis of a four-layer kernel by numerical graphical method. Case $\rho_1 : \rho_2 : \rho_3 : \rho_4 = 1:1/3:3:1/10$, $d_1:d_2:d_3 = 1:3:2$.

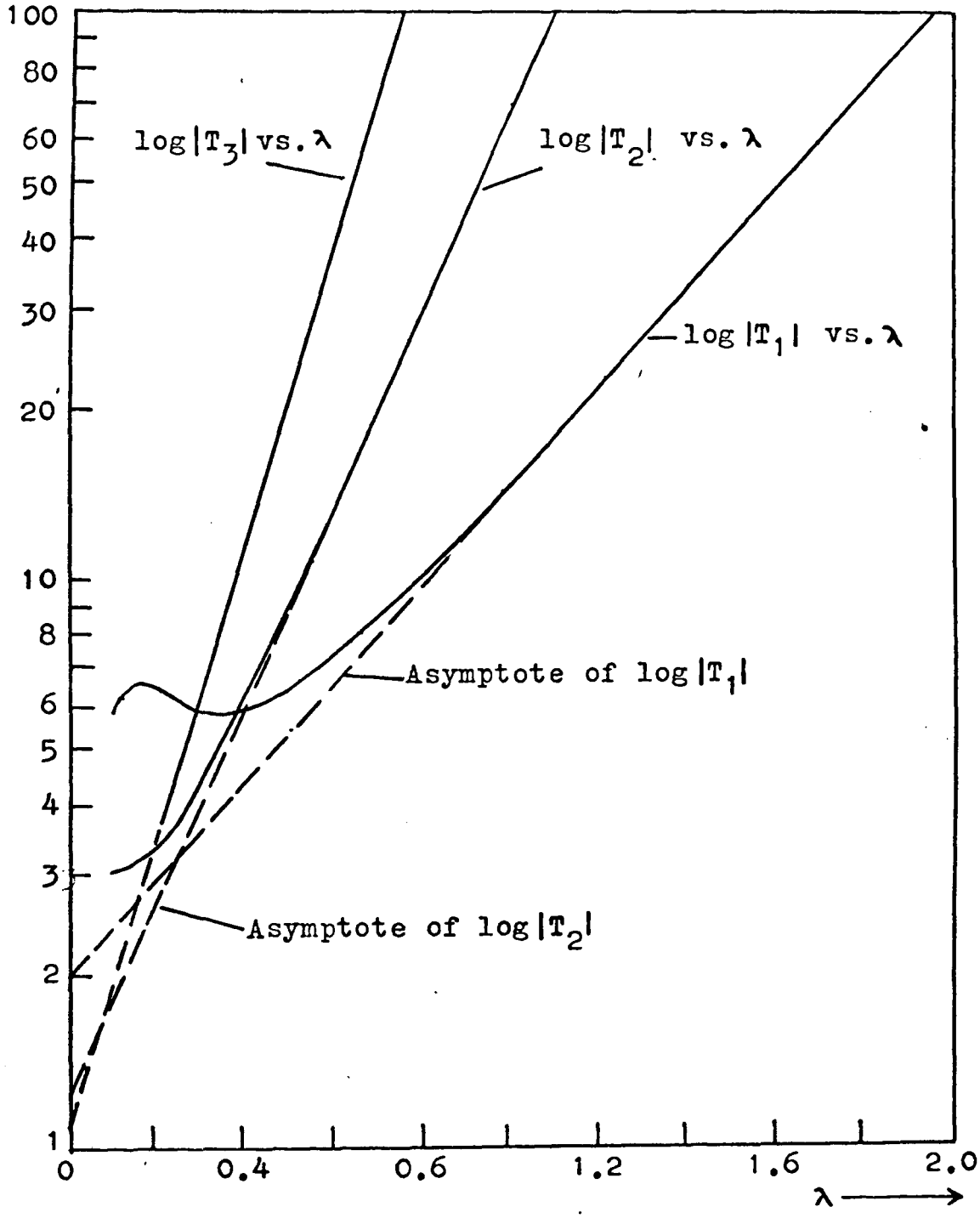

Fig. F.4. Analysis of a four-layer kernel by numerical graphical method. Case $\rho_1 : \rho_2 : \rho_3 : \rho_4 = 1:1/3:3:1/10$, $d_1:d_2:d_3 = 1:2:3$.

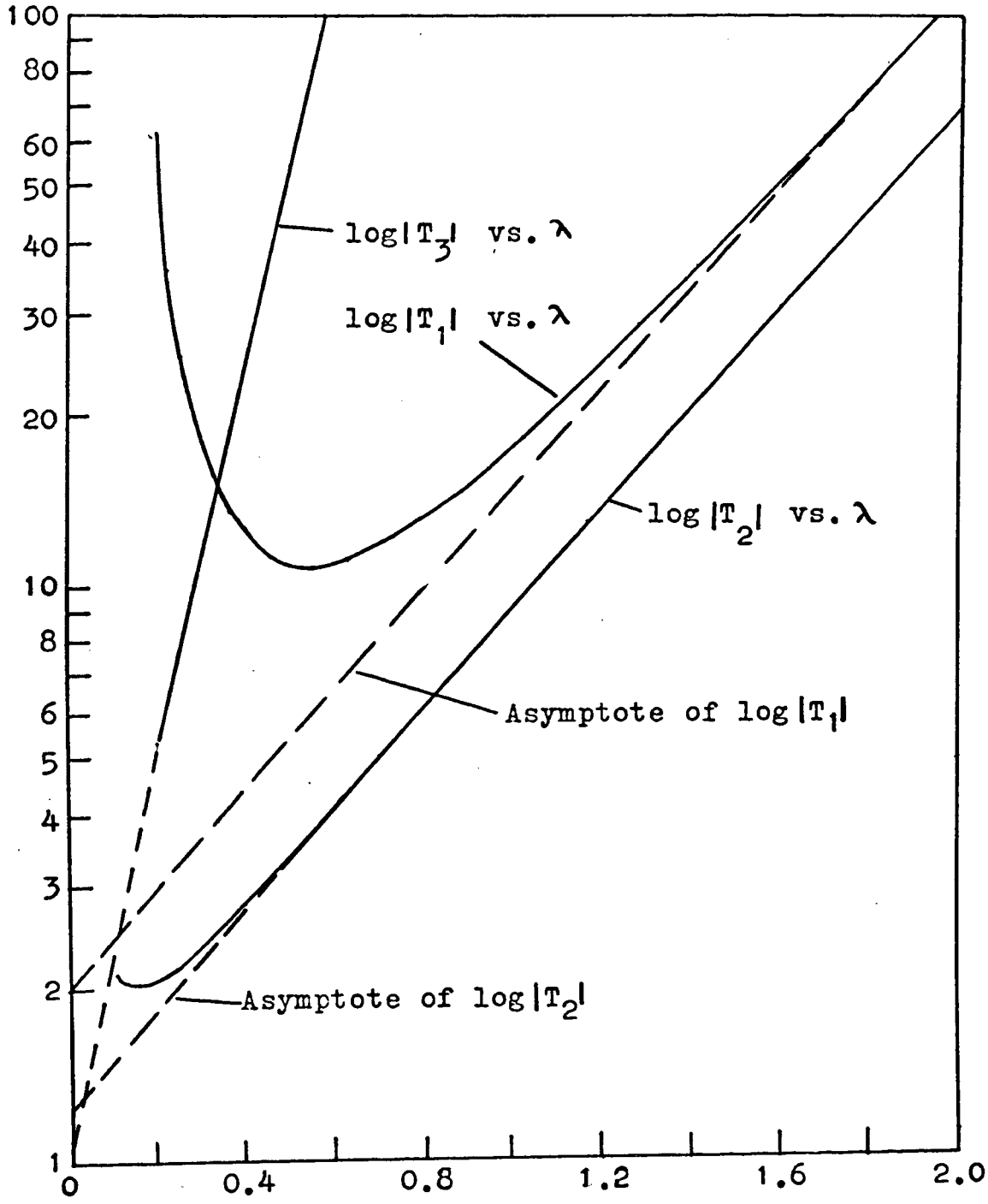

Fig. F.5. Analysis of a four-layer kernel by numerical - graphical method. Case $\rho_1 : \rho_2 : \rho_3 : \rho_4 = 1:1/3:3:1/10$, $d_1:d_2:d_3 = 1:1:4$.

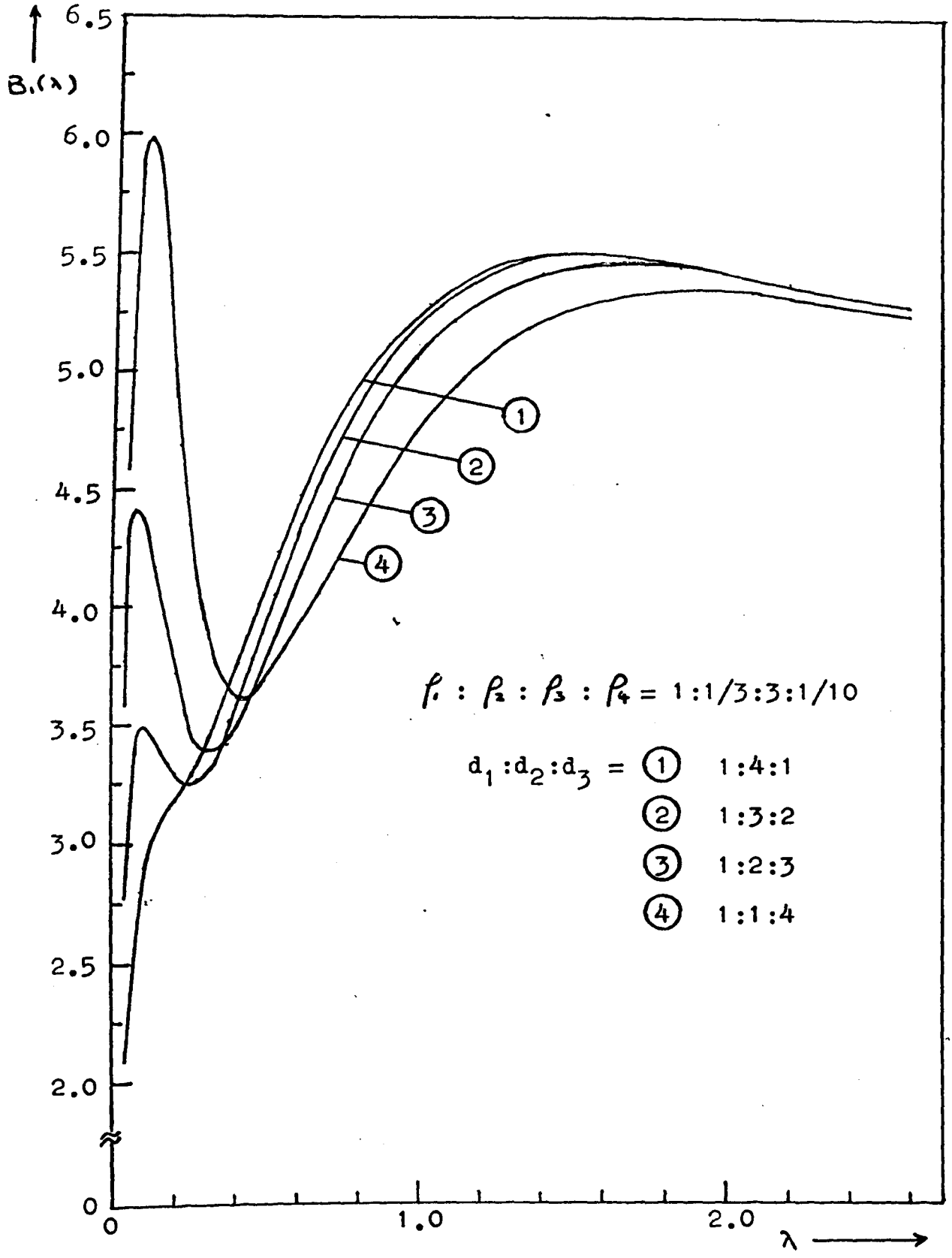

Fig. F.6. Examples of the curves of associated kernel of four-layer earth.

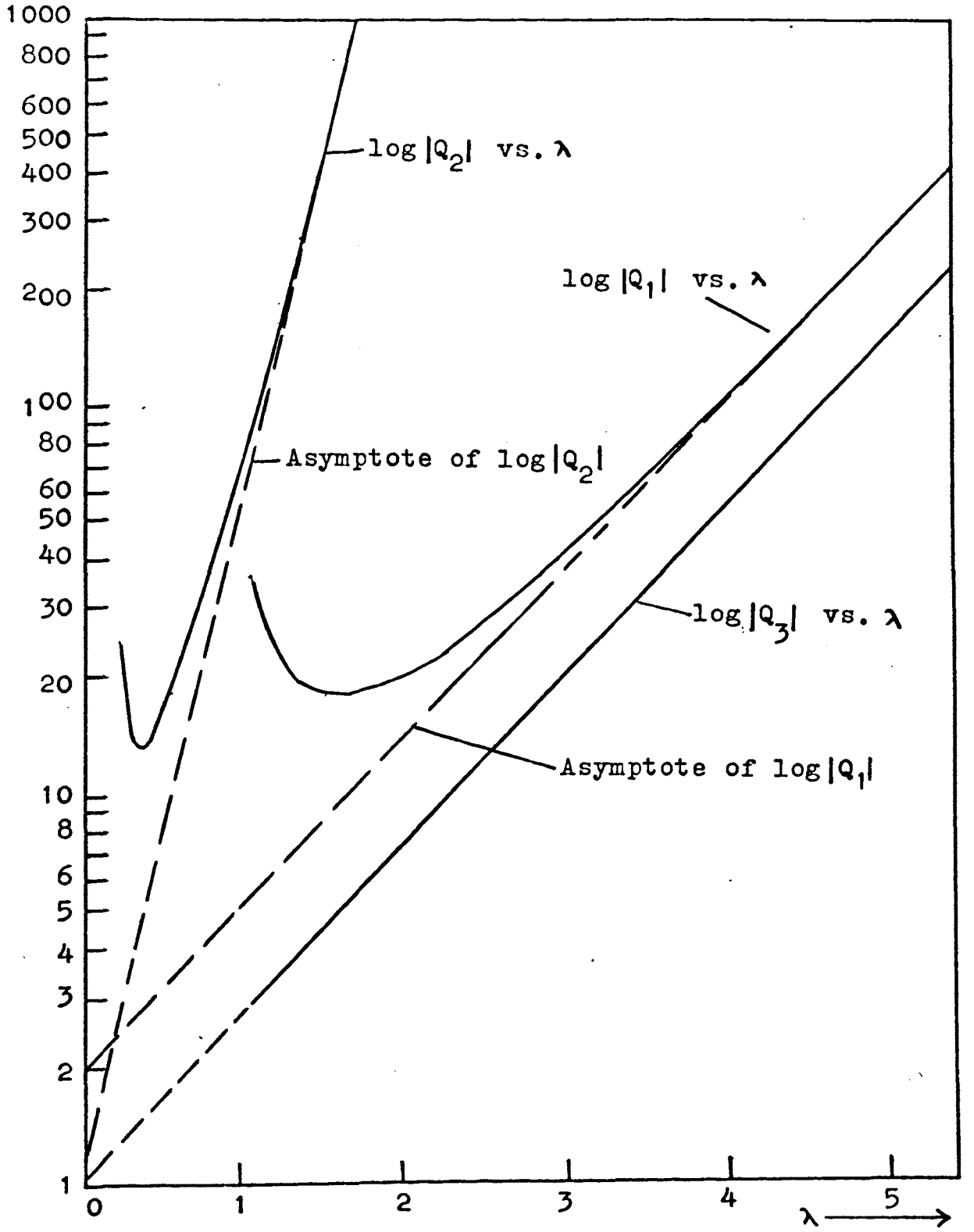

Fig. F.7. Analysis of a four-layer associated kernel by numerical-graphical method. Case $\rho_1 : \rho_2 : \rho_3 : \rho_4 = 1 : 1/3 : 3 : 1/10$, $d_1 : d_2 : d_3 = 1 : 4 : 1$.

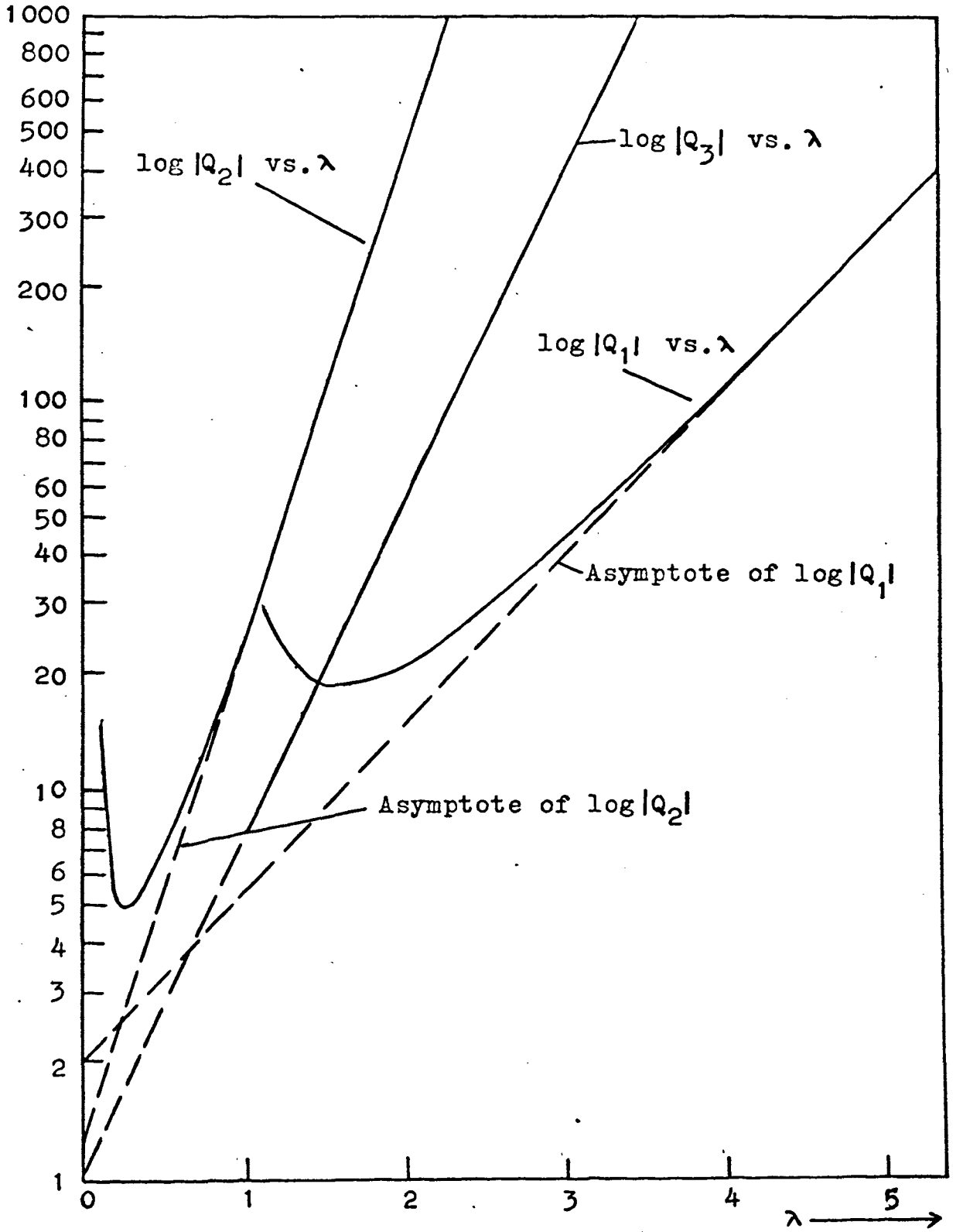

Fig. F.8. Analysis of a four-layer associated kernel by numerical-graphical method. Case $\rho_1 : \rho_2 : \rho_3 : \rho_4 = 1:1/3:3:1/10$, $d_1 : d_2 : d_3 = 1 : 3 : 2$.

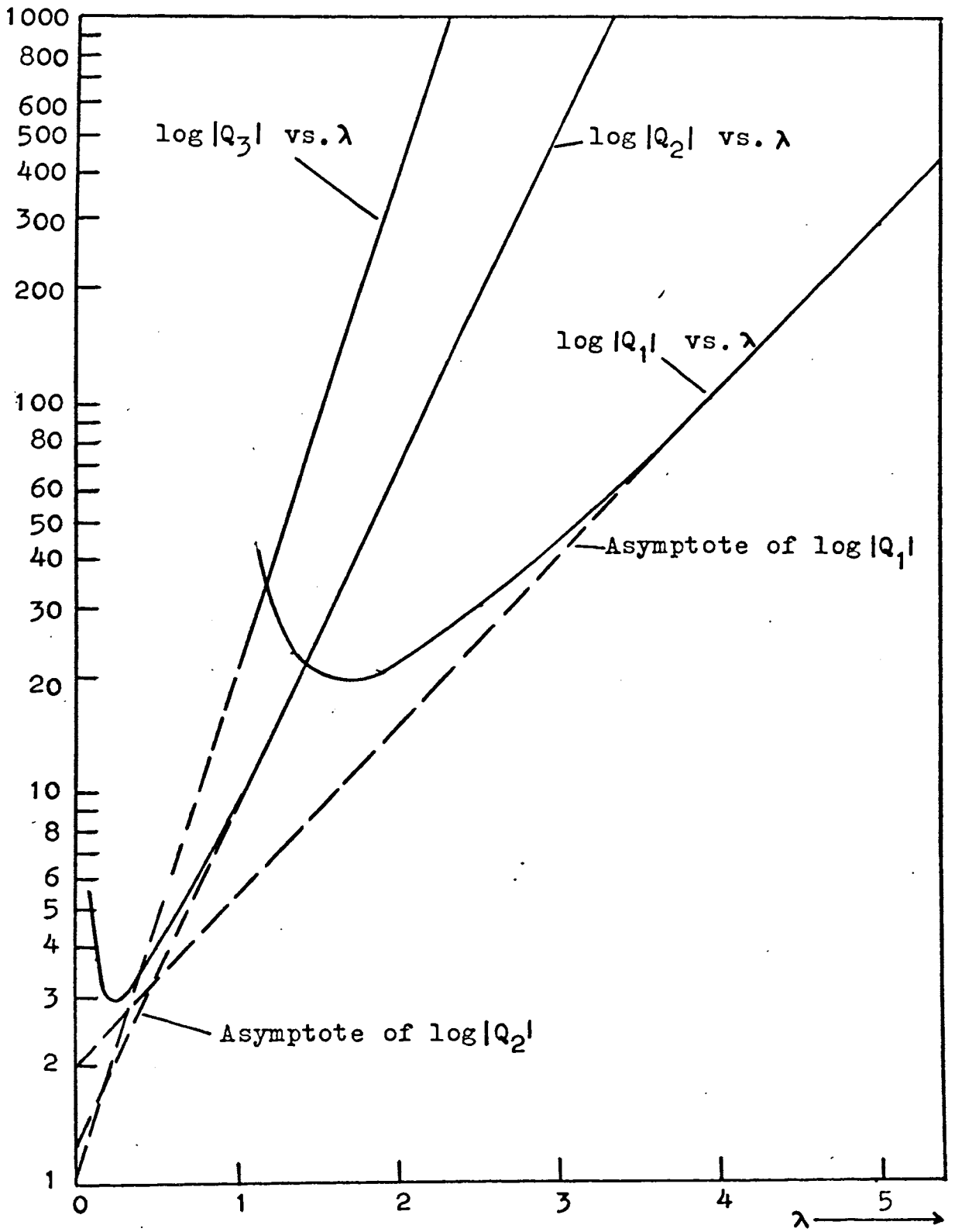

Fig. F.9. Analysis of a four-layer associated kernel by numerical-graphical method. Case $\rho_1 : \rho_2 : \rho_3 : \rho_4$ = 1:1/3:3:1/10, $d_1 : d_2 : d_3$ = 1:2:3.

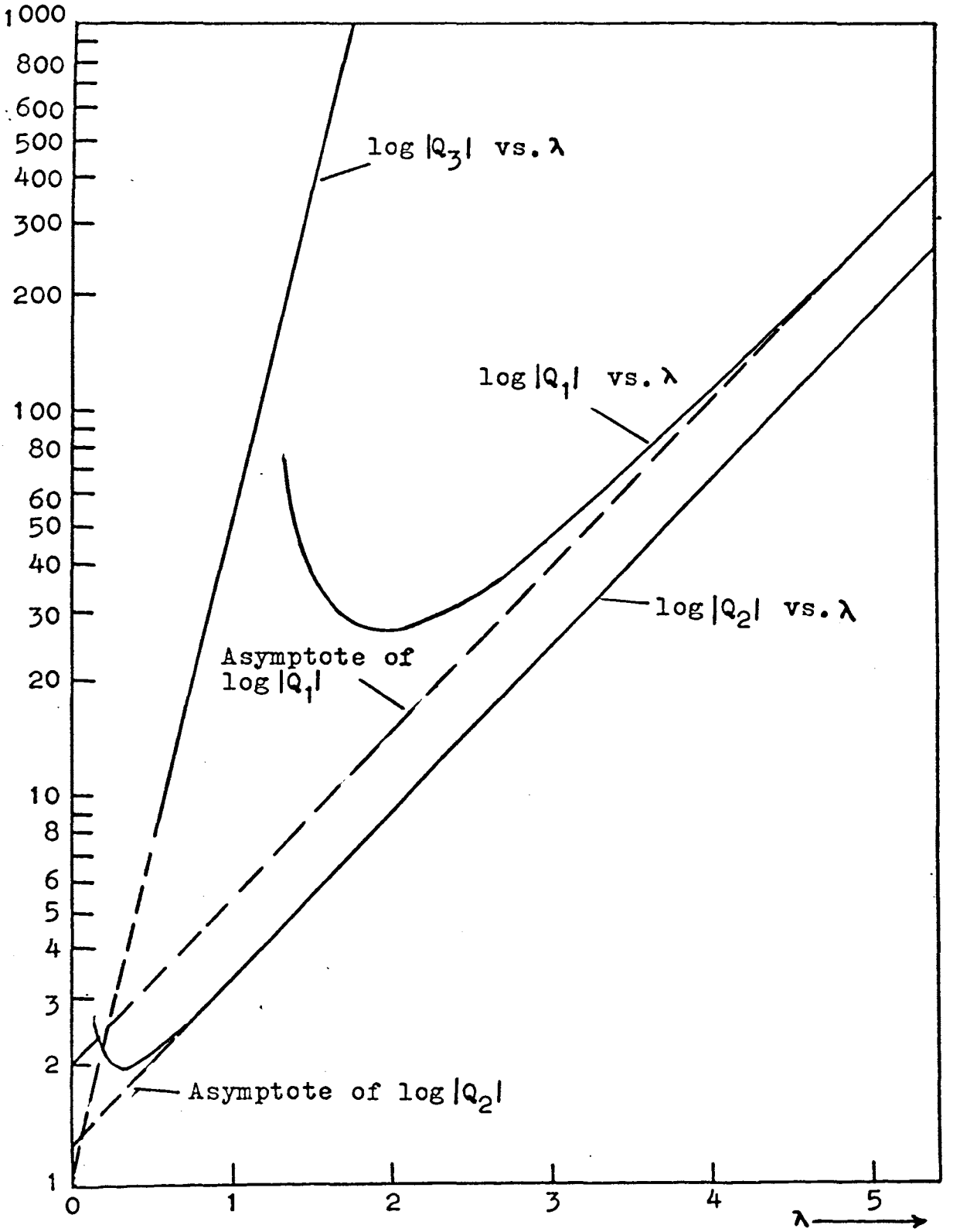

Fig. F.10. Analysis of a four-layer associated kernel by numerical graphical method. Case $\rho_1 : \rho_2 : \rho_3 : \rho_4 = 1:1/3:3:1/10$, $d_1 : d_2 : d_3 = 1:1:4$.

VITA

Siew Hung Chan, son of Wai Woh Chan and Ee Wan Au, was born September 21, 1937, in Tronoh, Perak, Malaysia. He attended the Yoke Choy Primary School in Ipoh, Perak, and graduated from the Chung Ling High School, Penang, in December 1956. In September 1957 he was enrolled into the Camborne School of Mines, Camborne, Cornwall, England, from which he received the first class Associateship of Camborne School of Mines (A.C.S.M.) in May 1960. He then proceeded to Missouri School of Mines and Metallurgy, Rolla, Missouri, to pursue graduate study in September 1960 and graduated with the degree of Master of Science in Mining Engineering in May 1962.

After graduated from Missouri School of Mines and Metallurgy he returned to Malaysia where he was employed as a prospecting engineer by the Eastern Mining and Metals Company, Kuala Lumpur, Selangor. His experience with the Eastern Mining and Metals Company was primarily concerned with the application of geophysical methods to the search for iron ore deposits in West Malaysia. In the following year he became the mine manager of the Segamat Iron Mine Ltd., in Segamat, Johore. In June 1964 he joined the Department of Geology, University of Malaya, as an assistant lecturer and was promoted to lecturer in January 1966. In August 1967 the Council of University

of Malaya granted him a study leave of three years, thus enabling him to return to the University of Missouri at Rolla to pursue his doctoral study in geophysical engineering. He has been granted research assistantship by the Department of Mining and Petroleum Engineering since September 1967. While he was in the University of Malaya he taught courses in engineering geology, economic geology of mineral deposits, and applied geophysics, and at the same time he also carried out research on the application of geophysical methods to the prospecting of alluvial tin deposits in West Malaysia.

In 1963 he was married to former Lee Kheng Beh of Singapore. They have a daughter Yik Wei Chan who is five years old.